Degradation of Aqueous Organic Pollutants by Catalytic Nonthermal Plasma based Advanced Oxidation Process

P. Manoj Kumar Reddy

A Dissertation Submitted to
Indian Institute of Technology Hyderabad
In Partial Fulfillment of the Requirements for
The Doctor of Philosophy

भारतीय प्रौद्योगिकी संस्थान हैदराबाद
Indian Institute of Technology Hyderabad

Department of chemistry

August, 2014

Declaration

I declare that this written submission represents my ideas in my own words. and where others' ideas or words have been included, I have adequately cited and referenced the original sources. I also declare that I have adhered to all principles of academic honesty and integrity and have not misrepresented or fabricated or falsified any idea/data/fact/source in my submission. I understand that any violation of the above will be a cause for disciplinary action by the Institute and can also evoke penal action from the sources that have thus not been properly cited, or from whom proper permission has not been taken when needed.

P. Manoj Kumar Reddy

(CY11P017)

Approval Sheet

This thesis entitled **"Degradation of Aqueous Organic Pollutants by Catalytic Nonthermal Plasma based Advanced Oxidation Process"** by P. Manoj Kumar Reddy is approved for the degree of Doctor of Philosophy from IIT Hyderabad.

A.K. Dikshit
18/11/2014
-Name and affiliation-
Examiner

18/11/14.
-Name and affiliation-
Examiner

Ch. Sarma
-Name and affiliation-
Adviser

G. Ne 18/11/2014
-Name and affiliation-
~~Co-Adviser~~

C. Krishna Mohan 18/11/2014
-Name and affiliation-
Chairman

Acknowledgements

I would like to express heartfelt thanks my supervisor, Dr.Ch. Subrahmanyam, Indian Institute of Technology-Hyderabad, for his extensive guidance, interests and helpful suggestions throughout the Ph.D. He has been and will always be my best source of inspiration and support.

I would like to thank Professor U. B. Desai (Director, Indian Institute of Technology Hyderabad) and Prof. F. A. Khan (Head of the chemistry department, IIT-Hyderabad) for providing necessary infrastructure and resources to accomplish my research work. My special thanks go to the faculty members in the department of chemistry, IIT-Hyderabad Dr. G. Satyanarayana, Dr. (Mrs.) M. Deepa, Dr. G. Prabusankar, Dr. T. K. Panda, Dr. (Mrs.) S. Sharada, Dr. Bhabani Shankar Mallik and Dr. Surendra Kumar Martha for their moral support during the completion of this research work.

I take this opportunity to thank all my friends especially Sk. Mahammadunnisa, A. Dayamani, K. Krushnamurty, E. Lingareddy, J. Karruppiah, B. Ramaraju Chandana and B. Laxminarayana for their help and moral support.

The students of "the department of chemistry" IITH are sincerely acknowledged for their valuable discussions and friendship without them the fulfillment of the thesis might not be materialized. I sincerely thank to Mr. Satyanarayana and team work shop in-charge for their help, and electrician Mr. Lingamaiah and Raju, for his great effort of help in our lab.

The work on my thesis has partly been financially supported by the Ministry of Environmental Forestry, Govt. of India. This support is highly acknowledged.

I would like to thank my wife and my family members whose spiritual supports and their patience are always the best encouragement for me.

P. Manoj Kumar Reddy

Abstract

Aqueous organic pollutants are a diverse group of chemicals, treated like potential environmental pollutants. Advanced Oxidation Process (AOP), which is based on the generation of highly reactive species, especially hydroxyl radicals has been receiving increasing attention as a possible remediation treatment for their removal. Nonthermal plasma (NTP) dielectric barrier discharge (DBD) reactor was developed as a possible new technology for the degradation and mineralization of aqueous organic compounds from water. The electrical discharges were produced in a parallel plane type coaxial NTP-DBD reactor. The combination of plasma discharge with different catalysts was investigated for the degradation and mineralization of model pollutants like dyes, pesticides, intermediates and pharmaceutical compounds. The effect of various operating parameters, such as initial concentrations, gas feed, applied voltage, catalyst on the performance of the reactor for mineralization was studied. Also, the degradation products were identified to understand the degradation pathways based on which possible mechanisms were proposed. Results indicated that the combination of the metal oxide catalyst with the NTP was found to enhance degradation as well as mineralization. Typical results showed that the pollutant structures were destroyed in plasma reactor, leading to mineralization. The identification by HR-MS analyses indicated that some organic acids could be the degradation products.

The present study investigates the quantification of hydrogen peroxide and O_3 formation in water and their transformation in the presence of catalyst to secondary oxidants like atomic oxygen and/or hydroxyl radical. The key parts of the present study were the identification and quantification of active species, mechanism of degradation and mineralization processes, removal efficiency and identification of the oxidation products and calculation of the energy yield.

Nomenclature

AC	Alternating Current
DC	Direct Current
DBD	Dielectric Barrier Discharge
PCD	Pulsed Corona Discharge
GC	Gas Chromatograph
NTP	Nonthermal Plasma
MFC	Mass Flow Controller
SMF	Sintered Metal Fiber
VOC	Volatile Organic Compound
MFC	Mass Flow Controller
XRD	X-ray diffraction
SS	Stainless Steel
Ppm	parts per million
AOP	Advanced Oxidation Processes
kV	Kilo volte
PCCPs	Pharmaceutical and personal care products

Contents

Title Page No.

List of Tables

List of figures

Chapter 1

Introduction and literature review

1.1. Preface

Almost all aspects of human life depend on water, and its quality is important in our lives because it is essential to all living organisms. Pure drinking water is a luxury in India, even today. Typical pollutants like dyes, fertilizers, pesticides, pharmaceuticals, personal care products and other hazardous effluents that are seeped into water and contaminating it [1]. The presence of these pollutants in water bodies causes several adverse effects, such as carcinogenicity, mutagenicity, generative impairment, endocrine disruption, and immune system damage [2-4]. Therefore, the removal of pollutants from water has become a major concern. Hence there is a need to address this issue.

1.2 Why is Water Quality Important?

Water is a part of everyday life, yet it is not an unlimited resource. Fresh water accounts for less than 2.5 percent of earth's water and 97.5 percent is salty found mostly in oceans and inland seas. Of all freshwater present on earth, nearly 80 percent is in the form of ice in the polar ice caps and glaciers of the world. This leaves only about 0.2 percent of earth's fresh water available for domestic use. The world is facing a global water quality crisis. Increasing population growth, urbanization, rapid industrialization, expanding and intensifying food production are putting pressure on water resources and increasing the unregulated or illegal discharge of contaminated water. In developing countries people are suffering from illnesses linked with contaminated water. It is estimated that 90 percent of wastewater is discharged untreated directly into rivers, lakes or the oceans. Such discharges are one of the reasons for growing dead zones in the seas and oceans.

The polluted water may have undesirable color, odor, taste, turbidity, organic matter contents, harmful chemical contents, toxic and heavy metals, pesticides, oily matters, industrial waste products, radioactivity, high total dissolved solids, acids, alkalis, domestic sewage

content, virus, bacteria, protozoa, rotifers, worms, etc. The organic content may be biodegradable or non-biodegradable. Water pollution is an even growing problem that arises from human activities. No unique solution seems possible for destroying all water pollutants due to the heterogeneous composition of real waste as well as the diversity of new chemical compounds that are continuously being generated.

1.3 Waste water treatment methods

Numerous methods (physical, chemical, and biological) have been proposed for the decontamination of polluted water and many research groups still are working for improved remediation processes [5, 6]. These methods include biological treatment and physico-chemical treatments such as air stripping, chemical oxidation, and adsorption. Each method has its own advantages and draw backs. Physical methods may transfer the pollutant to another phase against the desired mineralization [7]. Bio-treatment of effluents containing organic dyes is not effective due to their resistance to aerobic degradation, whereas, in anaerobic degradation, carcinogenic aromatic amines may be formed as by-products [8]. In this context chemical methods have been proved to be expensive as they require extensively large amount of chemicals and may also lead to large quantity of sludge. In this context, advanced oxidation processes (AOPs) have a great potential to remove organics from wastewater [9]. AOPs may offer specific advantages over conventional treatments due to *in-situ* generation of strong oxidants and may eliminate the problems associated with bio-remediation. AOPs by electric discharges is one of the techniques being used in the present study.

1.4 Advanced oxidation processes (AOPs)

In 1987, Glaze et al. [10] defined AOPs as "near ambient temperature and pressure water treatment processes which involve the generation of hydroxyl radicals in sufficient quantity to effect water purification". The hydroxyl radical (OH•) is a powerful non-selective chemical oxidant (as illustrated by Table 1.1), which reacts rapidly with most organic compounds. The AOPs are characterized by the formation of the highly oxidative hydroxyl radical (OH•) or superoxide (O_2•$^-$) at ambient temperature. AOPs are considered as a low or non-waste generation technology, which destroys the complex structures using short lived active species. The OH• radicals can be generated by chemical, electrical, mechanical or radiation energy.

Therefore, AOPs are classified under chemical, catalytic, photochemical, photocatalytic, mechanical and electrical processes. Oxidation processes aim at the mineralization of the contaminants to carbon dioxide, water and inorganic compounds or, at least, at their transformation into harmless products.

AOPs have gained attention due to their efficiency and ability to treat almost all organics in waste water [9]. Some of the most commonly used oxidants are photocatalysis, H_2O_2, UV, O_3, Fe^{2+} and ultra sound. The oxidizing potential of the most commonly used oxidants are shown in Table 1.1. A highly attractive advantage of the AOPs is that they are capable of mineralizing a variety of aqueous organic compounds such as dyes, phenolic compounds, amines, pesticides, pharmaceuticals and personal care products under ambient temperature. The process is non–selective to a very broad range of chemicals. The hydroxyl radical (OH•) can react with an organic substrate in three different ways, where the oxidation proceeds via abstraction of hydrogen atom to initiate chain reactions. OH• radicals are considered as reactive electrophiles due to their preference to electrons and hence they react rapidly towards electron rich organic compounds. The OH• has an oxidation potential of 2.80 V and can oxidize substances more efficiently than conventional oxidants. The organic substances are first attacked by the generated hydroxyl radicals (Eq-1.1), followed by hydrogen abstraction (Eq-1.2) and then the electron transfer (Eq-1.3) [11, 12].

- With hydrogen abstraction: $OH\bullet + RH \rightarrow R\bullet + H_2O$ (1.1)
- With electrophilic addition: $OH\bullet + PhX \rightarrow HOPhX\bullet$ (1.2)
- With electron transfer: $OH\bullet + RX \rightarrow RX^{\bullet+} + OH^-$ (1.3)

Species	Reduction potential, E^0_{red} (V)
Hydroxyl radical (OH•)	2.80
Atomic oxygen (O)	2.42
Ozone (O_3)	2.07
Hydrogen peroxide (H_2O_2)	1.78
Perhydroxyl radical (HO_2•)	1.70
Chlorine dioxide (Cl_2O)	1.57
Chlorine (Cl_2)	1.36
Oxygen (O_2)	1.23

Table 1.1: Reduction potentials of various oxidizing species

Hydroxyl radicals (OH•) are known to react nonselectively with all most all organic compounds in water [13]. OH• are capable of degrading organic substrates and causing structure destruction by hydrogen abstraction generating organic radicals, which yields peroxyl radical by the reaction with oxygen. These organic and peroxyl radicals initiate oxidative chain reactions leading to the mineralization, where the final products are carbon dioxide, water, and inorganic salts. Another mechanism is electron transfer to hydroxyl radicals leading to hydroxyl ion. AOPs are being studied for the degradation of contaminants in water and an increasing number of combinations of processes are being thought of. The techniques can be divided into different categories. Photochemical and photocatalytic and combinations of UV, ozone, hydrogen peroxide and TiO_2 as well as hybrid gas-liquid plasma reactors are used.

1.4.1 Ozonation

Ozone is the strongest commercially available oxidizing agent and is traditionally been used for treating water for the removal of odor and taste. Among the common oxidizers, only hydroxyl radical and fluorine have oxidation potential more than the ozone. An advantage of the use of ozone is the production of hydroxyl (OH) radicals that occurs through the self-decomposition of ozone. Ozone is a potential oxidant (E_0 = 2.07 V) and reacts with many organics via direct or indirect reactions (mainly hydroxyl radical). The rate of reaction by OH• are typically in the range of 10^6 to 10^9 times faster than that of ozone. Attack by ozone may occur at atoms with a

negative charge density or double/triple bonds etc. Indirectly, ozone can produce free radicals (OH•, E_0 = 2.80 V) that can react with almost all organic compounds [14, 15].

$$3O_3 + OH^- + H^+ \rightarrow 2OH^{\bullet} + 4O_2 \qquad (1.4)$$

Ozone itself is a selective oxidant but it oxidizes organic compounds through hydroxyl radical produced from the auto decomposition as shown below. Higher pH is recommended for ozonation to produce more hydroxyl radicals [16].

To enhance the radical formation and there by the degradation of contaminants, it is suggested to use to ozone in combination with UV light (O_3/UV) such that at UV radiation of 254 nm ozone decomposes to produce OH• [10]. This combined technique leads to reactions like photolysis, direct ozonation and radical oxidation

$$O_3 + H_2O + h\nu \rightarrow O_2 + H_2O_2 \quad \lambda < 300 \text{ nm} \qquad (1.5)$$

$$H_2O + h\nu \rightarrow 2HO\bullet \qquad (1.6)$$

1.4.2 UV/H_2O_2 process

The UV/H_2O_2 process is a homogeneous AOP in which OH• radicals are generated by the direct photo induced homolytic decomposition of H_2O_2 under UV irradiation and radical chain reactions. Oxidation with H_2O_2 alone or UV alone has not been recommended, due to low efficiency. The combination of H_2O_2/UV is found to be very effective in the degradation of organic compounds. The most accepted mechanism for this H_2O_2 photolysis is the rupture of the O-O bond by the action of ultraviolet light forming two hydroxyl radicals followed by OH• radical attack to hydrogen peroxide leading to the following sequence of reactions [17-19]:

$$H_2O_2 + h\nu \rightarrow 2OH\bullet \qquad (1.7)$$

$$H_2O_2 + 2OH\bullet \rightarrow HO_2\bullet + H_2O \qquad (1.8)$$

$$H_2O_2 + HO_2\bullet \rightarrow OH\bullet + H_2O + O_2 \qquad (1.9)$$

$$2HO_2\bullet \rightarrow H_2O_2 + O_2 \qquad (1.10)$$

1.4.3 Fenton processes

The Fenton reaction is a homogeneous catalytic oxidation generally that takes place in combination with an oxidizing agent (H_2O_2) and iron (II) catalyst (an oxide or metal salt). The ferrous ion initiated catalytic decomposition of H_2O_2, results in *in-situ* generation of hydroxyl radicals, HO• (Eq-1.11). This process involving Fe^{2+} ions and H_2O_2 was discovered by Fenton in the 19th century. However, its application for the oxidation of pollutants in water started only later in the 1960s. The advantage of the Fenton reagent is that no energy required to activate hydrogen peroxide for generation of active species. In the Fenton process, the addition of H_2O_2 to Fe^{2+} salts generates the hydroxyl radicals [20, 21].

$$Fe^{2+} + H_2O_2 \rightarrow Fe^{3+} + OH\bullet + OH^- \qquad (1.11)$$

The Fenton reagent has been successfully used in the degradation of several compounds. The Fe^{2+} regeneration follows different mechanisms and the recognized scheme is shown in the Eq-(1.12-1.1).

$$Fe^{3+} + H_2O_2 \rightarrow Fe^{2+} + HO^- + HO\bullet \qquad (1.12)$$

$$HO\bullet + H_2O_2 \rightarrow HO_2\bullet + H_2O \qquad (1.13)$$

$$Fe^{3+} + HO_2\bullet \rightarrow Fe^{2+} + H^+ + O_2 \qquad (1.14)$$

$$Fe^{2+} + OH\bullet \rightarrow Fe^{3+} + OH^- \qquad (1.15)$$

Photo-Fenton process

In this process in addition to the above reactions, the formation of hydroxyl radical also occurs by the photo induced homolytic cleavage of H_2O_2 by following reactions [19, 22].

$$H_2O_2 + UV \rightarrow HO\bullet + HO\bullet \qquad (1.16)$$

$$Fe^{3+} + H_2O + UV \rightarrow HO\bullet + Fe^{2+} + H^+ \qquad (1.17)$$

1.4.4 Photocatalytic process

Photocatalysis is generally a combination of photochemistry and catalysis. In general, the semiconductors are used as photocatalysts, which are activated by UV/Vis light. Photocatalysis has the capability of performing both oxidation and reduction which is a unique property when compared to other reactions where either oxidation or reduction may takes place. For a semiconductor to be photochemically active, the redox potential of the photo generated hole must be sufficiently positive to generate OH• radicals, which can subsequently oxidize the organics. The redox potential of the photo generated conduction band electron must be sufficiently negative to be able to reduce absorbed oxygen to superoxide**.** Many semiconductors such as TiO_2, ZnO, CdS, ZnS, SnO_2, Fe_2O_3 and WO_3 have been studied as photocatalysts [23-25]. When a photon of energy higher or equal to the band–gap value of the semiconductor is absorbed by a catalyst, an electron from the VB is promoted to the CB with simultaneous generation of a photo generated hole (h^+_{vb}) in the VB and photo generated electron (e^-_{cb}) in the CB (Eq-1.18). Photocatalytic degradation is carried out by two types of oxidizing species: the hydroxyl radicals and the positive holes [25-28].

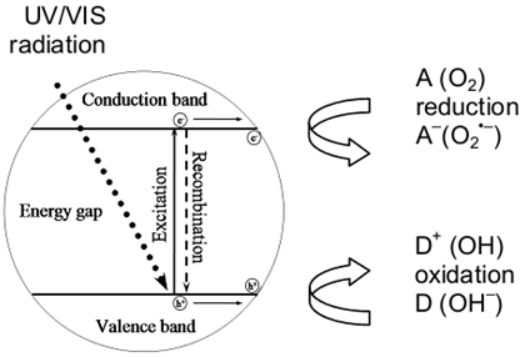

Figure 1.1: Processes involved in photocatalysis

Salient features of the electronic structures of semiconductors.

$TiO_2 \rightarrow e^-_{CB} + h^+_{VB}$ (1.18)

$h^+_{VB} + H_2O \rightarrow OH^{\bullet} + H^+$ (1.19)

$e^-_{CB} + O_2 \rightarrow O_2^{\bullet -}$ (1.20)

Pollutant + Active species → End product (1.21)

Where

TiO_2 (h^+_{VB}) = Valence band holes

TiO_2 (e^-_{CB}) = Conduction band electrons

1.4.5 Hybrid gas-liquid plasma reactors

Hybrid gas-liquid plasma reactors are units in which the electrical discharges and the liquid to be treated are in contact with each other [29-32]. Different types of hybrid reactors are being investigated for water treatment. Electric discharges at the water-gas interface is one of the AOP that offer specific advantages like generation of multiple oxidants [33]. Electrical discharges generated in water induce different physical and chemical effects like high electric fields, UV radiation, overpressure shock waves, and the formation of chemically active species [34]. The interaction of the high energy electrons created by the discharge with the water molecules produces highly oxidative species. The electrical breakdown in water produces UV radiation, shock wave, ions (H^+, H_3O^+, O^+, H^-, O^-, OH^-), molecular species (H_2, O_2, H_2O_2), and, most importantly, reactive radicals (such as O•, H•, OH•) [35-40]. In addition, the energetic electrons transform kinetic energy into potential energy of the excited species by energizing the atoms and molecules. There is an increasing interest in the application of plasma reactors in wastewater treatment; it produce electrons of the high energy, which scopes beyond the dissociation energy of water (5.16 eV) or even ionization energy of water (12.62 eV) [8, 37].

$$H_2O \rightarrow HO\bullet + H^+ \qquad (1.22)$$

The term plasma was first coined by Irving Langmuir in the year of 1928 to "describe a region containing balanced charges of ions and electrons".

1.5 Plasma

Plasma is often described as the fourth state of matter or ionized gas, since it has properties that are not found in the other three states: solid, liquid, and gas**.** From a fundamental definition, there are three states of matter: solid, liquid, and gas. These states are generally transformed by increases in temperature. Plasmas are generated when energy in the form of electrical, thermal, or magnetic is supplied to a gas. At some point the energy reaches a threshold and the gas is transformed into plasma. Plasmas are produced either by raising the temperature of a substance until high degree of ionization is obtained or by ionization processes that raise the degree of ionization much above its thermal equilibrium value. These plasmas represent a chemically rich environment of partially or fully ionized gas (Fig.1.2). For the quantitative description of plasma, the term of temperature is usually used.

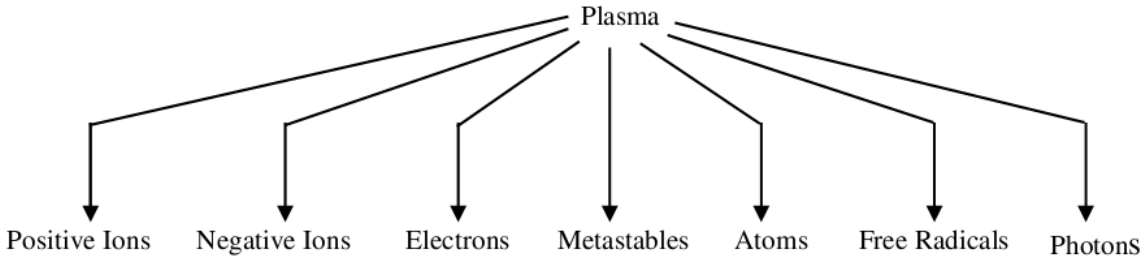

Figure 1.2: Constituents of plasma [40]

1.5.1 Types of Plasmas

Plasma can be generated naturally or artificially in the laboratory or in the industry using different types of plasma reactors. Based on the temperature, there are two main types of plasma: thermal equilibrium and non-thermal non-equilibrium plasmas with the primary difference being how energy is deposited into the plasma gas stream.

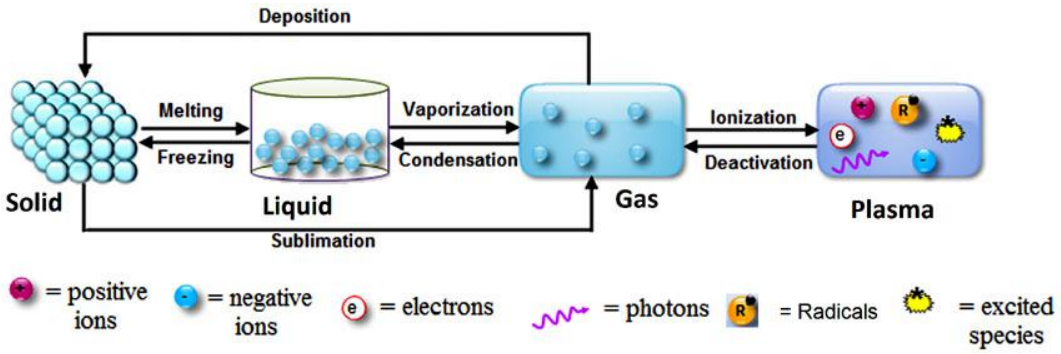

Figure 1.3: States of matter

1.5.1.1 Thermal plasma

The thermal plasma is characterized by almost all its components are at thermal equilibrium Te=Tg=Ti (Te is electron temperature, Ti is ion temperature, and Tg is gas temperature). When the kinetic energies are the same, the plasma is said to be in equilibrium. Plasma, as the ionized state of matter, consists of a quasi-neutral mixture of neutral species, positive ions, negative ions, and electrons with an average thermal energy typically exceeding 0.5eV. In thermal plasmas, the gas is heated to a temperature enough to ionize it (4000-20000K). Hence, all the species present are in thermal equilibrium with each other, i.e., Ti= Te =Tg (i=ion, e=electron, g=neutral gas) [41].

1.5.1.2 Non-thermal plasma.

As the non-thermal plasma (NTP) name implies, plasma also can occur at room temperature if the molecules are exposed to a strong electrical field. In NTP, much of the energy has been placed in excited electrons. In order to ignite and sustain NTP, the breakdown-voltage of the gas must be exceeded. In NTP, temperature (i.e. kinetic energy) is not in thermal equilibrium, and differs substantially between the electrons and the other particles (ions, atoms, and molecules). In this sense, NTP is also referred to as a ‘‘non-equilibrium plasma’’ or a ‘‘cold plasma”. Because of low mass of electrons, it can be easily accelerated to energies which are enough to ionize the gas atoms. The background gas molecules in NTP are often at or near room temperature. Due to the low gas temperatures, this type of plasma is called nonthermal or cold plasma. Te>>Tg and Te > Ti > Tg. Ion temperature, Ti, can lie anywhere between Te and Tg,

depending on the type of plasma. Furthermore, the degree of ionization in NTP is usually much lower than that of thermal plasmas (table 1.2). When viewed in large volumes, this NTP is assumed to have an equal number of negative and positive charges. This state of an equal number of positive and negative charge carries is referred to as quasi-neutrality [42, 43].

	Thermal	Nonthermal
Temperature	$T_i \approx T_e \approx T_g$ 4000-20000K	$T_e \gg T_g\ T_e > T_e > T_e$ T_e~$1 - 10eV$ (10^4-10^5)
Thermal equilibrium	Yes	No

Table 1.2: Characteristics of thermal and nonthermal plasma

Generation of nonthermal plasma

The most widely used method for the formation of nonthermal plasma is by the application of an external electric field between two electrodes surrounded by a volume of gas. The plasma can be operated either at low pressures (1–10^3Pa) or at atmospheric pressure and above. The breakdown voltage (Vb) defines the minimum voltage required to breakdown a gas to form a plasma discharge. Vb is dependent on the gas pressure (p) and the distance between the electrodes (D). This relationship is described by Paschen's Law (Eq-1.23), where 'a' and 'b' are constants that are dependent on the gas type [44-46].

$$V_b = \frac{a(pD)}{\ln(pD)+b} \qquad (1.23)$$

An applied voltage causes free electrons generation, which exists to some extent in a gas volume to become accelerated. At the point where the breakdown voltage is reached, the current flow will increase sharply due to an intensive avalanche of electrons in the discharge gap between the electrodes. These high energy electrons will collide with gas molecules leading to the formation of new 'active' plasma species including excited molecules and atoms radicals, ions and new molecules. These collision processes are shown in Figure 1.4 [47, 48].

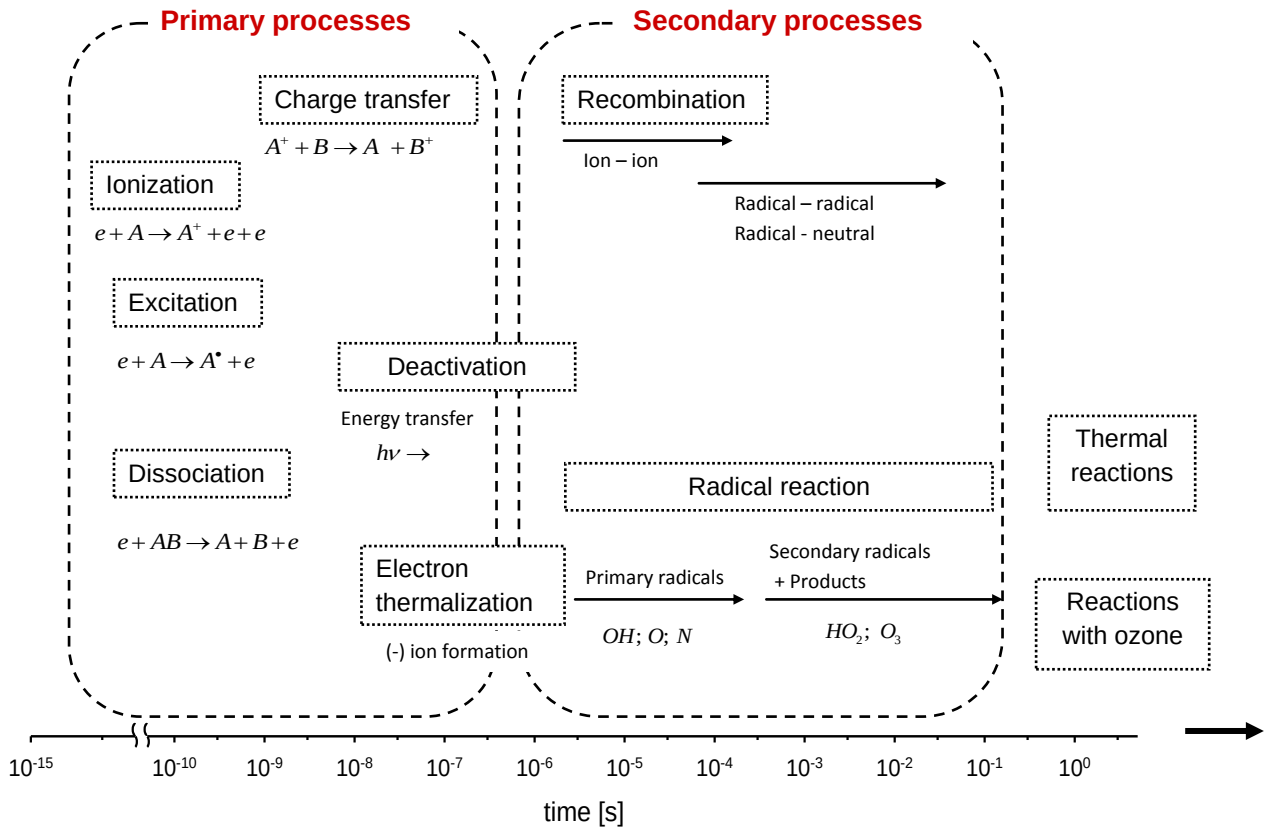

Figure 1.4: Schematic presentation of various processes and time scale [47,48].

In addition to the plasma species, photons are also generated in the plasma zone, the excited metastable state can spontaneously return to its stable ground state. When an electron is de-excited back to its lower energy orbital, the excess energy may be released in the form of a photon. This initiates a chain of reactive photon absorptions and emissions as molecules are excited and de-excited within the plasma. Consequently, the plasma can exhibit a visible glow if the energies of the emitted photons are in the visible region of the electromagnetic spectrum. In plasma processing, each of the plasma species may have different roles in the plasma chemistry. Electrons, being the first to receive energy from the electric field, distribute this energy through collisions, generating new reactive species.

In general, NTP reactors may be classified as the sub-atmospheric discharge reactors that demand a reduced pressure (radio frequency, microwave discharge, etc) and that are capable of operating at atmospheric pressure (Corona, dielectric barrier discharge, glow

discharge etc) . Several different types of nonthermal plasma can be formed depending on the type of applied electric field used to drive the plasma formation. The advantage of DBD over the other discharges lies in having the option to work at atmospheric pressure and comparatively straight forward scale-upto large dimensions. Dielectric barrier discharge (DBD) configuration is characterized by at least one insulating dielectric layers, which is placed between the electrodes. Its use in environmental applications can be tracked back to middle 19^{th} century, when Siemens (1857) used it to generate ozone. The classical DBD configuration is illustrated in Fig.1.5.

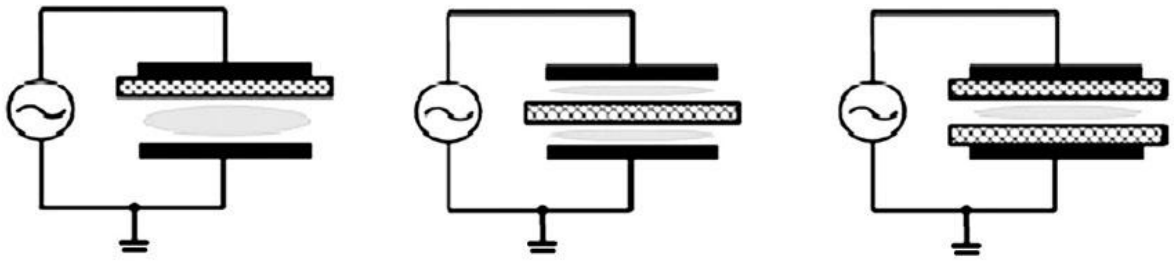

Figure 1.5: Schematic diagram of DBD discharge.

However, for environmental applications like decontamination of air and water pollutants DBD is widely tested. DBD configuration has been reported as a promising technique for the removal of air pollutants. An important property of DBD over other plasmas is that it distributes microdischarges evenly over the entire barrier. Due to the characteristic dielectric barrier, DC operation is not possible so a power source with pulsed DC or alternating current (AC) is used to generate the discharge. Typical configurations are found in either a planar or cylindrical geometry. In both geometries, a dielectric element is present in the current path between the electrodes.

1.6 Plasma-environmental applications

Low-temperature plasmas are at the core of numerous environmental applications. Non-thermal plasmas driven at atmospheric pressure (e.g. barrier discharges, coronas) are usually filamentary, i.e. the breakdown is dominated by the streamer mechanism which results in transient microdischarges. The application of plasmas in environmental application has grown at an exponential rate [43, 49-54]. Nonthermal plasma can be used in various fields, such as

- Indoor air cleaners (noxious organic compounds distraction),
- NOx and SOx removal from engine exhaust
- Conversion of the greenhouse gases CO_2 and CH_4 to synthesis gas or liquid fuels
- Waste water treatment (removal of hazardous organic pollutants)
- Soil sterilization
- Reduction of odors
- Fuel conversion and plasma-assisted combustion
- Pasteurization, disinfection of pathogenic microorganisms and sterilization
- Biological applications, etc.

Plasma AOPs are promising for removal of numerous waterborne contaminants. In this thesis, three groups of waterborne organic contaminants have been studied for degradation and mineralization in combination with homogeneous and heterogeneous catalysts. Specifically, the study compounds are different dyes like, methylene blue and crystal violet, intermediates like phenol, pesticides like endosulfan and pharmaceutical and personal care products (PPCPs) chemicals that include Sulfamethoxazole. Degradation and mineralization has been investigated under different conditions.

Plasma gas water interface have been found to be effective in degradation and mineralization of aqueous organic pollutants from water without adding any chemicals. Chemical and physical processes initiated by the high energy electrical discharges in water lead to the in-situ production of a variety of active species. In presence of feed gas the discharge is subsequently initiated inside the gas bubble.

1.7 Plasma Catalysis

One way to improve the efficiency of the plasma reactor is to integrate catalysts with plasma reactor. The amount of literature on the pollutant degradation by plasma catalysis in the liquid

phase electrical discharge is relatively limited. Catalysts can be homogeneous or heterogeneous. The effect of plasma catalysis, caused by the catalyst interaction of active species generated by plasma that may increase the life time of the activated species or may lead to more activated species. The combination of NTP with catalyst is an important method to improve selectivity and efficiency of the plasma process. The use of carbon materials, many metal ions and metal oxides (Fe_2O_3, Al_2O_3, MnO_2, CeO_2, TiO_2, Fe^{2+}, Fe^{3+} etc) catalyst have been studied [55-60]. Tong et al. have discovered that the possible mechanism of plasma catalytic integration is adsorption of organic molecule on the surface of catalyst and subsequent attack of ozone on adsorbed molecule [61].

1.8 Active species in plasma

Plasma generated at air-water interface is known to produce a variety of oxidants that are capable of mineralizing the target organic compounds. Among these oxidants, primary oxidants like ozone and H_2O_2 are important in that they can be converted to secondary oxidants like OH radicals.

1.8.1 H_2O_2 production

Hydrogen peroxide (H_2O_2) is a colorless liquid which is completely miscible with water. H_2O_2 has been known as benign and efficient oxidant for various purposes such as synthesis of organic compounds, pulp and paper industry, bleaching and also oxidation of organic pollutants in industrial wastewater via Fenton process. H_2O_2 is industrially synthesized through alkyl anthraquinone as an intermediate from hydrogen and oxygen.

H_2O_2 formation in plasma reactors was reported with a variety of feed gases (Ar, O_2, air and N_2) and interesting observation is that its formation takes place even in the absence of oxygen bubbling [62]. H_2O_2 formation in water for three model gases followed the order N_2 < Ar<air < O_2. Table 1.3 summarizes the selected reports that deal with quantitative information on H_2O_2 formation and the corresponding reactions responsible for its formation are summarized in table.1.3. It may be concluded that the feed gas may affect the formation of oxygen based reactive species such as OH, O_3, O and positive and negative charged ions like $\bullet O_2^+$, H_3O^+, $\bullet O_2^-$, $\bullet O_3^-$. H_2O_2 formed by the following reactions (Eq-1.24-1.29) [63-67].

$H_2O + e^- \longrightarrow H^\bullet + OH^\bullet + e^-$ (1.24)

$OH^\bullet + OH^\bullet \longrightarrow H_2O_2$ (1.25)

$2H_2O \longrightarrow H_2O_2 + H_2$ (1.26)

$H^\bullet + O_2 \longrightarrow HO_2^\bullet$ (1.27)

$HO_2^\bullet + H^\bullet \longrightarrow H_2O_2$ (1.28)

$HO_2^\bullet + HO_2^\bullet \longrightarrow H_2O_2 + O_2$ (1.29)

S.no	Reactor	Concentration	Operating parameters	Ref
1.	Water-Spray Gliding reactor	340ppm	25kV/250Hz/25 min	[68]
2.	pulsed streamer corona reactor	3.4 ppm	40kV/60Hz/12 min	[37]
3.	Pulsed Corona Discharge reactor	200 ppm	12kV/20Hz/30 min	[69]
4.	Gliding Arc Discharge reactor	130 ppm	10 kV/50Hz/60 min	[70]
5.	gliding arc discharge reactor	38 ppm	10kV/50Hz/25min	[71]
6.	Hybrid Electrical Discharge reactor	78 ppm	40kV/60Hz/40min	[29]
7.	Gliding-Arc Discharge reactor	81 ppm	25kV/170Hz/4min	[72]

Table 1.3: Summary of hydrogen peroxide generation in plasma reactor.

1.8.2 Ozone production

Ozone is yet another oxidant that is reported to have major applications during nonthermal plasma abatement of pollutants. The ozone formation reactions are summarized in Eq-(1.32). It was also proved that ozone generation in hybrid DBD was accompanied by a simultaneous production of hydrogen peroxide in the liquid phase. Ozone reacts with organic compounds present in wastewater directly via molecular and indirectly through radical type chain reactions. Both reactions may occur simultaneously. It is known that ozone reacts with unsaturated

functional groups present in organic molecules, leading to the conversion of the pollutants [73]. Simplified reaction mechanism of ozone in aqueous environment is given in Eq. (1.31-1.35).

$$O + O_2 \longrightarrow O_3 \quad (1.30)$$

$$3O_3 + H_2O \longrightarrow 2\,^{\bullet}OH + 4O_2 \quad (1.31)$$

$$H_2O_2 + 2O_3 \longrightarrow 2\,^{\bullet}OH + 3O_2 \quad (1.32)$$

$$O_3 + {}^{\bullet}HO_2 \longrightarrow {}^{\bullet}OH + O_2 + O_2^{-} \quad (1.33)$$

$$H_2O_2 + O_3 \longrightarrow {}^{\bullet}OH + O_2 + {}^{\bullet}HO_2 \quad (1.34)$$

$$O_3 + {}^{\bullet}OH \longrightarrow {}^{\bullet}HO_2 + O_2 \quad (1.35)$$

In addition, NTP is known to produce ultra-violet (UV) light due to excited gaseous molecules of the bubbling gas. Therefore, in aqueous solution, UV light induced dissociation of H_2O_2 molecules may lead to the formation of $^{\bullet}OH$ (Eq-1.36). Eq (1.37-1.40) summarizes the pathway to the possibilities in which ozone, H_2O_2 and UV light may induce the formation of various oxidants that can mineralize the pollutants.

$$H_2O_2 + h\nu \longrightarrow 2\,^{\bullet}OH \quad (1.36)$$

$$O_3 + H_2O + h\nu \longrightarrow H_2O_2 + O_2 \quad (1.37)$$

$$O_3 + h\nu \longrightarrow O_2 + O \quad (1.38)$$

$$2O_3 + H_2O_2 + h\nu \longrightarrow 2\,^{\bullet}OH + 3O_2 \quad (1.39)$$

$$^{\bullet}OH + H_2O_2 \longrightarrow H_2O + {}^{\bullet}HO_2 \quad (1.40)$$

1.9 Change of pH during plasma operation

Discharges in water may also significantly change the pH of the solution, mainly due to the formation of various inorganic and organic acids [63, 74]. The formation of inorganic acids is a

result of a series of reactions involving back ground gas like nitrogen, as shown in Eq (1.41-1.46). It has been observed that pH of the solution decreases rapidly due to the formation of water soluble ions. As a result, conductivity of the solution also increases significantly.

$$N_2 + e^- \longrightarrow 2N^{\bullet} + e^- \quad (1.41)$$

$$O_2 + e^- \longrightarrow 2O^{\bullet} + e^- \quad (1.42)$$

$$N^{\bullet} + O^{\bullet} \longrightarrow NO \quad (1.43)$$

$$NO + O \longrightarrow NO_2 \quad (1.44)$$

$$NO_2 + OH^{\bullet} \longrightarrow HNO_3 \quad (1.45)$$

$$NO_2 + H_2O \longrightarrow HNO_2 + HNO_3 \quad (1.46)$$

1.10 Energy efficiency

In the application of NTP for water treatment, designing an energy efficient reactor is if practical importance and a variety of reactors with liquid phase or gas–liquid phase electrical discharges have been developed. Dyes, pesticides and phenolic compounds are the commonly studied organic compounds. Energy efficiency values in g/kWh are provided in Table 1.4 is a straight forward comparison.

	Type of discharge	Target	Conc/Solution volume	Feeding gas	Conversion % at time (min)	yield (g/kWh)	Ref
2	Corona	Methyleneblue	150 ppm/100 ml	Oxygen	93 at 30 min	5	[69]
3	Corona	Methyleneblue	10 ppm/ 100 ml	Air	91at 20 min	4.6	[75]
	Corona	Methyl orange	10 ppm/ 100 ml	Air	90 at 20 min	4.4	
	Corona + Fe/H_2O_2	Methyleneblue	10 ppm/ 100 ml	Air	96 at 20 min	9.2	
	Corona	Methyleneblue	10 ppm/ 100 ml	Oxygen	91 at 20 min	4.6	
4	Pulsed	Methyl orange	80 ppm/200 ml	Oxygen	63 at 15 min	5.60	[76]
	Pulsed/(ACF/TiO_2)	Methyl orange	80 ppm/200 ml	Oxygen	98 at 15 min	8.86	
5	Dielectric barrier	Methyleneblue	50 ppm/300 ml	Oxygen	95 at 30 min	57	[77]
6	Dielectric barrier	Acid red 88	25ppm/100ml	Air	96 at 5min	11.14	[78]
7	Pulsed/TiO_2	Phenol	100ppm/250ml	Air	100at120min	0.46	[79]
8	Gliding arc	bisphenol A	28ppm/300ml	Air	100 at 30min	0.016	[70]
9	Gliding arc	Phenol	10ppm/100ml	Air	91 at 38 min	12.5	[80]
10	Glow	Phenol	300 ppm/250ml	Air	70 at 30 min	1.06	[81]
	Glow/ Fenton's	Phenol	300 ppm/250ml	Air	95 at 30 min	1.45	
11	Corona	p-Nitrophenol	300 ppm/250 ml	Air	86 at 60 min	0.20	[82]
12	Streamer	DCP	100 ppm/700 ml	Oxygen	29 at 60 min	0.275	[83]
	Streamer/Fenton's	DCP	100 ppm/700 ml	Oxygen	75 at 60 min	0.712	
13	Glow	Amoxicillin	500ppm/300 ml	Air	95 at 30min	4.649	[84]
14	Pulsed	Methyl orange	60 ppm /400 ml	Oxygen	98 at 18 min	26.41	[53]
15	Dielectric barrier	Methyl red	50ppm/200ml	Oxygen	93 at 10min	52.5	[85]
16	Corona	Phenol	94 ppm/100ml	Air	90 at 10min	48	[86]
17	circulatory airtight	Methyl orange	60 ppm/300 ml	Air	92 at 20 min	11.68	[87]

Table 1.4: Summary of nonthermal plasma configurations used for aqueous organic pollutants degradation.

1.11 Effect of applied voltage

Various process parameters determine the efficiency of plasma reactor. In the following section these parameters are discussed. A series of parameters may influence the microdischarge properties. One of them is the applied voltage. It was found that the number of microdischarges is proportional to the voltage applied on the electrode [88]. When the external voltage increases, the density of high energy electrons within the gap increases due to high applied electric field. The increase in the number of electrons may result in higher probability of breaking the bonds of pollutant or formation of more active species and thus increases the degradation. Kogelschatz et al. also confirmed that high voltage operations tend to spread and increase the number of microdischarges [89].

Lee et al., observed that the decomposition rate of Rhodium (RhB) was shown to increase with the increasing voltage level. This result indicates that a higher impressed voltage causes the more intense plasma, leading more hydroxyl radicals formation and leads to a higher de-composition efficiency of RhB [90]. Zhang et al., explained that at higher voltage the availability of more energetic electrons and active species may lead to higher degradation of malachite green(MG) [91]. Yan et al. also discovered that phenol degradation increases with rising voltage. It was found that increasing voltage could increase the solution's electric field intensity, generating more active species, such as •O, •OH, O_3 and H_2 O_2, capable of oxidizing more phenol into carbon dioxide [80]. However, at high applied voltage, although the discharge energy was high so more conversion of pollutants may be observed (Table 1.5).

Compound	Supply voltage (kV)	Removal efficiency (%)	Ref.
Phenol	7	55	[92]
	8	65	
	9	76	
	10	86	
Phenol	12	5	[80]
	24	19	
	36	23	
Ethanethiol	40	19	[93]
Trimethyamine		38	
Ammonia		40	
Ethanethiol	52	31	
Trimethyamine		55	
Ammonia		78	
Ethanethiol	62	45	
Trimethyamine		82	
methylene blue	12	84	[77]
	15	95	
Acid Red 27	20.3	30	[94]
	23.7	38	
	26.6	50	
	29	57	
indigo carmine	15	27	[95]
	20	70	
	25	88	
	30	95	
Acid Orange 7	24	8.8	[96]
	26	22	
	28	48	
	30	56	

Table 1.5: Effects of supply voltage on removal efficiency of organic compounds

1.12 Effect of the discharge gap

Another parameter that influences the microdischarge properties is the discharge gap. Gibalov et al. carried out experiments on ozone formation and confirmed that the amount of transferred charge to the microdischarges per half cycle is proportional to the discharge gap [97]. The explanation supported the fact that with increasing the gap value, the initiating gas breakdown voltage increases, the microdischarge current decreases and, therefore, the number of electrons with energies capable of initiating reactions also decreases.

Chen et al. also reported the effects of two different electrode distances on phenol removal from aqueous solution. Thus, we can understand that with a shorter electrode distance, it is easier to produce the plasma, and more energy can be deposited into the solution, leading to some photochemical and plasma channel effects and subsequently higher removal rate of phenol [92].

Hao et al. who varied the electrode separation between 10 to 20 mm and after 15 min, the conversion of 4-chlorophenol (4-CP) decreased with increasing the inter-electrode separation. Approximately 78% conversion of 4-CP was obtained with 10 mm inter-electrode separation that decreased to only 45% with 20 mm. With a relatively larger inter-electrode separation, more energy is required for plasma channel formation, whereas optimum separation may also provide plasma-photochemical effects and subsequently a faster degradation of 4-CP.

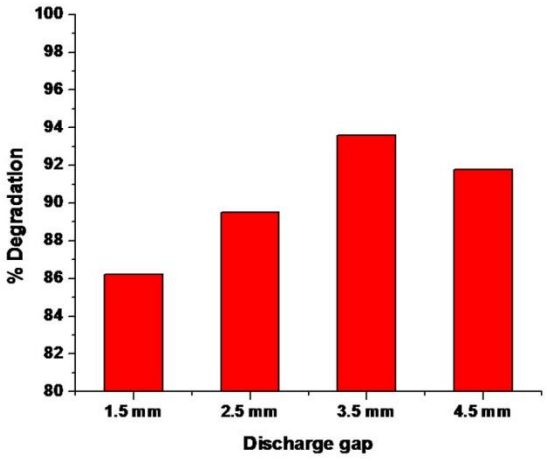

Figure 1.6: Effect of discharge gap on degradation of 100 ppm MB at16 kV with 200 ml/min gas flow rate.

Lang et al., conducted a series of experiments to investigate the dependence of the TNT degradation rates on the electrode gap. Electrode gap length was varied over the range of 6 -10 mm. It was observed that the time for complete conversion of TNT at a 6-mm electrode gap is the lowest, while time of the conversion for the 10-mm gap is the longest. With a smaller electrode gap it is easier to form the plasma channel, and more energy can be deposited into solution, which leads indirectly to photochemical and plasma channel effects and subsequently to a faster overall degradation and mineralization of TNT. With a larger electrode gap, more energy is required for plasma channel formation, and less energy is actually deposited into the chamber for TNT degradation [98].

1.13 Effect of the feed gas

Feed gas may also influence the degradation of the pollutants in plasma reactors. The gas flow rate may affect the formation of oxygen based reactive species such as OH•, O_3, O and positive and negative charged ions. On formation, these primary species react with each other or with pollutant and produce secondary radicals.

Chen et al., investigated the role of different oxidizing species in removing phenol from the aqueous solution; oxygen and nitrogen are bubbled into the phenol solution. Oxygen bubbling performs better than nitrogen bubbling; which is due to ozone formation due to oxygen bubbling. It is also observed that the high gas bubbling flow rate is beneficial to the removal of organic compounds. Higher gas flow supplies more O_2 molecules in the discharge region that may increase the quantity of ozone and other active species [92].

Zhang et al., studied the effect of gas flow rate and it was observed that it greatly affects the number of air bubbles presenting in the reactor, thereby affects the number of broken down bubbles and the quantities of active species formed. As the gas flow rate increases, the number of air bubbles presented in the reactor increases. The breakdown of air bubbles will thereby increase and more active species during the discharge process [91].

Du et al., studied different feed gases, including air, oxygen, nitrogen and argon during the degradation of a dye AO7. The degradation during the plasma treatment is highest for oxygen and least with nitrogen bubbling [62].

Magureanu et al., studied the degradation of methylene blue with different feed gases argon, air and oxygen and the results obtained with the three gases were compared. When using

argon the methylene blue conversion increased slower than in oxygen, so that after 30 min plasma treatment it was only 66%, while in oxygen the dye was almost completely degraded. In air the efficiency of the decomposition was very low, after 30 min treatment the methylene blue conversion was only 16%. [69]

Mok et al., studied the effect of feed gas on a model dye degradation and it was observed that ozone formation is deeply related to the content of oxygen in the working gas. When pure oxygen as the working gas showed best dye degradation. This result was due to high concentration of ozone when using oxygen [74].

1.14 Scope and objectives

The present study was aimed to present catalytic NTP-DBD reactor for the degradation of selected aqueous organic pollutants. The DBD configuration could lead to potential application for aqueous organic pollutants degradation. As an alternative to conventional techniques, nonthermal plasma approach has been investigated. A combination of catalyst and DBD was explored to increase the efficiency.

The thesis is divided into seven chapters. Chapter 1 consists of a thorough background and an overview presentation and literature review relevant to the project. It is followed by Chapter 2, which presents the details of the experimental setup and the materials and methods used throughout the project. The performance of designed reactor is evaluated for different categories of organic pollutants such as Dyes (chapter 3), pesticides (endosulfan in chapter 4), phenol (chapter 5) and pharmaceuticals (Sulfamethoxazole in chapter 6). Chapters 7 present the conclusions and recommendations for future work.

Chapter 2

Experimental Setup, Materials and Methods

This chapter deals with the experimental setup and operational aspects of the analytical instrumentation and catalyst characterisation techniques will be discussed.

2.1 Plasma reactor

Schematic representation of a dielectric barrier discharge (DBD) reactor is shown in Fig. 2.1. The system consists of an inner and an outer electrode which were separated by a dielectric barrier. The discharge was generated in quartz tube and the silver paste coated on the outer surface acts as the outer electrode. The inner electrode was a stainless steel metal rod (SS-316), which was connected to a high voltage generator. The alternating voltage generates the discharge, containing energetic electrons. These electrons collide with either the gas or target molecules to generate excited species, excited neutral molecules, free radicals, as well as positive and negative ions, which initiate the degradation and mineralization reactions. The dielectric barrier distributes the microdischarges throughout the discharge volume.

2.1.1 Operating conditions

The electrical discharge was produced in a coaxial NTP-DBD reactor by using a high-voltage AC source transformer (Jayanthi transformers). Quartz is used as the dielectric, due to its excellent dielectric properties. The reactor is a transparent quartz cylinder with an inner diameter of 19 mm and wall thickness of 1.6 mm. Silver paste painted on the outer surface of the quartz tube acted as the outer electrode, whereas a cylindrical stainless steel rod served as the inner electrode. The discharge length was 20 cm and the discharge gap was fixed at 3.5 mm. The applied voltage during the present study was varied between 14 to 18 kV. Discharge power (W) in the plasma reactor was measured by using a voltage–charge (V-Q) Lissajous method

(discharge power was calculated by multiplying the area of V-Q Lissajous figure with frequency) by using Tektronix TDS 2014B, 100MHz, 1.0GS/s oscilloscope.

$$P\ [W] = \text{area} \times \text{frequency} \qquad (2.1)$$

The gas bubbled through the reactor was controlled by a mass flow controller (AALBORG flow instruments-GFC 17). The gas outlet was connected to CO, CO_2 and NO_X analyzer (Siemens Ultramat 23) for qualitative analysis whereas; a pH meter (Systronics, l pH system 362, India) was used to measure of the pH variation during the plasma treatment. Degradation of pollutant was monitored as a function of the plasma treatment. The Energy efficiency of the removal was determined to understand the cost effectiveness. The energy yield of the degradation was calculated Eq-2.2.

$$\boldsymbol{Y(g/kWh) = \frac{C(g/l) \times V(L) \times \frac{1}{100} \times Conv(\%)}{P(kW) \times t\ (h)}} \qquad (2.2)$$

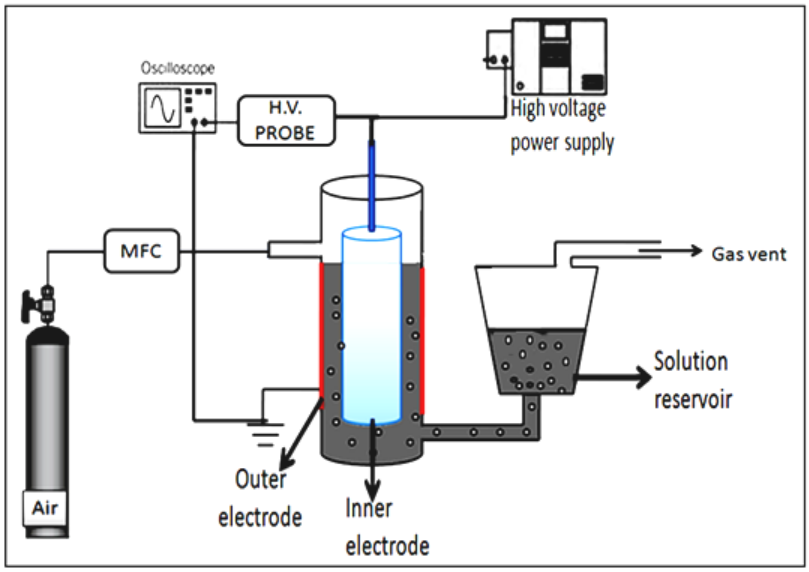

Figure. 2.1: Experimental set-up.

2.2 Experimental Procedure

In a typical experiment, the desired concentration (1-1000 mg/L) of the pollutant was weighed using a digital balance (Model No: BT 423S, Sartorius Instruments) and dissolved in the required amount of Millipore water and the absorption of the solution was determined by using

spectrophotometer (Shimadzu or T90 + UV/VIS Spectrometer, PG Instruments, Ltd, UK) or HPLC (HPLC-Waters Corporation 515 model). Then, the solution (100 ml) was fed into the reactor. The absorption of the samples was measured as a function of time ,till steady state was attained.

The Degradation and mineralization is defined by using the initial and final (after treatment) concentration of the target compound and were calculated as follows;

$$\text{Percentage degradation } (\%) = \frac{C_o - C_t}{C_o} \text{ x } 100 \qquad (2.3)$$

where C_o and C_t are the initial and the final concentrations of pollutant solution, respectively.

$$\text{Percentage TOC removal } (\%) = \frac{t_0 - t_t}{t_0} \text{ x } 100 \qquad (2.4)$$

t_0 and t_t are the initial and final TOC concentrations of pollutant, respectively.

2.3 Electrical characterization

2.3.1 Power supply and AC transformer

An AC transformer was supplied by Jayanthi transformer (India) and was used to regulate voltage and frequency. The power supply was connected to a standard 230 V AC, 50 Hz wall plug. The primary voltage was stepped up to secondary high voltage using transformer. The power supply was capable of delivering an output of 40 kV. High voltage wires were connected to the end of the metal rods by hose clamps. The power supply can be operated manually and both the transformer and the power source can be seen in Fig. 2.2.

(a)

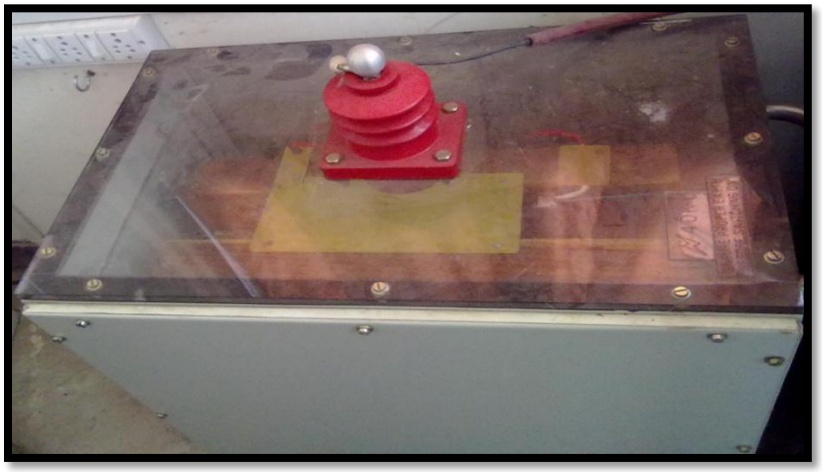

(b)

Figure 2.2: Shown in the photograph is the (a) Power supply and (b) High voltage transformer

2.3.2 High voltage probe and capacitor

During processing, electrical measurements of the reactor were measured through placement of a high voltage 1000:1 probe (Agilent technologies 34136A) on the high voltage electrode. The 1000X probe measured the voltage of the DBD reactor. NPN elektronik 1-250 decade capacitor substitution box contains 20 different capacitors in the range of 0.4 nF to 40nF and 0.1µF to

4µF was used. The total charge was measured with a non-inductive capacitor. HV probe/ capacitor is shown as shown Fig. 2.3 (a) & (b).

(a)

(b)

Figure. 2.3: (a) High voltage probe and (b) Capacitor.

2.3.3 Digital storage oscilloscope

A Tektronix 4-channel digital storage oscilloscope TDS-2014B with 100MHz and 1G/s oscilloscope was used to monitor current and voltage during processing. The voltage and charge (V-Q) waveforms were recorded by oscilloscope at channel 1 and 2, and stored in a USB flash drive.

Figure 2.4: Digital storage oscilloscope.

2.3.4 Electrical characterization and measurement of discharge power for DBD reactor

Electrical characteristics of the discharge voltage and charge waveforms are typical for a filamentary ac DBD with amplitudes of tens to hundreds mA and durations of nano second (ns) of both on the positive and on the negative alternance of the voltage waveform as shown in Fig. 2.5.

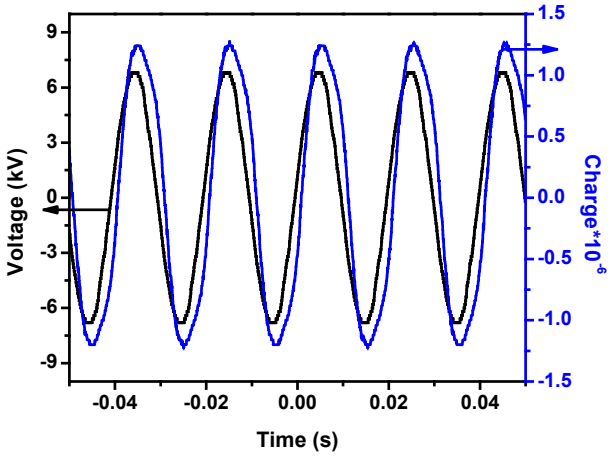

Figure 2.5: Voltage and charge waveform.

The charge and voltage waveforms were plotted to get Lissajous figure. Voltage of the DBD on the X-axis and the voltage of the capacitor on the Y-axis get Lissajous figure. From the Lissajous figure, one may obtain useful information regarding the DBD reactor parameters and discharge performance, capacitance of the DBD (C_t), discharge gap (C_g) and dielectric (C_d), an ideal DBD reactor was two capacitors (i.e. C_d and C_g) connected in series. Therefore, the total capacitance of a DBD reactor (C_t) was calculated by equation,

$$Ctot = \frac{Cgas.Cdiel}{Cgas + Cdiel}$$

When the amplitude of the applied voltage (V_{peak}) is low,

$$V_{peak} < V_b \frac{c_{diel} + c_{diel}}{c_{diel}}$$

The voltage across the discharge gap (V_{gas}) is not high enough to ignite a plasma, hence the voltage and the charge are in phase and the Lissajous figure (the charge plotted against voltage) is a straight line [85, 99]. When the voltage is higher than the breakdown voltage, a straight line changes to a parallelogram as shown in Fig. 2.6. The lines (a-b) and (c-d) are the capacitive transitions and their slope is equal to total capacitance of the reactor C_{tot}. The lines (b-c) and (d-a) are the discharge transitions and their slope is equal to C_{die}.

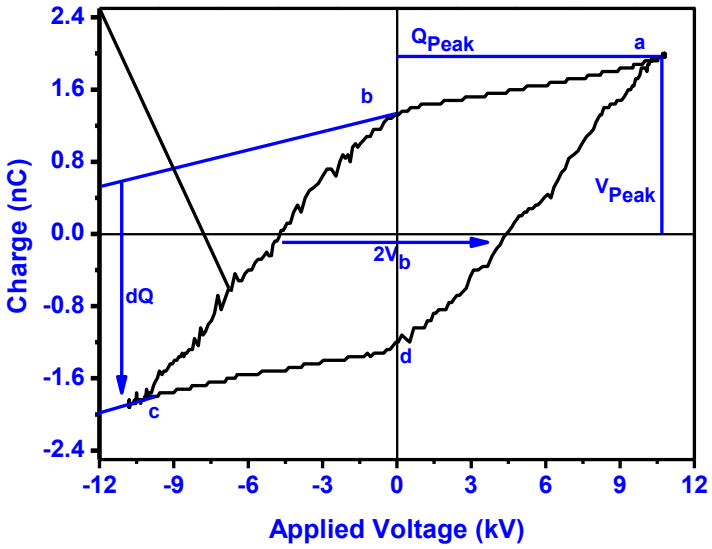

Figure 2.6: V–Q Lissajous plot at amplitude of 18 kV.

The Lissajous figure intercepts the voltage axis at values equal to $\pm V_b$; therefore V_b can be measured from the charge voltage plot. The dQ is the total charge transferred by the microdischarges per half cycle. Finally the area of the parallelogram is equal to the energy deposited in the cycle. The average power dissipated in the discharge can be calculated by multiplying this area with the frequency. Whereas, the energy yield was calculated using the relation

$$\boldsymbol{Y(g/kWh)} = \frac{\boldsymbol{C(g/l)} \times \boldsymbol{V(L)} \times \frac{\mathbf{1}}{\mathbf{100}} \times \boldsymbol{Conv}(\%)}{\boldsymbol{P(kW)} \times \boldsymbol{t}\ \boldsymbol{(h)}}$$

2.4 Analytical methods

2.4.1 UV-Vis Spectrophotometer

For determining the concentration of various compounds, UV-Vis spectrophotometer (Shimadzu) was used by using a quartz cell with a 1 mm path length. A PC based UV-Vis spectrophotometer was used for determination of concentration of model compounds as per the following procedure. To get the relationship between concentration and absorbance of the compound, a calibration curve was made. Calibration solutions were made from standard

solutions of known concentration. The absorbance is plotted against known concentration of the calibration samples.

The Beer-Lambert law states that there is a logarithmic dependence among transmittance of the light through a substance, the product of the absorption coefficient of the substance and the distance the light travels through the substance, as shown in Eq-2.5.

$$A = \varepsilon c l \qquad (2.5)$$

where A is the absorbance, ε is the absorbance coefficient, l the path length (cm) and c is the concentration (mol/L). Equation implies that the absorbance is linear with the concentration for dilute solutions.

2.4.2 Hydrogen peroxide quantification

The hydrogen peroxide (H_2O_2) formed during the reaction has been estimated spectrophotometrically. The method involves the quantification of the yellow color pertitanic acid formed when titanium sulfate reacts with hydrogen peroxide, as reported [100] . Titanium sulfate was prepared by dissolving 1 g of anhydrous titanium dioxide in 100 ml sulfuric acid(5M). The resulted solution was kept at 150 ^{0}C for 20 hours, cooled to room temperature, filtered and kept in reagent bottle.

$$Ti^{4+} + H_2O_2 + H_2O \longrightarrow H_2TiO_4 + 4H^+ \qquad (2.6)$$

2.4.3 Liquid chromatography

A high performance liquid chromatography (HPLC) was used to estimate the concentration of the pollutant in the solution. In liquid chromatography, a sample in a carrier flow i.e. eluent or mobile phase is introduced into a separation column containing a stationary phase. The sample components will partition between the stationary phase and the mobile phase due to component-specific physical interaction mechanisms. In this way component-specific separation is established. Detection of the eluting components is commonly performed by a UV absorbance detector but the detection by mass spectrometry, fluorescence, electrical conductivity or refractive index is also optional. In rp-HPLC the non-polar stationary phase is commonly an

alkyl-bonded silica packing e.g. a C8- or C18-alkane grafted on silica; the polar mobile phase is a mixture of water and an organic modifier.

The HPLC equipment make Waters Corporation 515 Series chromatograph, coupled with a Photo diode array detector (PDI). The chromatographic separations were run on a C18 column (SunFire C18 Column 250 mm × 4.6 mm, 5 μm) using a 50μL injection volume. The elution's of compounds were monitored by the PDI detector.

2.4.4 Infrared gas analyzer

To measure CO and CO_2 formed during the mineralization, an automated COx monitor was used (Siemens). The COx monitor used was ultramat 23 model Siemens instruments equipped with an IR detector. Infrared radiation (IR) is absorbed by gases such as CO, CO_2, SO_2 or NO at a characteristic wave number. The IR radiation passes through a measuring cell filled with the gas to be analyzed. An increase in the gas concentration causes a corresponding increase in IR absorption and thus a decrease in the radiation intensity received by the IR detector. To ensure selectivity for just one gas component two different principles are used. The dispersive principle uses radiation, which has been dispersed by a prism or grating before entering the measuring cell. Only two wavelength (or narrow wavelength ranges) of the entire spectrum are used, one that the component in question absorbs and one that not, as a reference. The ratio of absorption at these two wavelengths is a measure for the gas concentration. The non-dispersive (NDIR) principle uses a broad band of radiation from a lamp or glower without dispersion before entering the measuring cell. The working principle of the IR analyzer is shown in Fig. 2.7. When a component that does absorb IR radiation is present in the sample gas the radiation intensity reaching the detector will be reduced at the specific part of the spectrum. Two methods are in use for detecting the level of absorption a gas detector filled specifically with the gas of interest. Its variations caused by the varying concentration of the component in the sample gas passing through the measuring cell. Radiation absorption affects the gas pressure in the detector cell, these pressure variations are used to generate a detector signal as a measure of the concentration of the gas of interest. A solid state IR detector is used together with a narrow-band interference filter that allows the radiation range of the component of interest (e.g. CO_2) only to pass through, from the broadband spectrum of IR radiation. As the IR radiation

passes through the measuring cell a variation in CO_2 concentration will cause a proportional variation in the IR absorption and thus in the detector.

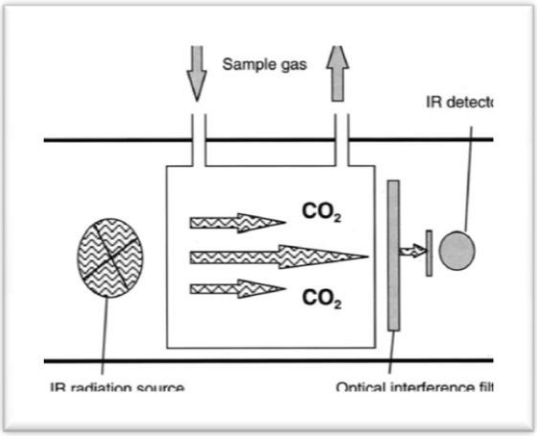

Figure 2.7: Working principle of the IR-analyzer.

2.4.5 Ozone measurement

Ozone formed in the plasma reactor was measured with a UV absorption ozone monitor (API-450 NEMA). A low pressure mercury vapor lamp provides a monochromatic source for 253.7 nm radiation. This UV wavelength is absorbed by ozone molecules. The principle of measurement is based on Beer-Lambers law. The detection of ozone molecules is based on absorption of UV light at 254 nm due to an internal electronic resonance of the O_3 molecule. The Model 450 NEMA uses a constructed mercury lamp so that the majority of light emitts at 254 nm wavelength. Light from the lamp shines through an absorption cell through which the sample gas being measured is passed. The ratio of the intensity of light passing through the gas to a reference measurement which does not pass through the gas forms the ratio I/Io. This ratio forms the basis for the calculation of the ozone concentration. The Beer-Lambert equation, shown below, calculates the concentration of ozone from the ratio of light intensities.

$$CO3 = -\frac{10^6}{\alpha \times l} \times \frac{T}{273°\mathrm{K}} \times \frac{14.695\,psi}{P} \times ln\frac{I}{\mathrm{I_o}}$$

Where:

I = Intensity of light passed through the sample

I_o = Intensity of light through sample free of ozone

α = absorption coefficient

l= path length

CO_3 = concentration of ozone in parts per million

T = sample temperature in degrees Kelvin

P = pressure in pounds per square inch (absolute)

The concentration of ozone also depends on factors other than the intensity ratio. Temperature and pressure influence the density of the sample. The density changes the number of ozone molecules in the absorption cell which impacts the amount of light removed from the light beam. These effects are addressed by directly measuring temperature and pressure and including their actual values in the calculation. The absorption coefficient is a number that reflects the inherent ability of ozone to absorb 254 nm light, the fact that ozone is a very efficient absorber of UV. Lastly, the absorption path length determines how many molecules are present in the column of gas in the absorption cell.

2.4.6 Total organic carbon (TOC)

TOC in the aqueous solution was measured by using TOC-V_{CPH} (Shimadzu, Japan) analyzer, which works on combustion method. Two types of carbons present in water: inorganic carbon and organic carbon. A different way to measure oxidation progress of an organic compound is the determination of the carbon content of the mixture. The total carbon content (TC) is defined as the sum of the total organic carbon TOC (hydrocarbons) and total inorganic carbon TIC (carbonate, bicarbonate, carbon dioxide). Due to oxidation, the carbon skeleton of an organic compound is gradually chopped into shorter carbon chain molecules containing oxygen-based functional groups viz. aliphatic aldehydes and carboxylic acids. The last member in the oxidation sequence is formic acid, which upon oxidation yields the unstable carbonic acid. The

TOC level of the oxidation product mixture decreases by the release of carbon dioxide (mineralization) and volatile or gaseous intermediates.

$$TOC = TC\text{-}IC \qquad (2.7)$$

Sample is introduced in to the TC combustion tube, which is filled with an oxidation catalyst that was heated to 680 ^{0}C. The sample is burned in the combustion tube and, as a result, the TC components in the sample are converted to carbon dioxide. Carrier gas, which flows at a rate of 150 ml/min to the combustion tube, carries the sample combustion products from the combustion tube to an electronic dehumidifier, where the gas is cooled and dehydrated. The gas then carries the combustion products through a halogen scrubber to remove chlorine and halogens. Finally, the carrier gas delivers the sample combustion products to the cell of a non-dispersive infrared (NDIR) gas analyzer, where carbon dioxide is detected. The TOC analyzer was calibrated with standard solutions of carbonate and potassium hydrogen phthalate. The NDIR outputs an analog detection signal that forms a peak; the peak area is measured by the TOC-Control V software. The peak area is proportional to the TC concentration of the sample.

2.4.7 Mass spectrometry

The progress of the reaction was followed by a gas chromatography mass spectrometer. Mass spectrometry is a highly sensitive method for identification, structure elucidation, quantification, and reaction mechanism analysis. It involves bombarding a target molecule with high-energy electron beam and the fragmentation pattern recorded as spectrum of positive/negative ions separated on the basis of mass/charge (m/z). The structure of a given compound can be determined from the fragments formed and the molecular ion peak. Analyses were performed on a Thermo scientific TRACE GC ULTRA capillary gas chromatograph coupled with a DSQ II mass spectrometer with electron energy of 70 eV. Injections into GC were made in splitless mode with an injector temperature of 250 ^{o}C. Helium was used as a carrier gas with a constant flow rate of 1 ml/min. A Thermo scientific capillary column (30 m×0.25 mm id 0.25-µm) was used. The mass spectrometer was operated in full scan mode in the mass range of 50-350 atomic mass units (m/z). Temperatures of the MS source and MS quadrupole were 250 ^{o}C.

2.5 Catalysts used

A common method for the preparation of supported metal oxide catalysts is the combustion technique. Nano sized CeO_2, 10 wt% Fe_2O_3/CeO_2 and 10 wt% ZrO_2/CeO_2 catalysts were prepared by combustion synthesis. For the preparation of CeO_2, in a typical synthesis method, 2.52 g of $Ce(NO_3)_3$ $6H_2O$ was added to 1.01 g of citric acid (CA) to maintain oxidant/fuel ratio = 1. Minimum amount of distilled water was added and the resulting solution was sonicated for 15 min and transferred into alumina crucible. Then the mixture was placed in a preheated furnace maintained at 573 K for 5 min to complete combustion. Then the catalyst was dried and calcined at 873 K for 60 min. In a similar manner, other catalysts are prepared.

2.6 Characterization techniques

2.6.1 Surface area analyses

surface area of the catalysts was obtained by N_2 adsorption–desorption carried out at 77 K using the multi point BET method, in a Quantachrome Nova 2200 physisorption analyzer. In a typical procedure about 1 g of each sample was weighed and degassed at 523 K and 10-6 torr for 6 h prior to nitrogen adsorption-desorption isotherm measurements. This instrument measures the adsorption and desorption isothermal curve (at 77 K) by the volume of adsorbed/desorbed N2, as a function of relative pressure. The BET surface area and pore volume of the metal oxide samples were calculated based on the nitrogen adsorption-desorption isotherm data using the accompanying software from Quantachrome.

The most well known and widely used BET equation may be written as follows;

$$\frac{P}{V(P_0 - P)} = \frac{1}{V_m C} + \frac{C - 1}{V_m C}\frac{P}{P_0} \qquad (2.8)$$

where P is the equilibrium experimental pressure, Po is the vapor pressure of the adsorbate gas at the experimental temperature, V (m^3/g) is the standardized experimental volume of the adsorbed gas per gram of adsorbent, Vm (m^3/g) is the volume of the adsorbate monolayer per gram of adsorbent and c is the a constant that relates to heat of adsorption.

A plot of $P/V(P_0\text{-}P)$ versus relative pressure of P/P_0 is a straight line with a slope of $(C–1)/(V_mC)$ and intercept of $1/(V_mC)$, respectively. Knowing slope and intercept permits

calculation of V_m. Subsequently the specific surface area (SA) of the sample can be determined by the following equation.

$$Specific\ surface\ area\left(\frac{m^2}{g}\right) = \frac{V_m\ X\ l\ X\ A_m}{W X\ V_o} \quad (2.9)$$

Where,

L is the Avogadro's constant (6.023 X 1023 molecules mol^{-1})

Am is cross sectional area of adsorbate molecule (N_2) is 0.162 nm^2 at 77 K

W is the weight of the sample

V_0 is 22414 mL mol^{-1}

2.6.2 X-ray Diffraction

X-ray diffraction (XRD) is an useful tool for studying a material's crystalline phases. As the X-ray bombards a sample at a range of incident angles, the X-rays are diffracted and detected. The detected diffraction pattern is indicative of the crystalline structure of a material. The diffraction relationship is given by Bragg's Law:

$$n\lambda = 2d\ sin\theta \quad (2.10)$$

where n is the order, d is the lattice spacing within the crystal, and Θ is the angle of the incident X-ray. From the diffraction pattern one can determine lattice dimensions of a crystal. Determination of the structure of a material is possible since different crystalline phases of each material have a unique diffraction pattern. A polycrystalline multi phase material will display pattern characteristics of each phase present within a material and the pattern can be checked against a reference library. The average crystallite size was determined from the width of the diffraction peak by use of the Scherrer formula:

$$L = \frac{K\lambda}{\beta cos\theta} \quad (2.11)$$

where L is the crystallite size, K is the shape factor, is determined by the peak shape, β is the full width at half of the maximum height (FWHM), Θ is the Bragg angle in degrees, needs to be converted into radians. λ is the wavelength of the X–ray radiation (CuKα=1.5406 Å). X'Pert Pro, PAN analytical diffractometer was employed for structural studies of all materials generated for this work with CuKα radiation (λ=1. 54 A°) in the range with a step size of 0.033. The X-ray tube was operated at 40 kV and 30mA. Diffraction patterns were compared with reference JCPDS (Joint Committee on Powder Diffraction Standards) powder diffraction files.

2.6.3 Raman Spectroscopy

Raman spectroscopy is an analytical tool used to understand chemical structure and bonding within a material. The sample is illuminated with a laser of known wave length. The light interacts with the vibration and rotational modes within the material, causing inelastic (Raman) scattering of the incident beam. Frequency shifts result from excitation of vibrational and modes within a structure.

Raman spectroscopic analysis was performed using Bruker optics SENTERRA multi-laser dispersive [2.33 eV (532 nm) and 1.58 eV (785 nm] laser excitation wavelengths. Spectrometer equipped with a liquid-nitrogen-cooled Spectrum One CCD. A Nikon 55 mm camera lens was employed both to focus the beam on the sample to an 0.25 mm 2spot and to collect the Raman scattered light.

2.7 Model compounds

In this study, organic pollutants chosen were synthetic dyes, pesticides, intermediate compounds and pharmaceutical compounds which are the most prominent pollutants of water. Millipore water and analytical grade chemicals were used to prepare initial solutions. Some technical information about these model compounds is given in Table 2.1. Compounds were used as received.

	Compound/ abbreviation	Formula (MW)	Structure/Figure 2.8 (a-e)	Make
1	Methylene blue/MB	$C_{16}H_{18}ClN_3S$ (319.85)	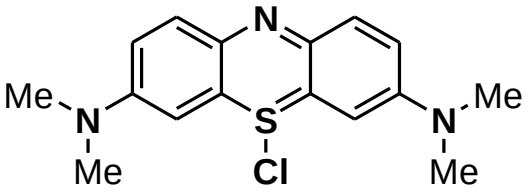	SD Fine-Chem Limited
			(a)	
2	Crystal violet/CV	$C_{25}H_{31}N_3$ (373.53)	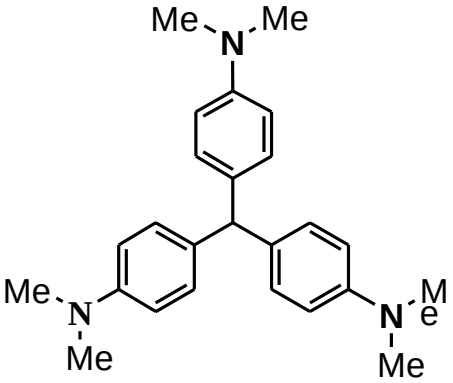	SD Fine-Chem Limited
			(b)	
3	Endosulfan/ES	$C_9H_6Cl_6O_3S$ (406.93)	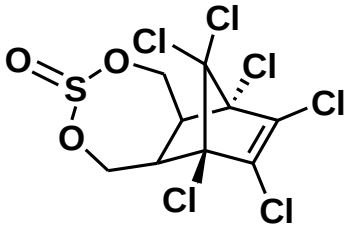	Aldrich Fine Chemicals
			(c)	
4	Phenol/Ph	C_6H_6O (94.11)	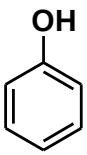	Merck Chemicals

			(d)		
5	Sulfamethoxazole/SM	$C_{10}H_{11}N_3O_3S$ (253.28)	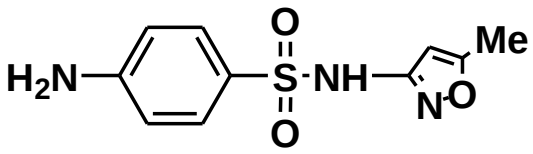		Aldrich Fine Chemicals
			(e)		

Table 2.1: Technical information about these model compounds.

Dyes:

Dyes are substances with considerable coloring capacity that are widely employed in the textile, pharmaceutical, food, cosmetics, plastics, photographic and paper industries. Thus, they constitute major components of wastewaters released from these industries. The dyes are generally designed to resist biodegradation, so they cause several ecological and environmental problems. The colored wastewaters reduce dissolved oxygen in rivers because they prevent sunlight from penetrating to algae at depth.

Methylene blue (MB)

Methylene blue an important cationic dye and used in many textile manufacturers and it releases aromatic amines and is a potential carcinogen. It belongs to the phenothiazinium class of compounds. The characteristic color of MB is caused by the strong absorption band in the 600-700 nm region. The structure of this dye is shown in Fig. 2.8(a).

Crystal violet (CV)

Crystal violet is also known under the name of gentian violet. Crystal violet is a cationic dye and widely used as a purple dye for textiles such as cotton and silk. Over the past many countries recognized the importance of wastewater treatment and it is estimated that 17 to 20% of industrial water pollution comes from textile dyeing and treatment plants. It provides a deep violet color for paints and printing ink. The characteristic color of CV is caused by the strong absorption band at 570 nm region.

Phenolic compounds:

Phenol is used as a general disinfectant, as a reagent in chemical analysis and for the manufacture of artificial resins, medical and industrial organic compounds and dyes. It is also used in the manufacture of fertilisers, explosives, paints and paint removers, drugs, pharmaceuticals, textiles and coke. It is produced in large volume, mostly as an intermediate in the production of other chemicals. Phenol is a highly toxic substance can be absorbed through the skin, gastrointestinal, respiratory and systemic symptoms of poisoning, a large number of short-term exposure to phenol can cause acute damage of the central nervous system, liver and kidney, cardiac muscle, blood and other multi-organ systems.

Pesticides [Endosulfan (ES)]:

A fundamental contributor to the green revolution is the development and usage of pesticides for controlling a wide variety of insectivorous and herbaceous pests that would otherwise affect the quantity of agro products. Hence, pesticides may pose threat to the ecosystems. Endosulfan (ES) metabolic compounds may cause adverse effects on humans and wildlife via interactions with the endocrine system. ES may be contaminated in air, surface water, groundwater, soil, and sediment. The World Health organization (WHO) puts it in Class II "moderately hazardous", (WHO, 2005), whereas, the US Environmental Protection Agency (USEPA) classifies it as a category 1b (highly hazardous). Because of growing concerns of the ES on the ecosystem, it has been banned in many countries, including India. Hence, removal of ES is a contemporary research topic and needs immediate attention.

PPCP:

The presence of trace pharmaceutical and personal care products (PPCPs) in the environment is a significant concern. Pharmaceutical products have been found in surface water, which is a common source of drinking water. After being administered for human or animal medical care, pharmaceutical products are excreted. They then reach the sewage treatment plant, which does not completely remove all the pharmaceuticals in the water. Aquatic and terrestrial pollution is also attributed to emission sources such as direct disposal of surplus in households or effluents of farms. Antibiotics, usually designed to control bacteria in humans and animals, have been found in surface water in concentrations that may rise to pg/L in surface and ng/L in ground water. Pharmaceuticals can enter the environment either in their original form or as metabolites

or degradation products. Sulfamethoxazole is an anti- bacterial sulfonamide. It prevents the formation of dihydrofolic acid, a compound that bacteria must be able to make in order to survive. Fig 2.8(e) shows the chemical structure of Sulfamethoxazole (SMX) or 4-amino-A-(5-methyl-3-isoxazolyl), which is a particular type of sulfonamide.

Chapter-3

Degradation and Mineralization of Dyes by dielectric barrier discharge non-thermal plasma reactor

3.1. Introduction

The wastewater**,** especially from paper and textile industries is highly colored due to the presence of dyes and hazardous compounds. For the treatment of water from these industries, various physico-chemical treatments, such as membrane filtration, ion exchange, activated carbon adsorptions etc. have been proposed [101]. Though on a large scale, many physico-chemical methods were tested for the treatment of wastewater from textile industry, in general, mineralization was not achieved. These methods may transfer the pollutant to another phase against the desired mineralization [102]. Bio-treatment of effluents containing organic dyes is not effective due to their resistance to aerobic degradation, whereas, in anaerobic degradation, carcinogenic aromatic amines may be formed as by-products [103]. In this context, advanced oxidation processes (AOPs) show specific advantages over conventional treatments like *in-situ* generation of strong oxidants and may eliminate the problems associated with bio-resistant organic compounds [104].

Oxidation of pollutant in AOPs proceeds via generation of powerful and non-selective hydroxyl radicals that may oxidize majority of the organic pollutants present in the water body. Hydroxyl radical has a high oxidation potential (E_0: 2.8 V) and only next to fluorine (E_0: 3.06 V). The main advantage with AOPs is the ability to mineralize the organic pollutants to CO_2 and H_2O. Various AOPs have been investigated for the degradation of organic pollutants in water. These techniques generate strong oxygen-based oxidizers that are expected to mineralize the pollutants [69, 105, 106]. However, in many cases, mineralization is not achieved that impose secondary problems with partially oxygenated products; hence there is a need to develop suitable AOPs to reduce toxicity.

Waste water treatment via electrical discharges recently has attracted much attention due to formation of highly reactive species such as OH, H, O, HO_2 radicals [9, 10]. A broad range of reactive species may be generated in NTP treatment, including excited species, excited neutral molecules, free radicals, as well as positive and negative ions. In addition, at the gas-liquid interface, highly reactive species like H_2O^+, $H^{\bullet}$, O_3, $OH^{\bullet}$, or $HO_2^{\bullet}$ that may promote the destruction of the target pollutants may be formed [40, 63, 94].

The present study was aimed at the mineralization of model dyes present in water. For this purpose, the NTP is generated in a dielectric barrier discharge (DBD) configuration. Physico-chemical characterization of the reactor was done and formation of H_2O_2 in DBD reactor that may promote the oxidization of targeted compound has been quantified. Influence of various parameters like the applied voltage, dye concentrations, flow rates of air, the effect of SO_4^{2-} and Fe^{2+} on the performance of the reactor has been studied.

3.2. EXPERIMENTAL

3.2.1. Experimental setup

Figure 3.1 presents the NTP-DBD schematic diagram employed in the present study**.** The reactor is a quartz tube with an inner diameter of 19 mm and wall thickness of 1.6 mm. Silver paste painted on the outer surface of the quartz tube acts as the outer electrode, whereas a cylindrical stainless steel rod placed at the center of the reactor serves as the inner electrode. The discharge length was 20 cm and the discharge gap was around 3.5 mm. Inner electrode was connected to AC high voltage and the electrical discharge was ignited by applying an AC high voltage in the range 14–18 kV (peak-to-peak), which was generated by a high voltage transformer (Jayanthi Transformer) at 50 Hz. Discharge takes place in air and air-water interface. The air flow rate was regulated by using a mass flow controller (MFC). The gas after passing through the solution was connected to a CO_x analyser.

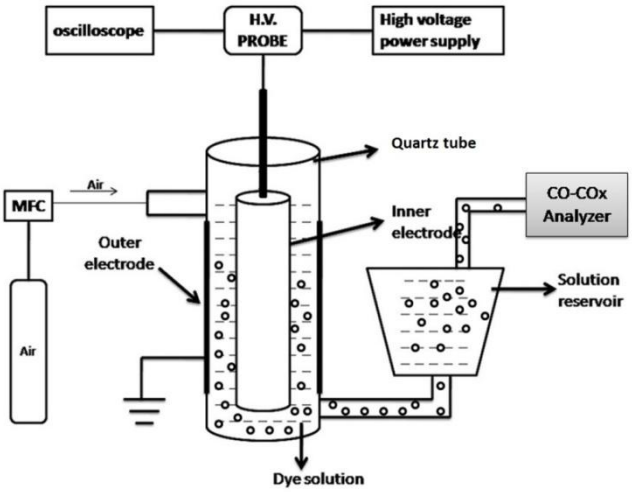

Figure. 3.1: Schematic representation of dielectric barrier discharge reactor.

The power used by the discharge was calculated by voltage (V) and charge (Q) Lissajous method [107]. The V and Q waveform are shown in Fig 3.2(a). Where the charge *Q* (i.e. time integrated current) was recorded by measuring the voltage across the capacitor of 100 nF connected series to the ground electrode. The voltage measured with a high voltage probe (Agilent 34136A HV, 1/1000). The signals of V and Q were recorded with a digital oscilloscope (Tektronix, TDS 2014B) and plotted to get a typical V-Q Lissajous diagram for 14 kV and 50 Hz as shown in Fig 3.2(b).

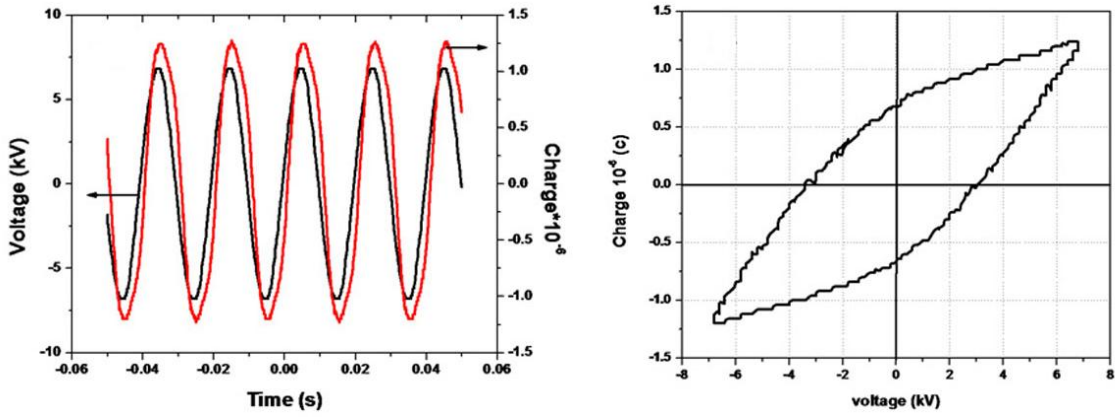

(a) (b)

Figure. 3.2: (a) Voltage and charge waveforms (**b)** V–*Q* Lissajous figure at 50 Hz and 14 kV.

The energy yield of the degradation was calculated from Eq-(3.1) [69],

$$\boldsymbol{Y(g/kWh) = \frac{C(g/l) \times V(L) \times \frac{1}{100} \times Degradation(\%)}{P(kW) \times t\,(h)}} \qquad (\mathbf{3.1})$$

Where C is initial dye concentration, V is the volume of the solution, Degradation (%) is % degradation at time t, P is power and t is time. It has been observed that increasing applied voltage increases the power and decreases the energy yield.

3.2.2. Material and methods

A 500 mg/L stock solution of dye (Methylene blue and Crystal violet) was prepared by dissolving required amount of analytical grade dye in Millipore water. The experimental solutions (50-100 mg/L) were obtained by diluting the stock solution in accurate proportions. The air flow rate (100 and 200 ml/min) was adjusted by using Aalborg calibrated mass flow controller (MFC). The gas outlet was connected to CO, CO_2 and NO_X analyzer (Siemens Ultramat 23) for qualitative analysis of CO, CO_2 whereas; a pH meter (Systronics, µ pH system 362, India) was used to measure of the pH variation during the plasma treatment. Degradation of dye was monitored for every five minute intervals of plasma treatment by using a double beam UV spectrophotometer (Shimadzu) at 668 nm for Methylene blue (MB) and at 588 nm for Crystal violet (CV). The degradation percentage was calculated by using the following Eq-(3.2).

$$\text{Percentage degradation (\%)} = \frac{C_o - C_t}{C_o} \text{ x } 100 \qquad (3.2)$$

where C_o and C_t are the initial and the final concentrations of dye solution, respectively.

The hydrogen peroxide (H_2O_2) formed during the reaction has been estimated spectrophotometrically. The method involves the quantification of the yellow color pertitanic acid formed when titanium sulfate reacts with hydrogen peroxide Eq-(3.3), as reported [100]. Titanium sulfate was prepared by dissolving 1 g of anhydrous titanium dioxide in 100 ml sulfuric acid. The resulted solution was kept at 150 ^{0}C for 20 hours, cooled to room temperature, filtered and kept in reagent bottle.

$$Ti^{4+} + H_2O_2 + H_2O \longrightarrow H_2TiO_4 + 4H^+ \qquad (3.3)$$

The total organic carbon (TOC) in the aqueous solution was measured by using a TOC-VCPH (Shimadzu, Japan) analyzer, which works on combustion method. TOC content was determined from the difference of total carbon (TC) content and inorganic carbon (IC) content.

When the dye solution exposed to the plasma, a noticeable pH decrease was observed. As throughout the present study the back ground gas was air, as reported earlier the pH decrease may be due to nitric and nitrous acids formation that originate from the nitrogen in air as given in Eq-(3.4-3.8) [108, 109]. In addition, the pH decrease may also be due to the formation of intermediate organic acids. Fig 3.3(a) confirms the decrease of pH with time due to the formation of acids.

$$*e^- + O_2 \longrightarrow 2*O + e^- \quad (3.4)$$

$$*e^- + N_2 \longrightarrow 2*N + e^- \quad (3.5)$$

$$*N + *O \longrightarrow NO \quad (3.6)$$

$$*O + NO \longrightarrow NO_2 \quad (3.7)$$

$$NO_2 + {}^{\bullet}OH \longrightarrow HNO_3 \quad (3.8)$$

Hence, the production of NO and NO_2 may consume some of the oxygen in the system, hence concentrations of O_3 may be limited. The overall degradation process of the dye in solution proceeds via the formation of intermediates to carbon dioxide and water [110].

3.3 Results

3.3.1 Kinetics of dye degradation

Kinetics of dye degradation was followed for 50, 75 and 100 ppm concentrations. As shown in Fig 3.3(b) $\ln(C/C_0)$ are proximately linear with the degradation time and the degradation obeys first order kinetics. The first-order integral rate Eq-(3.9)

$$\ln(C/C_0) = -k_1 t \quad (3.9)$$

where C, C_0, and k_1, are the concentration of dye for a given reaction time, initial concentration, and first-order rate constant (min^{-1}), respectively. The Table 3.1 shows the rate constant and R^2 values for different conditions. The coefficient indicated the linearity and confirms the first-order kinetics behaviour.

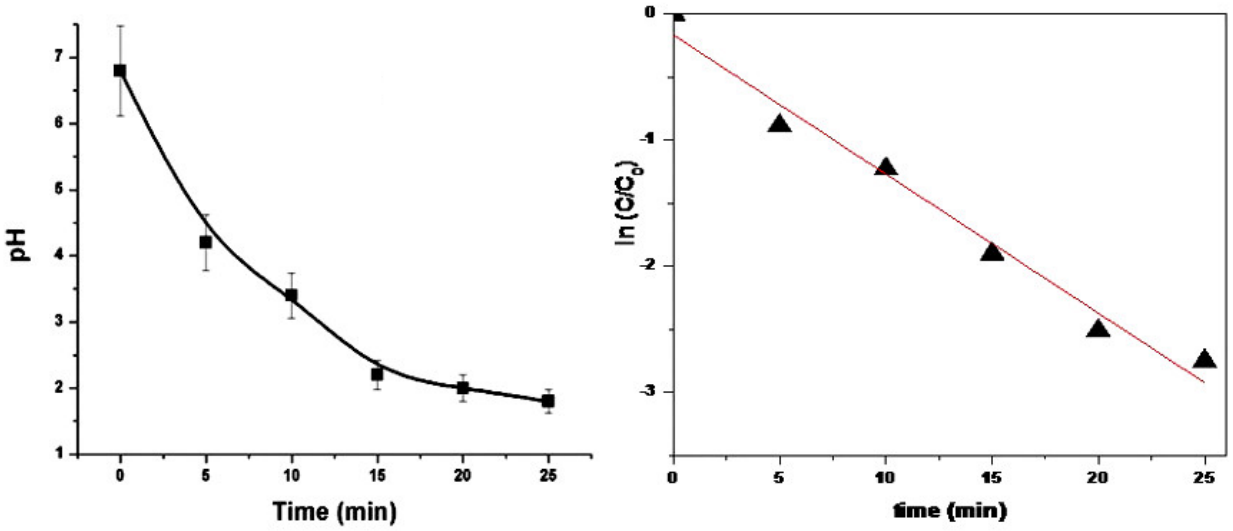

(a) **(b)**

Figure 3.3: (a) Variations of pH during plasma treatment **(b)** First-order kinetics of 50 mg/L MB degradation at 14 kV.

3.3.2 Formation of H_2O_2

As stated earlier hydrogen peroxide may be formed during in NTP-DBD treatment in air water interface by the electron impact dissociation of water molecules. Fig 3.4 shows the concentration of H_2O_2 as a function of time at different applied voltages for 200 ml/min flow rate of air. As seen in Fig 3.4, significant amount of H_2O_2 was generated in DBD and its concentration increases with increasing applied voltage. Also, H_2O_2 concentration increases with time for any applied voltage and nearly 60 ppm of H_2O_2 was observed at 18 kV after 25 min of plasma treatment.

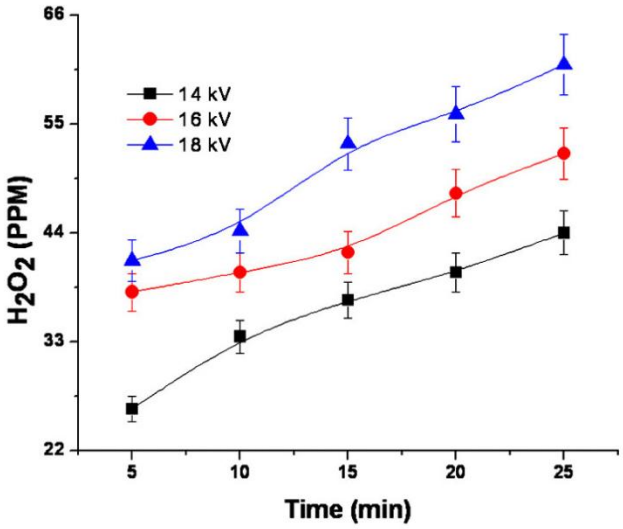

Figure. 3.4: Hydrogen peroxide concentration measurements during plasma treatment

Ozone is one of the major active species in NTP-DBD reactor. The main ozone generation reactions are given in Eq-(3.10). Ozone is a widely applied oxidizing agent for the treatment of wastewater. Ozone reacts almost indiscriminately with all organic compounds present in the reacting system [111]. Ozone reacts with wastewater compounds directly via molecular and indirectly through radical type chain reactions. Both reactions occur simultaneously. Simplified reaction mechanisms of ozone are given in Eq-(3.10-3.14).

$$O + O_2 \longrightarrow O_3 \qquad (3.10)$$

$$3O_3 + H_2O \longrightarrow 2\,{}^{\bullet}OH + 4\,O_2 \qquad (3.11)$$

$$H_2O_2 + 2O_3 \longrightarrow 2\,{}^{\bullet}OH + 3\,O_2 \qquad (3.12)$$

$$O_3 + {}^{\bullet}HO_2 \longrightarrow {}^{\bullet}OH + O_2 + O_2^{-} \qquad (3.13)$$

$$H_2O_2 + O_3 \longrightarrow {}^{\bullet}OH + O_2 + {}^{\bullet}HO_2 \qquad (3.14)$$

these active species are responsible for dye degradation.

3.3.3. Degradation of a model textile dye Methylene blue (MB)

3.3.3.1 Effect of initial concentration and applied voltage

Figure 3.5 presents the effect of applied voltage (14, 16 and 18 kV) on the degradation of 50 and 100 mg/L MB with 100 ml/min air. As seen in Fig 3.5, the degradation efficiency increases with increasing applied voltage. For 100 mg/L MB, the degradation was 90% at 14 kV that increased to 95 % at 18 kV. It can be seen that degradation decreases with increasing the initial concentration. At 14 kV and 100 ml/min flow rate of air, increasing initial dye concentration from 50 mg/L to 100 mg/L decreases the % degradation of dye decreases from 95 to 90 %. Table 3.1 presents the % of MB degradation after 25 min plasma treatment for different applied voltages and concentrations.

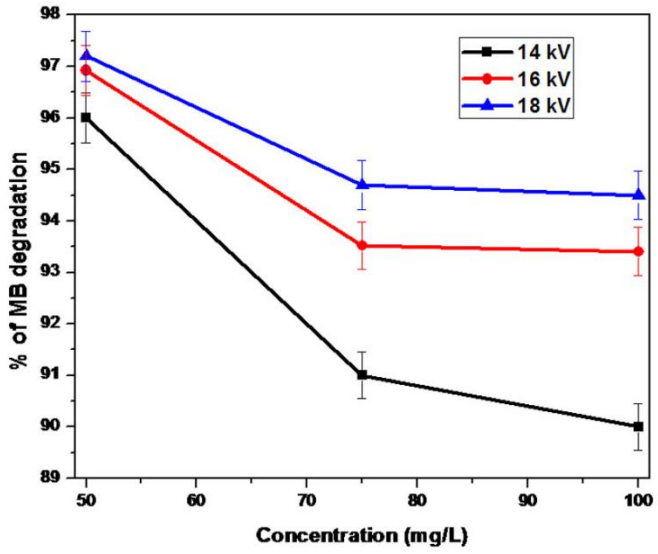

Figure. 3.5: Amount of MB degraded after 25 min with different initial concentrations and different voltages.

Flow rate	C_0 (ppm)	Voltage (kV)	% of degradation at 25 min	Initial TOC (ppm)	Final TOC (ppm)	TOC Decrease in %	Rate constant (min^{-1})	R^2
100 ml/min	50	14	96.81	30	27.0	10.0	0.119	0.96
		16	96.92		25.2	16.0	0.130	0.95
		18	97.20		23.5	21.6	0.133	0.94
	75	14	91.48	45	38.6	14.2	0.105	0.96
		16	93.52		38.2	15.1	0.117	0.96
		18	94.79		37.7	16.2	0.124	0.96
	100	14	90.77	60	49.0	18.3	0.101	0.95
		16	93.40		49.0	18.3	0.119	0.96
		18	94.57		48.0	20.0	0.120	0.95
200 ml/min	50	14	97.47	30	28.0	7.5	0.133	0.95
		16	97.77		25.5	15.0	0.141	0.93
		18	97.80		23.5	21.6	0.148	0.93
	75	14	91.78	45	37.5	16.6	0.140	0.95
		16	94.02		37.3	17.1	0.130	0.95
		18	95.10		37.0	18.0	0.117	0.94
	100	14	91.81	60	48.3	19.5	0.113	0.95
		16	93.67		49.0	18.3	0.122	0.94
		18	94.70		47.5	20.8	0.138	0.93

Table 3.1: Changing the parameters (% of degradation, initial TOC, final TOC,% of TOC decreased, $k_1(min^{-1})$ and R^2 value) During the experiment at 25 min.

3.3.3.2 Effect of gas flow rate

The effect of flow rate of air on degradation of 100 mg/L dye is shown in Fig 3.6. At a fixed voltage of 14 kV, changing the flow rate of air from 100 to 200 ml/min has not shown any significant change in degradation efficiency. This may be due to the fact that for the dye concentrations tested, the amount of oxidizing species formed in the discharge may be sufficient even at the 100 ml/min flow rate; hence increasing flow rate may not have noticeable change**.** In order to ensure this observation, ozone concentration was measured at the outlet, which showed 300 and 330 ppm, respectively at 100 and 200 ml/min flow rate, at 18 kV applied voltage respectively. The value corresponds to the O_3 formed in the presence of MB solution, but not used in the reaction with MB.

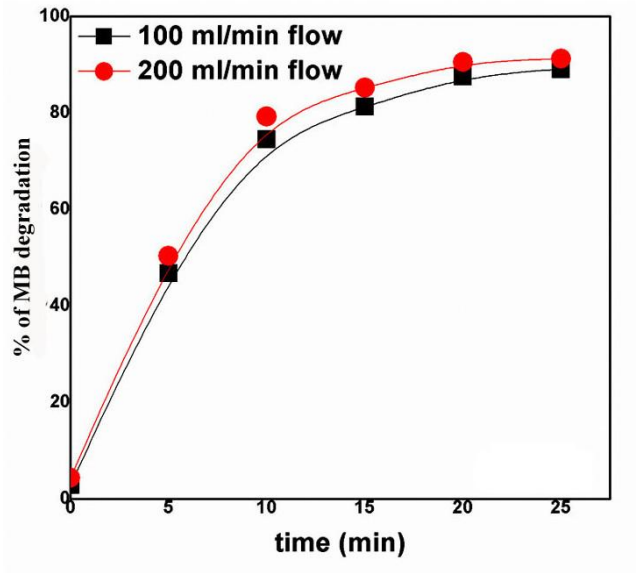

Figure. 3.6: Degradation % of 100 mg/L MB at 14 kV with 100 and 200 ml/min flow rates.

3.3.3.3 Effect of chemical additives

Effect of Na_2SO_4

Large amounts of sulphate are generally essential in the dye bath for successful dyeing, which results in high concentrations of sulphate discharge in the effluent. To examine the effect of Na_2SO_4 concentration on decolorization efficiency, 50 mg/L of SO_4^{2-} in 100 mg/L MB was prepared. Fig 3.7 shows the positive effect of Na_2SO_4 on dye degradation in DBD plasma. The excess SO_4^{2-} may react with the hydroxyl radicals to generate $SO_4^{-\bullet}$, which is more reactive than hydroxyl radicals Eq-(3.15).

$$SO_4^{2-} + {}^{\bullet}OH \longrightarrow SO_4^{-\bullet} + OH^- \quad (3.15)$$

The excess SO_4^{2-} decreases the dye concentration, since the oxidation potential of $SO_4^{-\bullet}$ (E^0 = 2.6 V) is comparable to $^{\bullet}OH$ (E^0 = 2.8 V) [112]. The oxidation potential of $^{\bullet}OH$ is > $SO_4^{-\bullet}$, they participate in different reactions. It is known that $SO_4^{-\bullet}$ and $^{\bullet}OH$ react with organic compounds mainly by three mechanisms like hydrogen abstraction, hydrogen addition, and electron transfer [26]. In general, $SO_4^{\bullet-}$ is more likely to participate in electron transfer reactions, whereas $^{\bullet}OH$

may participate in hydrogen abstraction or addition reactions [113], and hence during the present study $^{\bullet}OH$ may be less selective than $SO_4^{\bullet-}$.

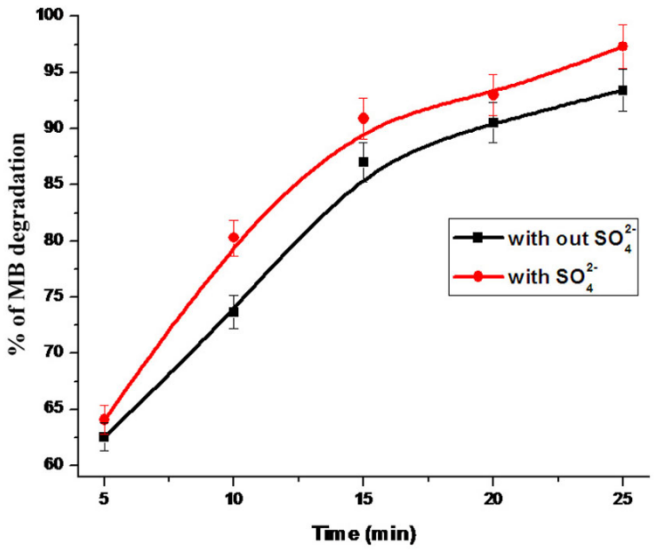

Figure. 3.7: Effect of the addition of SO_4^{2-} on degradation of 100 mg/L MB at16 kV with 100 ml/min gas flow rate.

Effect of Fe^{2+}

As the present study confirmed the formation of H_2O_2, Fe^{2+} (ferrous sulphate) was added to study its effect on degradation, via the Fenton reaction (Eq-3.16), which involves the following reactions Eq-(3.17-3.20) [17, 20, 114].

$$Fe^{2+} + H_2O_2 \longrightarrow Fe^{3+} + {}^{\bullet}OH + OH^- \quad (3.16)$$

$$Fe^{2+} + {}^{\bullet}OH \longrightarrow OH^- + Fe^{3+} \quad (3.17)$$

$$Fe^{3+} + H_2O_2 \longrightarrow Fe^{2+} + {}^{\bullet}HO_2 + H^+ \quad (3.18)$$

$${}^{\bullet}HO_2 + H_2O_2 \longrightarrow O_2 + H_2O + {}^{\bullet}OH \quad (3.19)$$

$$Fe^{3+} + e^- \longrightarrow Fe^{2+} \quad (3.20)$$

Figure 3.8 shows the change in % degradation for 100 mg/L MB with the addition of 60 mg/L of Fe^{2+}. From this figure it may be concluded that Fe^{2+} improves the % degradation. As shown in Eq-(3.11 and 3.13), on addition of Fe^{2+}, H_2O_2 may be lead to the formation of $OH^{\bullet}$ and $HO_2^{\bullet}$via Fenton's reaction. As the oxidation potential of $^{\bullet}HO_2$ is higher than that of H_2O_2, addition of Fe^{2+} may have improved the degradation.

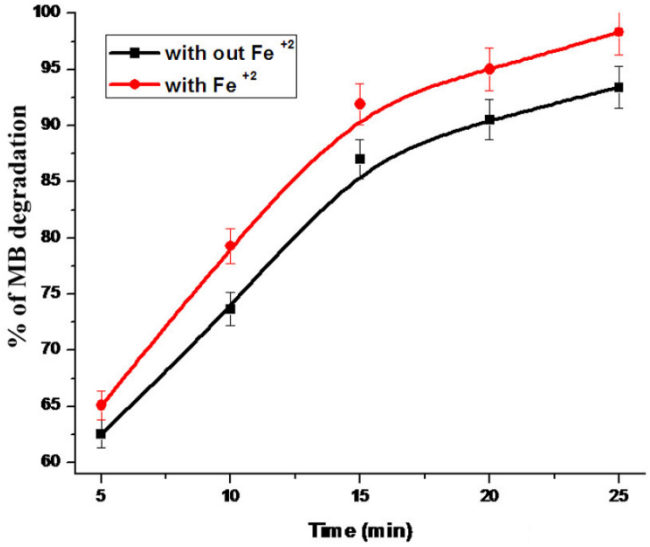

Figure. 3.8: Effect of addition of Fe^{2+}on degradation of 100mg/L MB at16 kV with 100 ml/min gas flow rate.

3.3.3.4 Mineralization of dye

The degradation of the dyes was followed by TOC (total organic carbon), which indicates the degree of mineralization of the target compound. The plasma treatment decreased the TOC with time and Table 3.1 presents the data on the decrease of TOC under different flow rates and voltages. The decreasing TOC with increasing treatment time indicated that the degraded organic carbon may be converted into CO and CO_2 [92]. The CO, CO_2 released during the reaction confirms that some amount of degraded dye was mineralized. However, during the present study, CO_X analyzer was utilized only for qualitative analysis. Mineralization depends on several conditions like concentration of the dye and flow rate. As seen from the Table 3.1, 50 mg/L of MB and 100 ml/min gas flow rate showed lowest mineralization (10 %) and highest mineralization (21 %) was observed for 100 mg/L of MB and 200 ml/min flow rate at 25 min.

3.3.3.5 Energy efficiency of the MB degradation

The dye degradation efficiency may be better illustrated by the amount of MB decomposed per unit of energy (yield). The energy yield is shown in Fig 3.9 as a function of % of MB degradation for 100 mg/L MB initial concentration at 14 kV applied voltage. It may be clear that at any voltage and concentration, The energy yield decreases with increasing voltage (increasing in power) and increases with concentration and flow rate (decreasing power). The best performance obtained in this study was 76 g/kWh for 100 mg/L MB at 14 kV and 200 ml/min flow rate. Table 3.2 presents the yield (g/kWh) after 10 min degradation of MB for different concentration and air flow rate.

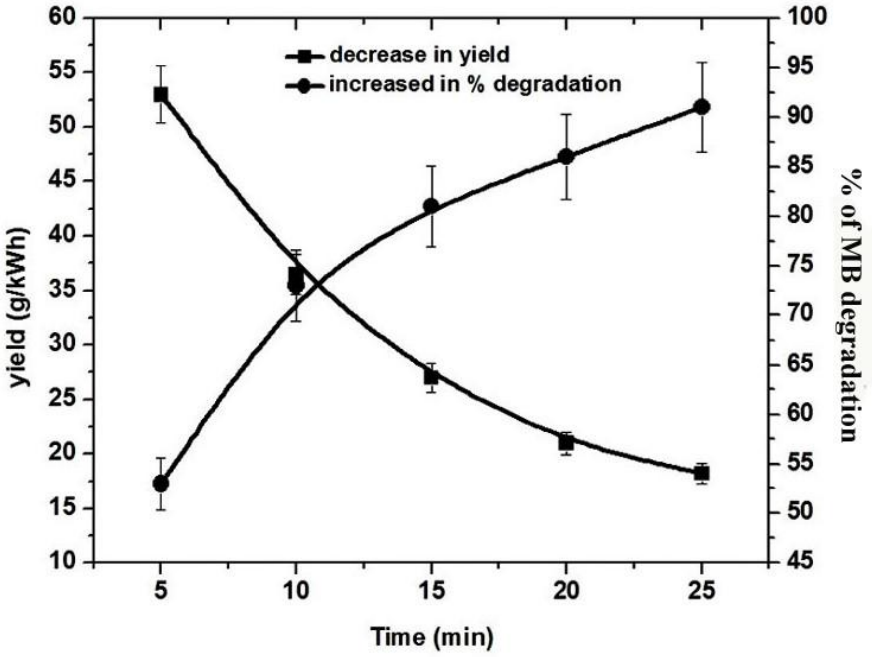

Figure. 3.9: Yield as a function of % of MB degradation for 100 mg/L MB concentration at 14 kV applied voltage.

Flow rate	C_0 (ppm)	Voltage (kV)	Power (W)	Yield (g/kWh)	% of degradation at 10 min
100 ml/min	50	14	1.2	21.5	86
		16	1.7	15.8	90
		18	2.1	13.1	92
	75	14	1.2	28.5	76
		16	1.7	21.1	80
		18	2.1	17.3	81
	100	14	1.2	36.5	73
		16	1.7	25.7	74
		18	2.1	22.0	77
200 ml/min	50	14	0.68	44.0	88
		16	1.1	24.8	91
		18	1.82	15.5	94
	75	14	0.68	57.7	77
		16	1.1	35.7	81
		18	1.82	20.5	83
	100	14	0.68	76.0	76
		16	1.1	43.1	79
		18	1.82	27.7	84

Table 3.2: Amount of yield (g/kWh) during the experiment after 10 min

3.3.4. Degradation of a model textile dye Crystal Violet (CV)

3.3.4.1 The effect of initial concentration and applied voltage

In order to understand the influence of dye concentration and applied voltage during the degradation of the CV, concentration varied at 50 to 100 ppm in the applied voltage range 14 to 18 kV and the results are shown in Fig 3.10 and Table 3.3. It was observed that the % degradation increased with the applied voltage as shown in Table 3.3 and Fig 3.10. At higher voltage more reactive species may form that increases the rate of degradation. As seen in Fig 3.10, removal of low concentration is beneficial and the performance of the technique decreases with increasing concentration of the dye.

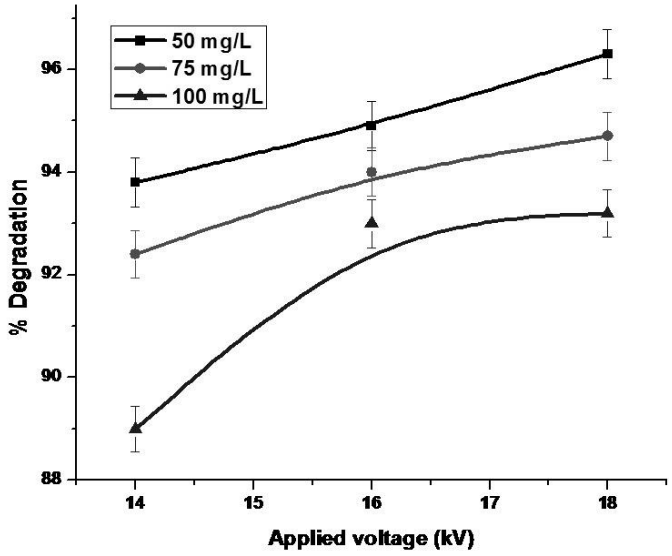

Figure. 3.10: Effect of variation in initial concentration and applied voltages on CV degradation after 25 min of plasma treatment for 100 ml/min flow rate.

The major degradation intermediates are identified by using gas chromatography with mass spectrometer (HR-MS) and plausible degradation mechanism is given in Fig 3.11.

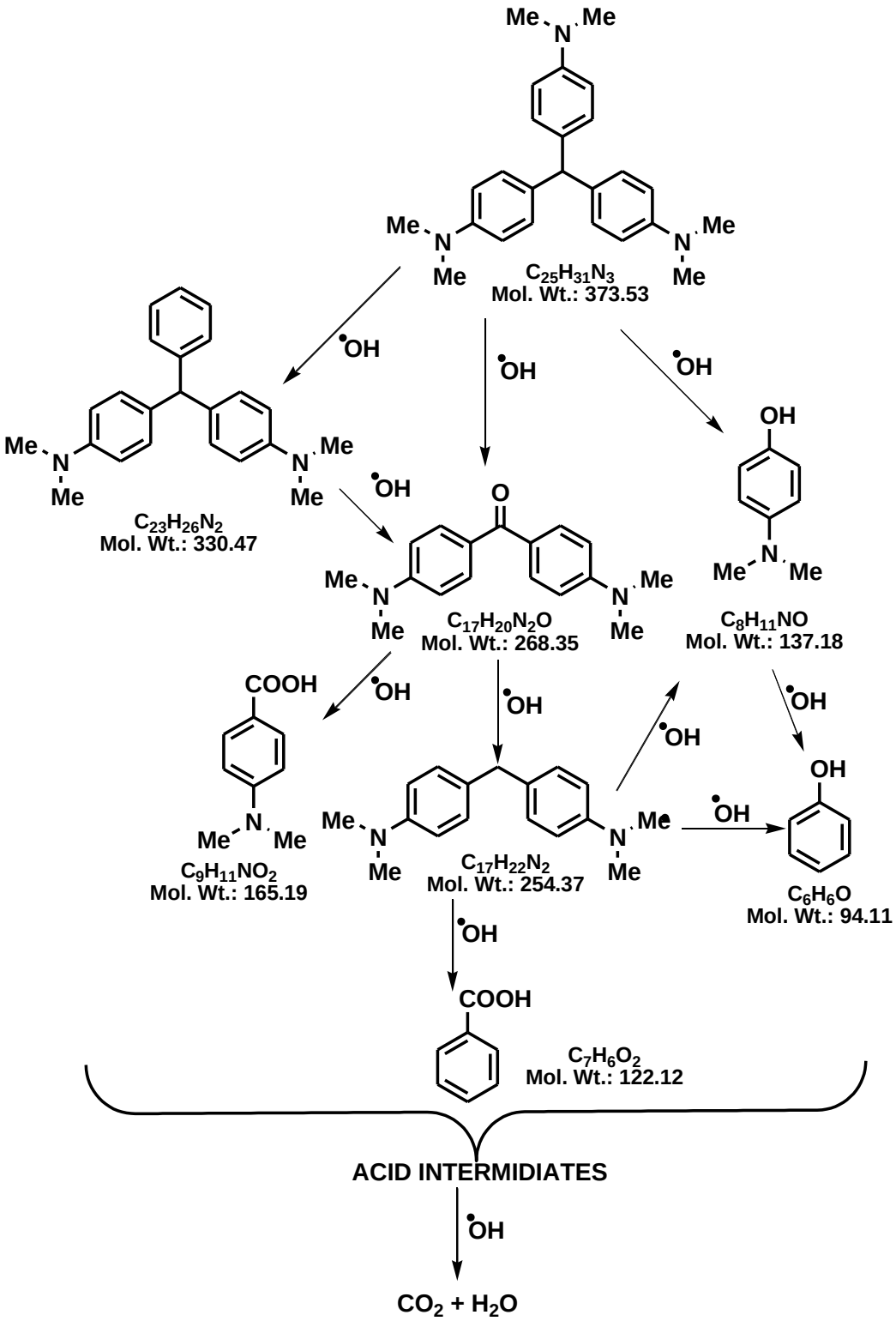

Figure. 3.11: Plausible mechanism of Crystal violet degradation and its intermediates.

3.3.4.2 Effect of chemical additives

As explained earlier, electric discharges produce various reactive species. One of the ways of improving the performance is by adding suitable additives that may improve the efficiency. The chemical additives for enhancement of the degradation efficiency of the dye wastewater are one of the advocated methods. Since the H_2O_2 formation was confirmed, the addition of Fe^{+2} may be a logical approach from the view point of Fenton type reactions. Hence, the effect of Fe^{2+} has been investigated on the degradation of CV.

Effect of hydrogen peroxide

In order to understand whether 60 ppm of H_2O_2 formed in the DBD reactor is sufficient or not, the reaction was followed with the addition of hydrogen peroxide. The reactivity of hydroxyl radicals is extremely high; In contrast to other active species this is considered relatively high reaction rates. The prominent increase of degradation most probably appears due to the reactions of dyes with hydroxyl radicals formed UV induced homolytic fission of the O - O bond (Eq-3.21) in H_2O_2 which attack the organic pollutants to initiate oxidation. H_2O_2 may increase the concentration of active $OH^{\bullet}$ and thus accelerate the degradation rate.

$$H_2O_2 + h\nu \rightarrow 2OH^{\bullet} \qquad (3.21)$$

Effect of Fe^{2+}

The presence of iron significantly enhanced the rate of CV degradation. The addition of iron increases the formation of $OH^{\bullet}$ radicals by the decomposing of H_2O_2 in Fenton-type reactions, and provides an additional source of hydroxyl radicals. Fe^{2+} [0.5 g/lit] was added to the reaction solution and the formation of active species are expected as per the Eq-(3.22).

$$Fe^{2+} + H_2O_2 \rightarrow OH^{\bullet} + OH^{-} + Fe^{3+} \qquad (3.22)$$

It was found that addition of Fe^{2+} in smaller doses was more successful in degradation of CV by utilizing hydroxyl radical are shown in Fig 3.12.

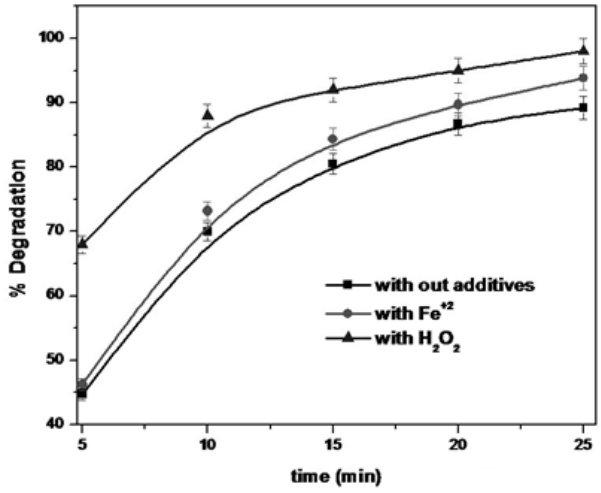

Figure. 3.12: Effect of chemical additives on enhancement of the dye degradation at 14 kV applied voltage, 100 ml/min flow rate and 100 ppm CV concentration.

Flow rate	C_0 (ppm)	Voltage (kV)	Initial TOC (ppm)	Final TOC (ppm)	TOC Decrease in %	% of degradation at 25 min	Rate constant (min^{-1})	R^2
100 ml/min	50	14	36.85	33.12	10.12	93.8	0.99	0.95
		16		32.17	12.70	94.9	0.111	0.93
		18		30.76	16.52	96.3	0.116	0.96
	75	14	55.27	47.23	14.54	92.4	0.94	0.99
		16		45.4	17.85	94	0.105	0.99
		18		43.87	20.62	94.7	0.111	0.98
	100	14	73.7	62.13	15.69	89	0.91	0.97
		16		59.7	18.99	93	0.97	0.97
		18		57.6	21.84	93.2	0.101	0.94
200 ml/min	50	14	36.85	31.92	13.37	95.1	0.114	0.96
		16		30.02	18.53	96	0.123	0.95
		18		29.23	20.67	97	0.129	0.95
	75	14	55.27	45.93	16.89	93	0.106	0.98
		16		44.04	20.31	93.9	0.117	0.95
		18		42.36	23.35	94.6	0.121	0.94
	100	14	73.7	60.87	17.40	90.6	0.99	0.97
		16		58.47	20.66	93.3	0.109	0.98
		18		55.89	24.165	94.2	0.102	0.97

Table 3.3: Changing the parameters (% of degradation, initial TOC, final TOC, % of TOC decreased, k_1 (min^{-1}) and R^2 value) during the experiment at 25 min of plasma duration.

3.3.4.3 Mineralization of dye

As mentioned in the introduction, mineralization by avoiding the formation of the unwanted products is the best way to remove the organic compounds, the total organic carbon (TOC) is the amount of carbon bound in an organic compound and is often used as a non-specific indicator of water quality. A different way to measure mineralization of the target compound is to determine the carbon content. Due to oxidation, the carbon skeleton of an organic compound is gradually chopped into shorter carbon chain molecules. The TOC level of the oxidation product mixture decreases by release of oxides of carbon (mineralization) [39], and gaseous intermediates. The amount of CO and CO_2 released during the reaction are shown in Fig 3.13(a) and % of degradation and TOC with respect time shown in Fig 3.13(b). From Table 3.3 it can be seen that % TOC removal increases as a function of applied voltage, concentration and flow rate. The highest removal % was observed at 100 ppm, 18 kV and 200 ml flow rate at 25 min and shown in Table. 3.3 that increased to 48 % at 60 min.

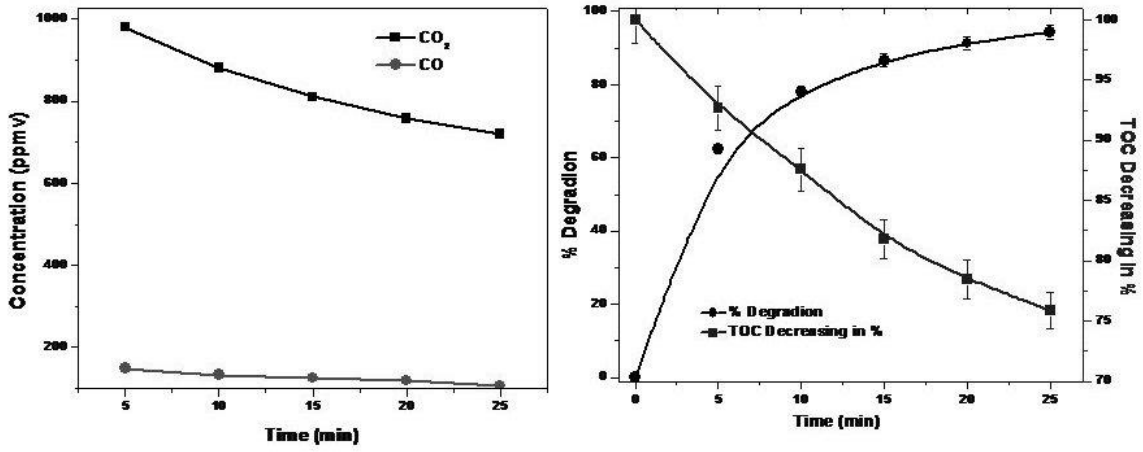

(a) (b)

Figure. 3.13: (a) CO, CO_2 released during degradation **(b)** % of degradation and TOC decrease % as a function time at 18 kV applied voltage, 200 ml/min flow rate and 100 ppm CV concentration

3.3.4.4 Energy efficiency

The dye degradation efficiency may be better illustrated by the amount of CV decomposed per unit of energy (yield). The energy yield depends on the type of discharge

reactor, initial concentration and nature of the compound. During the degradation of CV, ~ 80% degradation was observed within 10 min and Table 3.4 presents a detailed data of energy yield under various conditions. It was observed that as a function of time the energy yield decreases and % degradation increases as shown in Fig 3.14(a) and change in yield with voltage, initial dye concentration and gas flow rates are shown in Fig 3.14 (b), (c) and (d), respectively. It is clear with increasing applied voltage from 14 to 18 kV, the yield decreased from 42.2 to 24.5 g/kWh for 50 ppm, from 36.4 to 22.5 g/kWh for 75 ppm and from 34.9 to 21.04 g/kWh for 100 ppm at 100 ml/min flow rate. With increasing flow rate from 100 to 200 ml/min, yield increased from 42.2 to 86.5 g/kWh for 50 ppm initial concentration even at 14 kV applied voltage. The energy efficiencies of various conditions are given in Table 3.4.

Flow rate	C_0 (ppm)	Voltage In kV	Yield (g/kWh)	% of degradation at 10 min
100 ml/min	50	14	42.19	84.3
		16	30.5	86.6
		18	24.5	87.0
	75	14	36.4	72.8
		16	26.9	76.4
		18	22.6	79.3
	100	14	34.9	70.1
		16	26.5	75.2
		18	21.04	76.3
200 ml/min	50	14	86.3	86.3
		16	51.6	87.7
		18	29.4	89.3
	75	14	76.7	76.7
		16	47.9	81.4
		18	27.4	83.3
	100	14	71.17	71.2
		16	43.7	74.4
		18	25.75	78.1

Table 3.4: Energy yield (g/kW h) during the experiment after 10 min plasma treatment

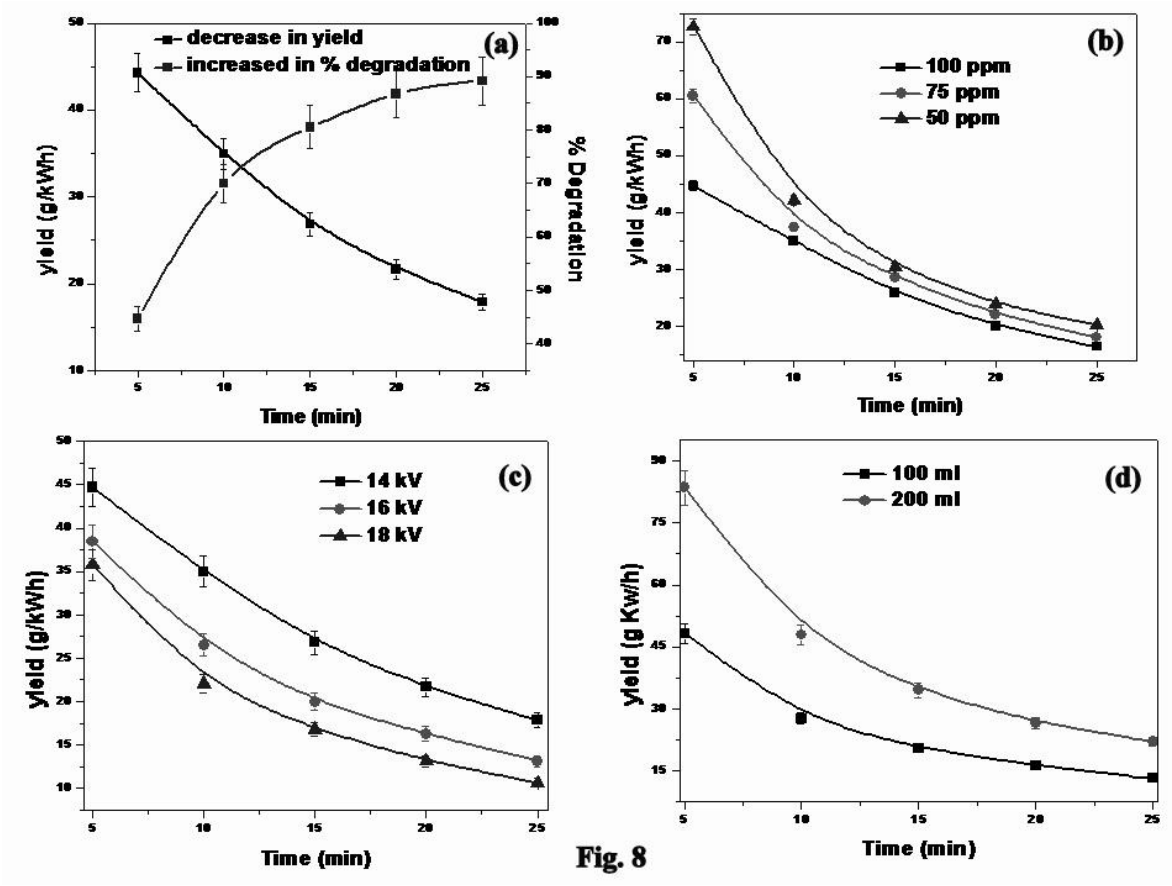

Fig. 8

Figure. 3.14: (a) Energy yield and the % of dye degradation As a function of time during plasma treatment for 100 ppm CV at 14 kV with 100 ml flow rate, **(b)** Energy yield as a function of time for various initial concentrations at 14 kV applied voltage and 100 ml flow rate **(c)** Energy yield as a function of time for various applied voltages for 75 ppm initial CV concentration and 100 ml/min flow rate. **(d)** Energy yield as a function of time for two flow rates at 16 kV applied voltage with 75 ppm initial CV concentration.

3.4. Discussion

Discharge in water is different to that in air due to different physical characteristics of water and air [63, 115]. Electrical discharge in air and air-water interface generates plasma that may cause a variety of chemical and physical effects such as generation of high electric field, intense UV radiation, over pressure shock waves and highly reactive electrons which are called

active species. These high energy electrons may react in air and aqueous solution to produce secondary reactive species as given in Eq-(3.4), (3.5), (3.23)-(3.25).

$$*e^- + H_2O \longrightarrow {}^\bullet OH + {}^\bullet H + e^- \quad (3.23)$$

$$^\bullet OH + {}^\bullet OH \longrightarrow H_2O_2 \quad (3.24)$$

$$*e^- + O_2 \longrightarrow O_2^+ + 2e^- \quad (3.25)$$

Ozone production is one of the major applications of NTP. The main ozone generation reaction is given in Eq-(3.26). Ozone is a widely applied strong oxidizing agent for the treatment of wastewater. Ozone reacts with organic compounds present in wastewater directly via molecular and indirectly through radical type chain reactions. Both reactions occur simultaneously [116]. It is known that ozone reacts with unsaturated functional groups present in organic molecules. Simplified reaction mechanism of ozone in aqueous environment is given in Eq-(3.27-3.30).

$$O + O_2 \longrightarrow O_3 \quad (3.26)$$

$$3O_3 + H_2O \longrightarrow 2\ {}^\bullet OH + 4\ O_2 \quad (3.27)$$

$$H_2O_2 + 2O_3 \longrightarrow 2\ {}^\bullet OH + 3\ O_2 \quad (3.28)$$

$$O_3 + {}^\bullet HO_2 \longrightarrow {}^\bullet OH + O_2 + O_2^- \quad (3.29)$$

$$H_2O_2 + O_3 \longrightarrow {}^\bullet OH + O_2 + {}^\bullet HO_2 \quad (3.30)$$

It was reported that NTP produces ultra-violet (UV) light due to excited nitrogen molecules present in air [92]. This UV light may dissociate hydrogen peroxide molecules present in aqueous solution to form hydroxyl radicals Eq-(3.31) [34,37,38]. Eq-(3.32-3.34) are the combination of ozone, H_2O_2 and UV light and are most effective and are capable of mineralizing the pollutants. Most of UV light can also be absorbed by water. It is worth mentioning that during the present study, H_2O_2 was formed in adequate amount (60 mg/L) and Equation 23 may be responsible for the use of H_2O_2 for the generation of even stronger oxidizing agent hydroxyl radical. However, excess H_2O_2 may also scavenge the hydroxyl radical, making the H_2O_2/UV process less effective [117, 118]. In addition, H_2O_2 may react with $^\bullet OH$ and generate $^\bullet HO_2$ as shown in Eq. (3.35).

$H_2O_2 + h\nu \longrightarrow 2\,{}^{\bullet}OH$ (3.31)

$O_3 + H_2O + h\nu \longrightarrow H_2O_2 + O_2$ (3.32)

$O_3 + h\nu \longrightarrow O_2 + O$ (3.33)

$2O_3 + H_2O_2 + h\nu \longrightarrow 2{}^{\bullet}OH + 3O_2$ (3.34)

${}^{\bullet}OH + H_2O_2 \longrightarrow H_2O + {}^{\bullet}HO_2$ (3.35)

3.5. Conclusions

An advanced oxidation process based on electrical discharges has been demonstrated for treatment of wastewater containing model dyes methylene blue and crystal Violet. Typical results indicated the DBD is an efficient technology for the removal of dyes. It was observed that the major reactive species involved in the degradation process are hydroxyl radical, hydrogen peroxide and ultraviolet. Formation of H_2O_2 was confirmed and it increases with treatment time. It was observed that addition of Fe^{+2} further promoted the degradation via Fenton reactions. The specific advantage of the present process is the mineralization of the dye and best energy yield upto 86.3 g/kWh for CV and 76.0 g/kWh for MB. It was observed that dye degradation followed first order kinetics.

Chapter 4
Catalytic Nonthermal Plasma Reactor for Mineralization of Endosulfan in Aqueous Medium

4.1. Introduction

A fundamental contributor to the green revolution is the development and usage of pesticides for controlling a wide variety of insectivorous and herbaceous pests that would otherwise affect the quantity of agro products [119-121]. Even though pesticides are expected only to reach the target organisms, they may also affect the non-target organisms such as humans and wildlife and may cause loss of biodiversity [119]. Endosulfan (ES) metabolic compounds may cause adverse effects on humans and wildlife via interactions with the endocrine system [122]. ES may be contaminated in air, surface water, groundwater, soil, and sediment [123]. The World Health organization (WHO) puts it in Class II "moderately hazardous", (WHO, 2005), whereas, the US Environmental Protection Agency classifies it as a category 1b (highly hazardous). Because of growing concerns of the ES on the ecosystem, it has been banned in many countries, including India [124]. Hence, removal of ES is a contemporary research topic and needs immediate attention [125].

Various physico-chemical techniques like adsorption [126], membranes [127, 128], biobed [129] and advanced oxidation processes (AOPs) like photocatalysis [130], UV/ozone [131], ultrasonication have been tested for the removal of ES. However, the scope of many of these processes is limited to transfer the contaminant from one phase to another; however a complete oxidation is desired. Stated earlier, application of NTP for the removal of ES may offer specific advantages due to the presence of multiple oxidants like $OH^{\bullet}$, $H^{\bullet}$, $O^{\bullet}$, $HO_2^{\bullet}$, $O_2^{\bullet}$, H_2O_2, O_3, UV radiation and shock waves [74, 132-134]. As NTP reactors produce ozone, various catalysts can be integrated with plasma for the effective utilization of ozone [135, 136].

The objective of the present study is test the feasibility of NTP dielectric barrier discharge (NTP-DBD) reactor during the mineralization of the ES in aqueous medium. At a later stage, NTP is combined with a catalyst, as some of the oxidants like ozone, etc may

transform to secondary oxidants like atomic oxygen that are capable of promoting the complete oxidation. Various parameters like applied voltage, concentration and the addition of a catalyst were studied.

4.2. Experimental Section

4.2.1 Materials and Methods

Endosulfan was obtained from Sigma-Aldrich, 15 mg of endosulfan dissolved in 30 ml of acetonitrile then make it up to 1 liter with water. It is a mixture of two biologically-active isomers, the alpha and beta isomers (α and β), in the proportions α/ β = 70/30. Nano sized CeO_2 was prepared by combustion synthesis. In a typical synthesis method, 2.52 g of $Ce(NO_3)_3.6H_2O$ was added to 1.01g of citric acid (CA) to maintain oxidant/fuel ratio = 1. Minimum amount of distilled water was added and the resulting solution was sonicated for 15 minutes and transferred into alumina crucible. Then the mixture was placed in a preheated furnace maintained at 573K for 5 min to complete combustion. Then the catalyst was dried and calcined at 873 K for 60 min. Crystal structure was confirmed with XRD patterns recorded on X'Pert Pro, PAN analytical diffractometer with CuKα radiation (λ=1. 54 A°). The X-ray tube was operated at 40 kV and 30mA. Nitrogen adsorption-desorption isotherms at 77 K were carried out using a Quantachrome Nova 2200. The samples were degassed at 300°C for 3 hours. The Raman spectrum was recorded with Bruker optics SENTERRA multi-laser dispersive Raman microscope at room temperature.

4.2.2 Discharge reactor

Plasma is generated by applying a high voltage (in the range 1 to 40 kV) between ground and the inner electrodes that were separated by a 3.5 mm discharge gap. The inner electrode is a stainless steel rod placed at the center of a quartz tube coated with silver paste that also acts as the ground electrode. The applied voltage was measured with a high-voltage probe (Agilent 34136A HV 1/1000). Charge and voltage are recorded with a 100-MHz bandwidth (maximum 1GS/s) oscilloscope (Tektronix TDS 2014B). The flow rate of the bubbling air (200 ml/min) was adjusted by using a mass flow controller from AALBORG flow instruments (GFC 17).

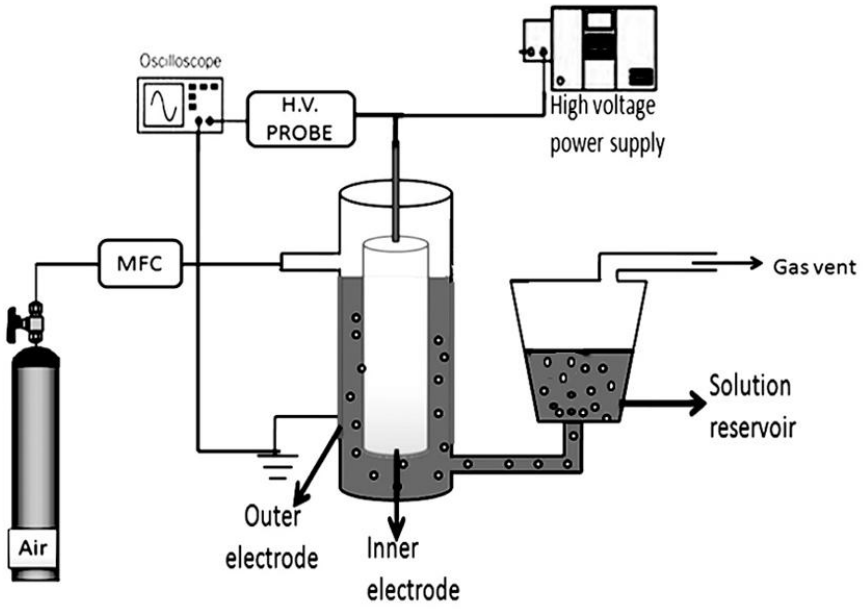

Figure. 4.1: Experimental setup

Endosulfan concentration in aqueous medium was monitored as a function of time and quantified by using High Performance Liquid Chromatography (HPLC-Waters Corporation 515 model) with a photodiode array detector with a mobile phase consisted of acetonitrile: water solution (70:30). The degradation percentage was calculated by using Eq-(4.1)

$$\text{Degradation percentage}\,(\%) = \frac{C_o - C_t}{C_o} \times 100 \qquad (4.1)$$

C_o and C_t are the initial and the final concentrations of ES, respectively. The energy yield of the degradation was calculated from Eq-(4.2).

$$Y(\text{g/kWh}) = \frac{C(\text{g/l}) \times V(\text{L}) \times \frac{1}{100} \times \text{Conv}(\%)}{P(\text{kW}) \times t\,(\text{h})} \qquad (4.2)$$

Where C is initial ES concentration, V is the volume of the solution, P is power and t is time.

Hydrogen peroxide (H_2O_2) produced in water by the discharge was quantified by following earlier mentioned procedure, which involves the spectrophotometric quantification of the pertitanic acid formed when Titaniumsulphate reacts with H_2O_2 at 418 nm [32].

The measurements of TOC are based on calibration with potassium hydrogen phthalate standards**.** The mineralization percentage was calculated by using Eq-(4.3)

$$\text{TOC removal percentage (\%)} = \frac{t_0 - t_t}{t_0} \text{ x } 100 \qquad (4.3)$$

t_0 and t_t are the initial and the final TOC concentrations of ES, respectively.

Qualitative analysis of CO, CO_2 released during the mineralization reaction was monitored by a gas analyzer (Siemens Ultramat 23) equipped with an IR detector; whereas, ozone concentration at the outlet of the reactor was measured with an UV-absorption ozone monitor (Teledyne instruments API 450 NEMA). It was observed that 264, 300 and 356 ppmv of ozone was detected at the outlet of reactor for 14, 18 and 22 kV applied voltages, respectively.

4.3 Catalyst characterization:

The formation of ceria fluorite structure was confirmed by XRD pattern as shown in Fig 4.2 (JCPDF#810792).The crystal size calculated from Debye-Scherrer method was found to be around 15 nm.

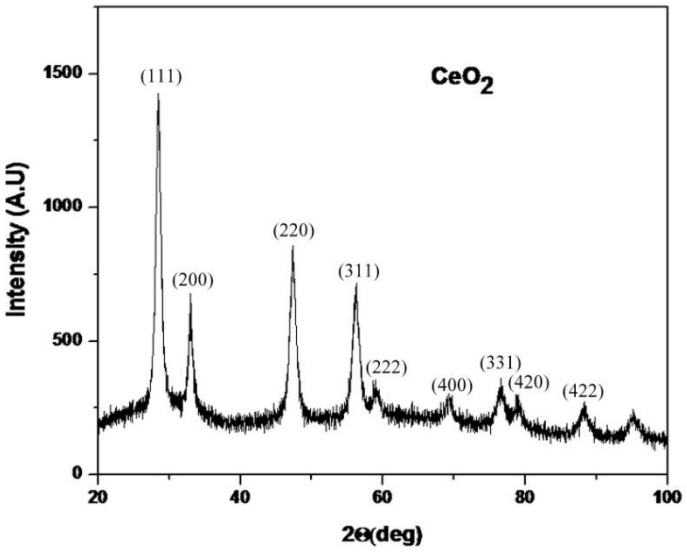

Figure. 4.2: XRD diffraction patterns of the CeO_2 catalysts

The N_2 adsorption – desorption isotherms are shown in Fig 4.3. The BET surface area of ceria was around 90 m^2/g and pore size was 19.2 Aº and pore volume was 0.073 cc/g.

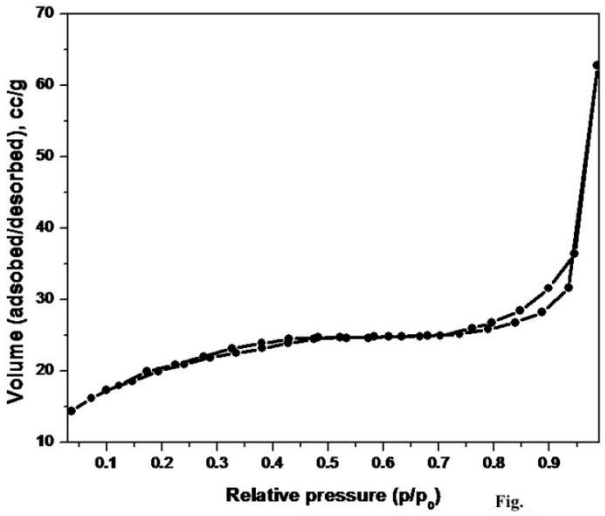

Figure. 4.3: Nitrogen adsorption and desorption isotherm of powder CeO_2 prepared by combustion synthesis.

Raman spectroscopy is one of the powerful tools for characterization of ceria. The strong peak at 464 $cm^{-1}$was assigned to F_2g Raman active interior phonon mode of CeO_2 fluorite structure, whereas, the second peak around 600 cm^{-1} (Fig. 4.4) was due to the presence defect induced oxygen vacancies (D-band) on the surface. The presence of Ce^{+3}/Ce^{+4} (oxygen vacancies) is believed to be the cause of the high reactivity of CeO_2 for ozone decomposition catalyst.

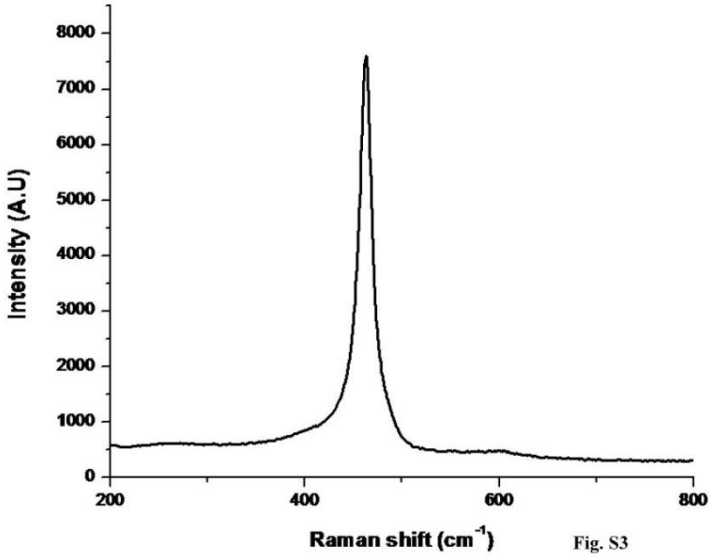

Figure. 4.4: Raman of the CeO_2 catalysts

4.4. RESULTS

4.4.1 Characteristics of the DBD reactor

The power dissipated in the discharge was found to be dependent on the applied voltage and it increases with applied voltage, as shown in Fig 4.5.

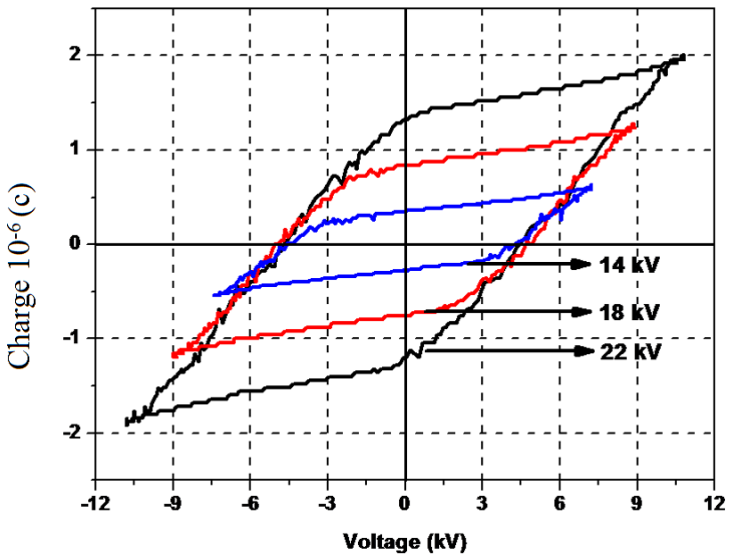

Figure. 4.5: V-Q diagram (Lissajous Figure) at different applied voltages.

H_2O_2 and ozone are the major active species in the NTP-DBD process. H_2O_2 formed by the following reaction Eq-(4.4-4.9) [30, 36, 37] was quantified and Fig 4.6 presents the concentration of H_2O_2 as a function of time and voltage.

$$H_2O + e^- \longrightarrow H^\bullet + OH^\bullet + e^- \quad (4.4)$$

$$OH^\bullet + OH^\bullet \longrightarrow H_2O_2 \quad (4.5)$$

$$2H_2O \longrightarrow H_2O_2 + H_2 \quad (4.6)$$

$$H^\bullet + O_2 \longrightarrow HO_2^\bullet \quad (4.7)$$

$$HO_2^\bullet + H^\bullet \longrightarrow H_2O_2 \quad (4.8)$$

$$HO_2^\bullet + HO_2^\bullet \longrightarrow H_2O_2 + O_2 \quad (4.9)$$

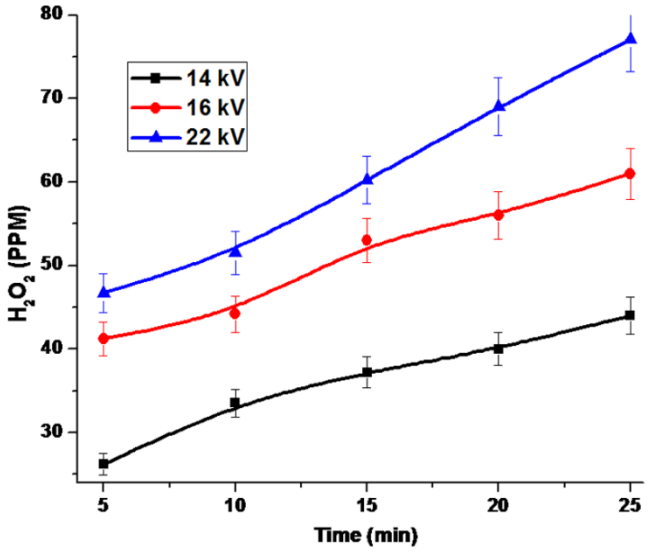

Figure. 4.6: Concentration of H_2O_2 formed as a function of time with different applied voltage.

Ozone is a widely applied strong oxidizing agent for the treatment of wastewater. The ozone generation reactions are given in Eq (4.10). Ozone reacts with target compounds via molecular and radical reactions [38-40]. Simplified reaction mechanisms of ozone are given in Eq-(4.10-4.15) [30].

$$O + O_2 \longrightarrow O_3 \quad (4.10)$$

$$3O_3 + H_2O \longrightarrow 2\ {}^{\bullet}OH + 4\ O_2 \quad (4.11)$$

$$H_2O_2 + 2O_3 \longrightarrow 2\ {}^{\bullet}OH + 3\ O_2 \quad (4.12)$$

$$O_3 + {}^{\bullet}HO_2 \longrightarrow {}^{\bullet}OH + O_2 + O_2^{-} \quad (4.13)$$

$$H_2O_2 + O_3 \longrightarrow {}^{\bullet}OH + O_2 + {}^{\bullet}HO_2 \quad (4.14)$$

$$O_3 + {}^{\bullet}OH \longrightarrow {}^{\bullet}HO_2 + O_2 \quad (4.15)$$

In order to evaluate the performance of NTP-DBD reactor, degradation of the ES was followed as a function of time with three different initial concentrations, for voltage variation between 14 to 22 kV (corresponding power input was 0.6 and 2.67 W, respectively). The volume of the aqueous solution was 100 ml. As seen in Fig 4.7, the degradation of ES increases with the increasing applied voltage and decreased with increasing concentration. As seen in Table 4.1, maximum degradation efficiency of ES was achieved with 5 mg/L at 22 kV, whereas, higher concentration decreases the conversion.

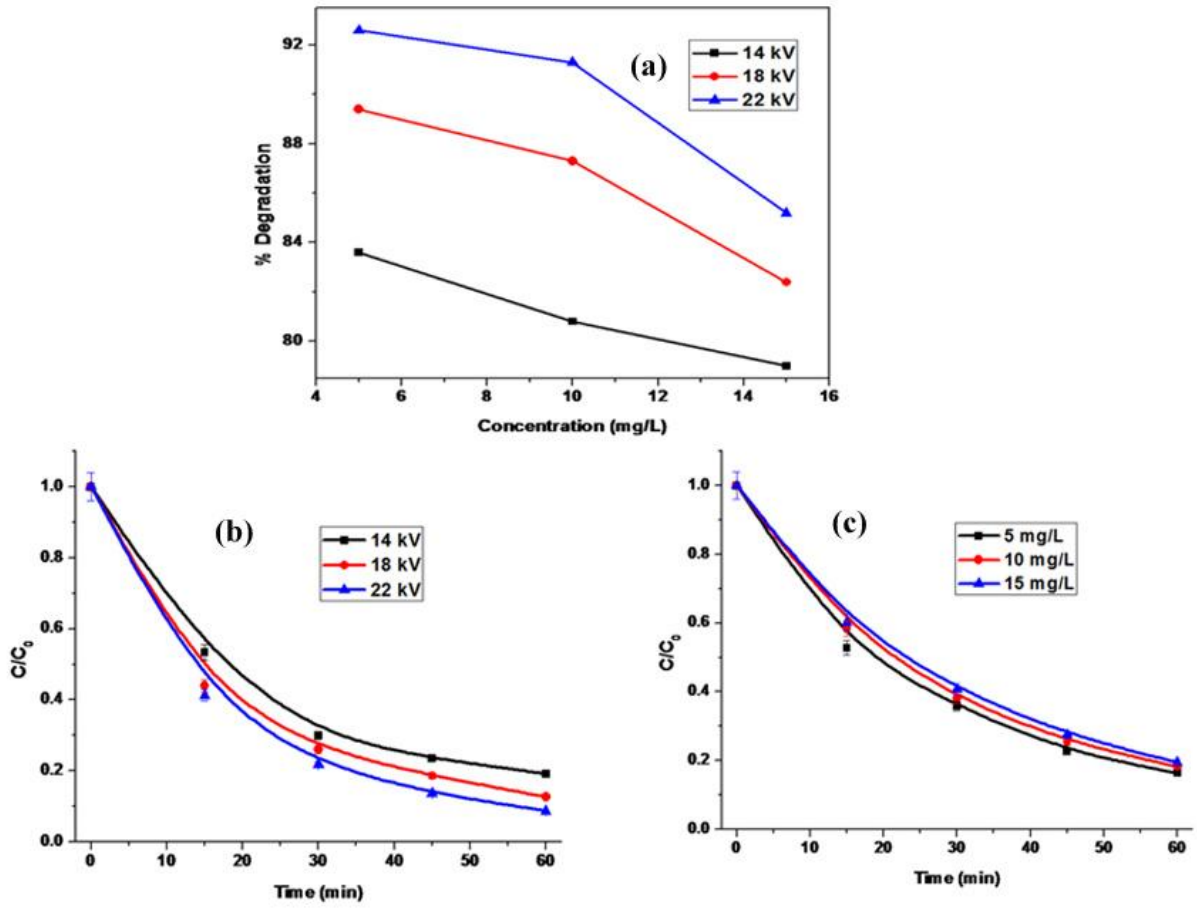

Figure. 4.7: Experimental results of ES degradation (a) degradation as a function of initial concentrations with different applied voltages at 60 min (b) with 10 mg/L initial concentration (c) with 14 kV applied voltage.

4.4.2. Mineralization

As mentioned earlier, the conventional physical treatments, at best may transfer the pollutant to another phase/compound against the desired mineralization. In order to understand the potentials of NTP for oxidation of ES, TOC was monitored as a function of time. Due to oxidation, the carbon frame of organic compound is gradually sliced into shorter carbon frame and finally to mineralization that should decrease the organic carbon content. During the oxidation of ES, TOC levels have been measured after every 15 minutes. Interestingly, NTP mineralizes the pollutant by the following reaction Eq-(4.16)

$$\text{Pollutant + plasma (Active species)} \rightarrow CO + CO_2 + H_2O \qquad (4.16)$$

% of degradation and TOC change with time are shown in Fig 4.8 for 10 mg/L initial ES concentration at 22 kV applied voltage and typical results are summarized in Table 4.1. As seen from Table 1, the extent of the mineralization increases as a function of applied voltage and concentration. At the end of the 60 min, for 15mg/L ES, highest TOC removal (22%) was observed at 22 kV. As the conversion levels are not high, it may be concluded that NTP alone is not very effective in mineralizing ES.

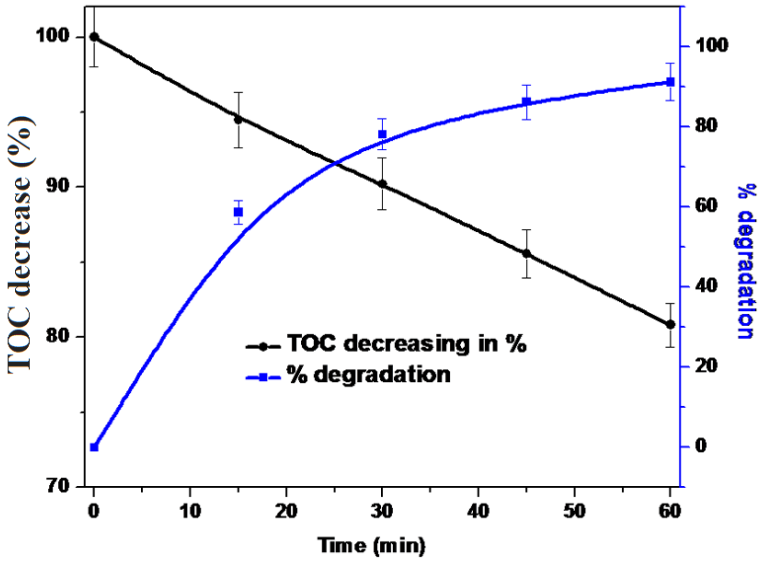

Figure. 4.8: TOC removal % during degradation of ES as a function time with 10 mg/L at 22 kV.

4.4.3. Effect of catalyst addition

As both degradation and mineralization of ES in NTP-DBD is not 100 % even after 60 min, catalyst combination with NTP was proposed. Recently, synergy effect on addition of transition metal oxide catalyst to NTP during the abatement of air pollutants was reported [33, 41]. Also, various supported and unsupported metals and metal oxides were tested for the ozonation of organic compounds in water. As stated earlier, nearly 300 ppm of ozone was observed at the out let of the reactor, which is also a potential oxidant with oxidation potential 2.07 V. It is also known that ozone in-situ decomposition may lead to atomic oxygen, which is even a stronger oxidant than ozone (oxidation potential 2.42 V). In order to understand the role of ozone decomposition on the performance of the reactor, CeO_2 catalyst was combined with NTP.

During the present study, 1 g/L of CeO_2 was added during the degradation of 15mg/L ES at 18 kV applied voltage. As seen in Fig 4.9, CeO_2 alone is not effective in decomposing ES and the observed decrease of ~3% may be due to adsorption. The catalytic NTP process on addition of CeO_2 to NTP leads to higher conversion compared to NTP alone, which is in agreement with the decreasing amount (125 ppmv) of ozone at the outlet of the reactor. However, after 60 min, NTP-CeO_2 showed the highest degradation of 95% against 80and 3%, respectively for NTP and CeO_2. Interesting observation is that NTP-CeO_2 also showed highest mineralization of ~ 48% against 16% with NTP alone. This improved performance on CeO_2 addition may be due to catalytic decomposition of ozone [42,43] as given Eq-(4.17-4.21).

Ozone adsorption

$$O_3+S\leftrightarrow O_3\text{-}S \qquad (4.17)$$

ES adsorption

$$E+ S\leftrightarrow E\text{-}S \qquad (4.18)$$

Reaction of adsorbed ES with adsorbed ozone

$$O_3\text{-}S + E\text{-}S\leftrightarrow 2P\text{-}S \qquad (4.19)$$

Desorption of products

$$2P\text{-}S\leftrightarrow 2S+CO_2+H_2O \qquad (4.20)$$

Where, S represents active centers of CeO_2 catalyst and E represents endosulfan. It is worth mentioning that the direct oxidation of ES by ozone as presented in Eq (4.21) is limited due to sluggish nature of the reaction.

$$O_3\text{-}S + E\text{-}S\leftrightarrow P\text{-}S \qquad (4.21)$$

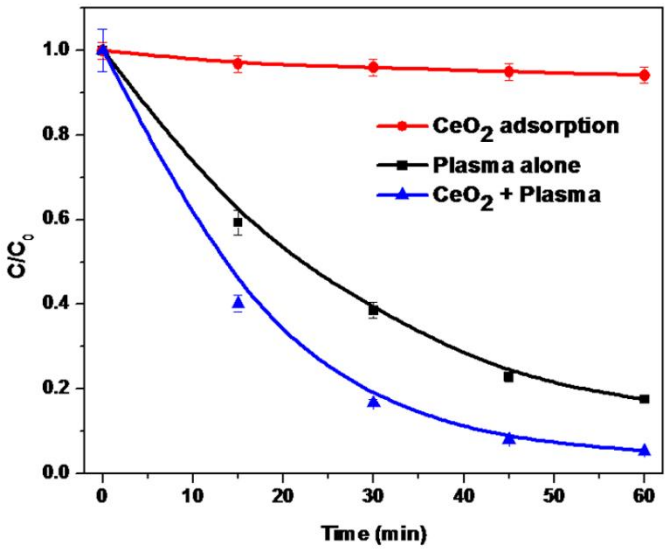

Figure. 4.9: Effects of catalyst on the degradation of 15 mg/L ES at 18 kV.

4.4.4. Kinetics

The kinetics of the ES degradation and rate constants have been determined and presented in Table 4.1. The rate constant was calculated by the first-order integral rate equation Eq-(4.22)

$$\ln(C/C_0) = -k_1 t \qquad (4.22)$$

where C, C_0, and k_1, are the concentration of ES for a given reaction time, initial concentration, and first-order rate constant (min^{-1}), respectively. As shown in Fig 4.10, the reaction follows typical first order kinetic behavior and plot of $\ln(C/C_0)$ vs time is a straight line. Table 4.1 shows the R^2 values and first-order rate constants for given conditions. The coefficient indicated the linearity and confirms the first-order kinetic behavior.

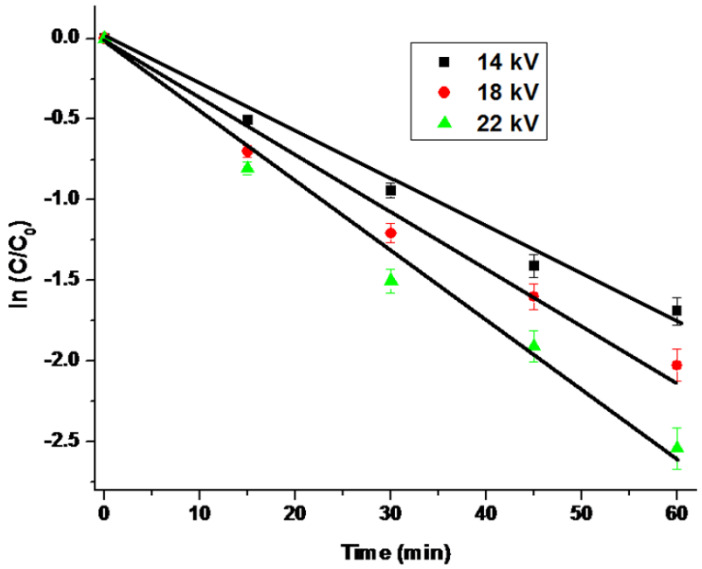

Figure. 4.10: Apparent first order kinetics plots for aqueous ES degradation with 10 mg/L initial concentrations.

Table 4.1: Changing the parameters (% of degradation, % of TOC decreased, Rate constant and R^2 value) during the experiment at 60 min of plasma treatment.

C_0 (mg/L)	Voltage (kV)	% of degradation at 60 min	TOC Decrease in %	Rate constant (min^{-1})	R^2
5	14	83.6	7.2	0.089	0.986
	18	89.4	11.2	0.107	0.991
	22	92.6	18.6	0.128	0.975
10	14	80.8	7.7	0.082	0.974
	18	87.2	13.4	0.099	0.963
	22	91.3	19.1	0.119	0.977
15	14	80.5	6.07	0.081	0.995
	18	82.4	15.8	0.085	0.996
	22	85.2	22.1	0.095	0.992
15	With catalyst at 18	95.0	48.0	0.145	0.995

4.4.5 Energy yield

The degradation efficiency may be best illustrated by the amount of ES decomposed per unit of energy (yield). The energy yield depends on the type of discharge reactor, initial concentration and nature of the compound. During the present study, ~ 60% degradation within 30 min was observed and the energy efficiency for different conditions is given in Table 4.2. It was observed that energy yield decreases as a function of time whereas % degradation increases, (Fig 4.11). With increasing applied voltage from 14 to 22 kV (power 0.6 w to 2.67 w), the energy yield decreased from 1.072 to 0.29 g/kWh for 5mg/L, 2.03 to 0.58 g/kWh for 10mg/L and from 3.02 to 0.72 g/kWh for 15mg/L initial concentrations, respectively. Hence, higher concentration leads to a better performance.

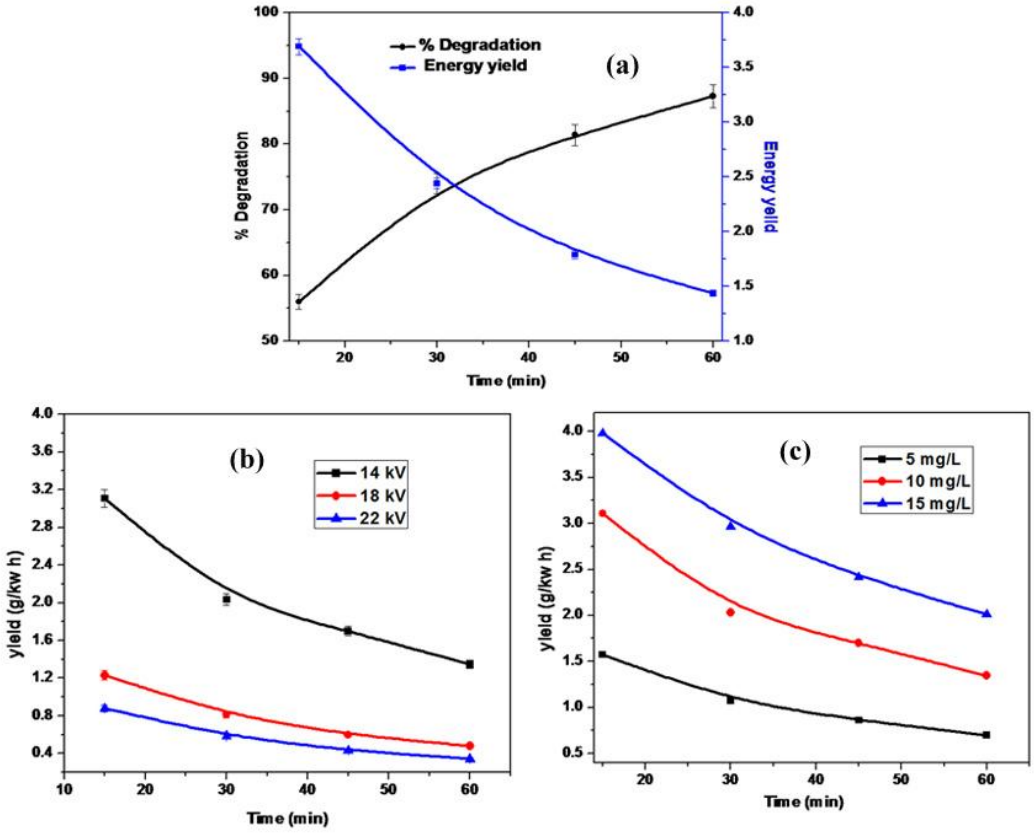

Figure. 4.11: (a) Energy yield and the % of ES degradation As a function of time during plasma treatment for 10 mg/L concentration at 18 kV applied voltage, (b) Energy yield as a function of time for various applied voltages for 10 mg/L initial ES concentration (c) Energy yield as a function of time for various initial concentrations with 14 kV applied voltage.

Table 4.2: Energy yield (g/kWh) during the experiment at 30 min plasma treatment

C_0 (mg/L)	Voltage (kV)	Power (W)	Yield (g/kWh)	% degradation after 30 min
5	14	0.68	1.07	64
	18	1.82	0.421	76
	22	2.67	0.298	79
10	14	0.68	2.03	61
	18	1.82	0.813	74
	22	2.67	0.585	79
15	14	0.68	3.02	60
	18	1.82	1.03	63
	22	2.67	0.721	65

4.5. Conclusions

An advanced oxidation process based on nonthermal plasma generated in a dielectric barrier discharge configuration has been reported for the mineralization of a model pesticide endosulfan. Typical results highlighted the potentials of DBD process for the removal of endosulfan. On addition of catalyst CeO_2 to the discharge, best performance was achieved, which was assigned due to in-situ decomposition of ozone on the surface of the catalyst leading to the formation of strong oxidant atomic oxygen. The conversion decreases with increasing ES concentration, whereas, higher input powers favor high conversion. The degradation kinetics of ES follows first order kinetics. Typical results during degradation of 15 mg/L of ES indicated conversion upto 82% and mineralizationupto15%. Combination of cerium oxide catalyst to NTP increased the conversion to 94% and mineralization upto48%.

Chapter 5

Mineralization of Phenol in water by Catalytic Non-Thermal Plasma Reactor

5.1 Introduction

Phenolic compounds are one of the abundant pollutants discharged into industrial waste waters and removal of these compounds is of great interest due to their toxicity and stability [137-143]. Hence, research in this direction has been diverted to develop technologies that may mineralize the pollutant rather converting pollutant to either partial degradation products or to another form. Among the options available for mineralization of aqueous organic compounds, bio-remediation has unique advantages like specificity and low cost. However, bio-remediation is a slow process and time consuming [105]. In this context, application of electrical discharges in water appeared to be a potential alternative [38, 83].

The aim of the present study is to design a catalytic DBD plasma reactor capable of mineralizing phenol in water. Influence of various parameters like applied voltage, initial concentration and addition of CeO_2 catalyst was studied to achieve the best degradation efficiency.

5.2. Experimental

5.2.1. Materials

As reported in the earlier section, CeO_2, 10 wt% Fe_2O_3/CeO_2 and 10 wt% ZrO_2/CeO_2 catalysts were prepared by following same procedure [144]. Briefly, in a typical synthesis, metal nitrate solution was added to citric acid (CA) to maintain oxidant/fuel ratio of 1. Minimum amounts of distilled water was added and the resulting solution was sonicated for 15 minutes and transferred into alumina crucible and heated at 573 K in a preheated furnace for 5 min. During the catalytic plasma experiments, 100 mg of the catalyst was dispersed in aqueous solution.

5.2.2. Analysis

Phenol concentration was measured using a high performance liquid chromatography (Waters Corp 515 HPLC) equipped with a photodiode array detector, at 254 nm using acetonitrile /water = 70:30 (V/V) as the mobile phase. The gas after passing through the solution was connected to an online COx analyzer to identify CO-CO_2, whereas a total organic carbon analyzer was used to quantify the mineralization. Total organic carbon (TOC) was estimated as a function of time by a total organic carbon analyzer (TOC-V_{CPH}, Shimadzu). The % degradation was calculated as follows Eq-(5.2)

$$\text{Percentage degradation (\%)} = \frac{C_o - C_t}{C_o} \times 100 \qquad (5.2)$$

C_o and C_t are the initial and the final concentrations of phenol, respectively. The TOC removal was calculated from Eq-(5.3)

$$\%\text{TOC decrease} = [(TOC_i - TOC_t)/TOC_i] \times 100 \qquad (5.3)$$

Where, TOC_i= the initial total organic carbon of phenol solution and TOC_t= the total organic carbon at time t of treated phenol solution.

5.3. Results and Discussion

5.3.1. Catalyst characterization

Figure 5.1 shows the XRD patterns of CeO_2, 10wt% Fe_2O_3/CeO_2 and 10 wt% ZrO_2/CeO_2 which confirm the fluorite structure of CeO_2 with intense peaks at d-spacing of 5.42, 5.38 and 5.39A°. The XRD pattern of Fe_2O_3/CeO_2 and ZrO_2/CeO_2 catalyst is similar to that of pure CeO_2 and no

additional peaks corresponding to $Fe_2O_3$and ZrO_2 were observed, indicating that $Fe_2O_3$and ZrO_2 are well dispersed on CeO_2 surface to form solid solutions.

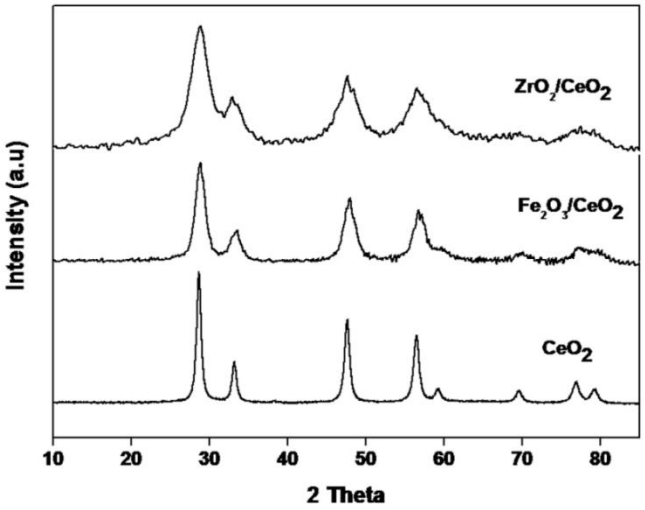

Figure. 5.1: X-ray diffractograms for the cerium oxide catalysts.

Figure 5.2 presents N_2 adsorption-desorption isotherms of catalysts used in the present study. The, surface area of CeO_2, 10 wt% Fe_2O_3/CeO_2 and 10 wt% ZrO_2/CeO_2 is around $90\pm5 m^2/g$.

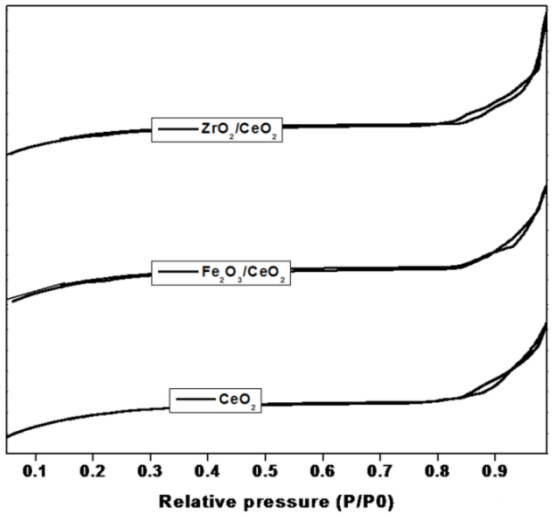

Figure. 5.2: Adsorption isotherms of cerium oxide catalysts.

Raman spectra of pure CeO_2, Fe and Zr-doped CeO_2 samples are presented in Fig 5.3, that showed a strong peak at 462 cm^{-1} due to the F_{2g} Raman active mode characteristic of the fluorite structure of CeO_2 [145]. Beside this, a weak band observed at around 588 cm^{-1} that originated from intrinsic oxygen vacancies [145].

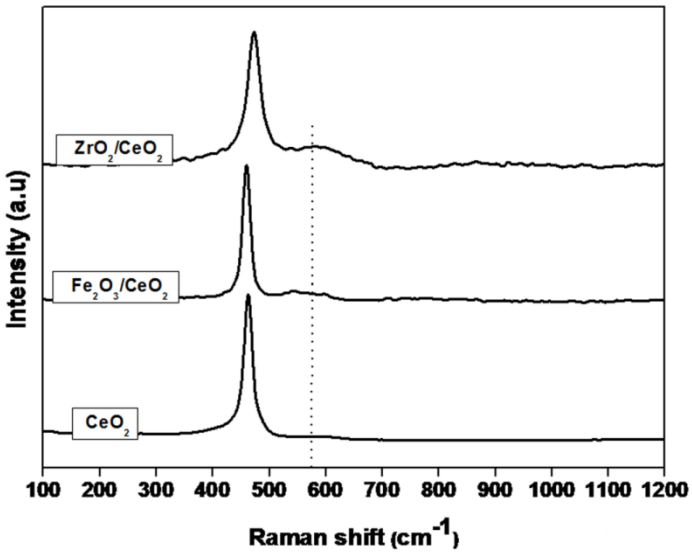

Figure. 5.3: Raman spectra for the cerium oxide catalysts

5.3.2. Effect of the applied voltage on the degradation of phenol

In order to understand the influence of the applied voltage on phenol degradation, voltage was varied between 14 to 18 kV and conversion was followed for 50 ppm initial concentration of phenol at 200 mL/min gas flow rate. Fig 5.4 presents the typical results of phenol degradation. As seen in Fig 5.4, degradation efficiency was 82% at 14 kV that increased to 92% at 18 kV after 30 min. At any time, high voltage leads to higher conversion. This increase may be due to the high electric filed strength at high input voltage that may generate more number of active species such as ions (H^+, H_3O^+, O^+, H^-, O^-, OH^-, $\mathbf{O_2^-}$), molecular species (H_2, O_3, H_2O_2) and reactive radicals (such as $O^\bullet$, $H^\bullet$, $OH^\bullet$) that may enhance the oxidation of the phenol. The oxidation of phenol may proceed via decomposition to lower molecular weight products, such as intermediate organic acids and finally to CO_2 and H_2O.

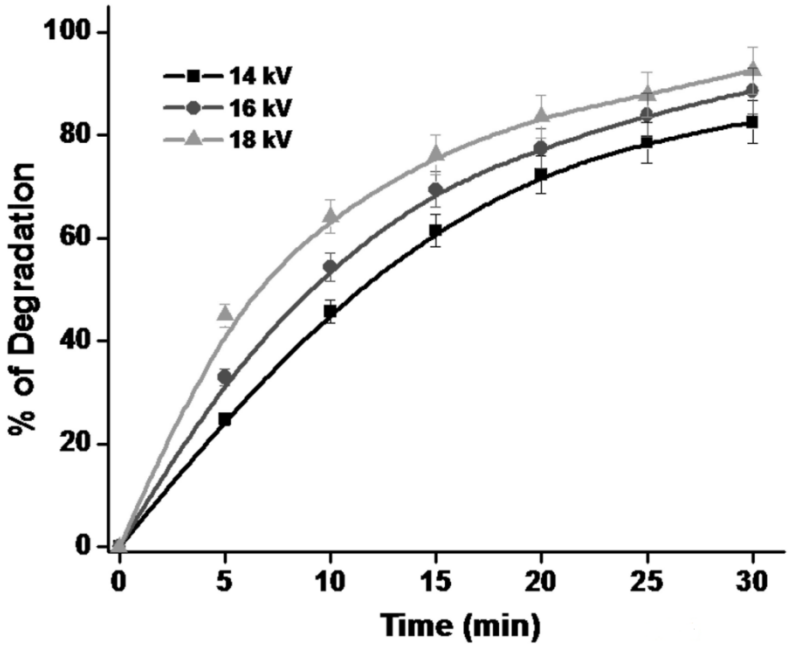

Figure. 5.4: Effect of applied voltage on phenol degradation for 50 ppm initial phenol concentration.

5.3.3. Effect of initial concentration

The effect of initial concentration of phenol on the rate of degradation is investigated at a fixed voltage (18 kV) by varying the concentration between 50 to 100 ppm and the results are shown in Fig 5.5. It was observed % degradation was more at lower concentrations, which may be due to the limited number of pollutant molecules available to react with the active species generated in plasma. For example, after 30 min of treatment, 92% degradation was achieved for 50 ppm that decreased to 60% for 100 ppm. As the reaction was carried out a fixed voltage, at higher concentration, only a limited number of active species may be available to react with more number of reactant molecules. As conversion was not 100% a catalyst combination to plasma was tested.

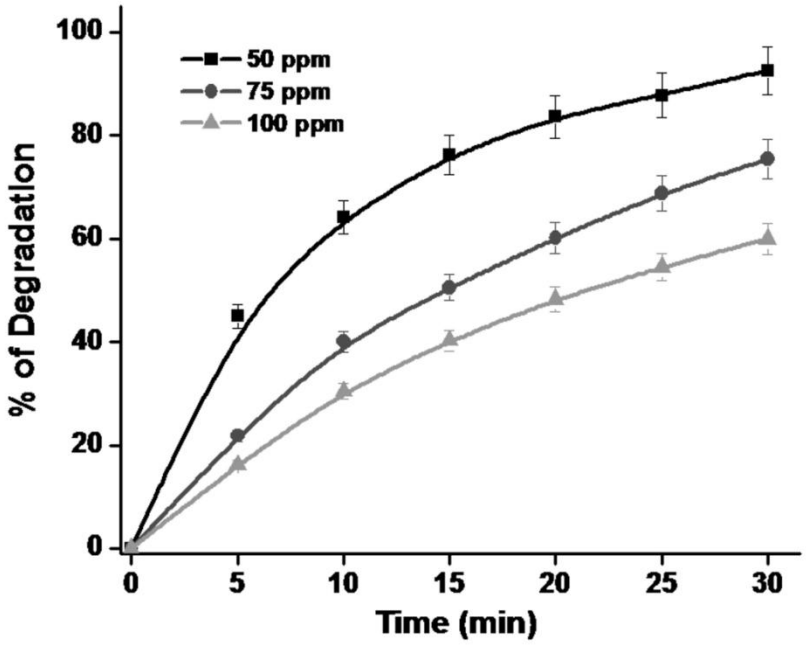

Figure. 5.5: Effect of initial concentration on phenol degradation with 18 kV applied voltage.

5.3.4. Effect of catalyst addition on phenol degradation

Figure 5.6 presents the influence of modified CeO_2 catalysts during degradation of 100 ppm phenol at 18 kV. It is worth mentioning that the adsorption capacity of catalyst is almost negligible (1.5 %). Interesting observation is that catalyst addition to plasma improves the % degradation of phenol. At 18 kV the order of activity of different catalysts followed the trend: CeO_2< Plasma< CeO_2+ Plasma< Fe_2O_3/CeO_2+ plasma and ZrO_2/CeO_2+ plasma. The highest conversion achieved was close to 91% with ZrO_2/CeO_2+Plasma against 60% with plasma lone. It is known that many of the excited species produced in NTP are short-lived. Hence, addition of a catalyst may either enhance the life time of short-lived species or/and facilitate the formation of secondary oxidants like atomic oxygen by in-situ decomposition of ozone. DBD reactor used in the present study produces 300 ppm of ozone. The improved performance of ceria (CeO_2) modified with ZrO_2 and Fe_2O_3 may be due to catalytic decomposition of ozone as given in Eq-(5.4-5.8) [146, 147]. Fe and Zr metal oxides loaded on CeO_2 showed the best degradation efficiency when compared to CeO_2 with plasma, which is in agreement with the decreasing amount of ozone (with oxidation potential of 2.07 V) at the outlet (226, 192, and 167 ppm respectively).The best ozone decomposition efficiency of Fe_2O_3/CeO_2 and ZrO_2/CeO_2

systems .when compared to CeO_2 may be due to creation of defect induced oxygen vacancies (D-band) on CeO_2, as confirmed by the presence of the Raman band at 588 cm^{-1}[146-148]. As stated earlier, metal oxides catalysts are capable of converting ozone to activate oxygen, which is even a stronger oxidant than ozone with oxidation potential (2.42 V) [149].

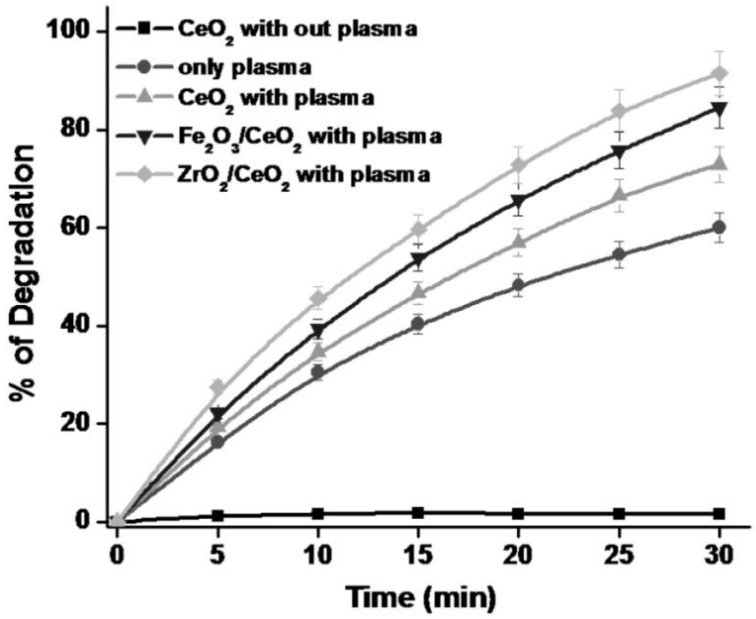

Figure. 5.6: Effect of catalyst addition on phenol degradation with 18 kV applied voltage and 100 ppm initial concentration.

The catalytic decomposition of ozone may be explained as shown in Eq-(5.4-5.8)**.**

Ozone adsorption

$$O_3 + A \leftrightarrow O_3\text{-}A \qquad (5.4)$$

Phenol adsorption

$$Ph + A \leftrightarrow Ph\text{-}A \qquad (5.5)$$

Reaction of adsorbed phenol with adsorbed ozone

$$O_3\text{-}A + Ph\text{-}A \leftrightarrow 2P\text{-}A \qquad (5.6)$$

Desorption of products

$$2P\text{-}A \leftrightarrow 2A + CO_2 + H_2O \qquad (5.7)$$

Where, 'A' represents active centers in catalyst, Ph represents Phenol and P represents products.

An additional possibility is the direct oxidation of phenol by ozone as presented in Eq-(5.8).

$$O_3\text{-}A + Ph\text{-}A \leftrightarrow P\text{-}A \qquad (5.8)$$

5.3.5. Energy yield

During the removal of pollutants, often energy yield (grams of the pollutant degraded per kWh input energy) is taken as a practical measure of applicability. Fig 5.7a presents the energy yield as a function of time. As seen in Fig 5.7a, at any fixed voltage energy yield decreases on time and plasma alone showed least performance. However, addition of catalyst improved energy yield. For 50 ppm phenol, the best performance obtained was 20.5 g/kWh at 14 kV and 200 ml/min flow rate. Fig 5.7b present the effect of catalyst addition on yield; it is clear that the best degradation was achieved with catalytic DBD reactor. The yield increased from 8.1 to 13.1 on catalyst addition (10% ZrO_2/CeO_2). Table 5.1 presents the yield (g/kWh) after 15 min for different experimental conditions.

Table 5.1: % degradation, TOC removal, R^2 value and Energy yield during the plasma treatment.

C_0 (ppm)	Voltage (kV)	Catalyst	At 30 min of plasma treatment		Rate constant (min^{-1})	R^2	At 15 min of plasma treatment	
			% of degradation	% of TOC removal			% of degradation	Energy yield (g/kWh)
50	14	----	82.6	12.4	0.078	0.995	61.48	20.5
50	16	----	88.6	18.6	0.091	0.997	69.46	13.6
50	18	----	92.56	24.4	0.125	0.992	76.2	8.4
75	18	----	75.42	30.3	0.088	0.991	50.48	8.3
100	18	----	59.99	35.6	0.071	0.998	40.28	8.1
100	18	CeO_2	72.9	46.8	0.076	0.994	46.66	10.3
100	18	Fe_2O_3/CeO_2	84.49	46.4	0.081	0.997	53.88	11.8
100	18	ZrO_2/CeO_2	91.49	47.3	0.084	0.998	59.74	13.1

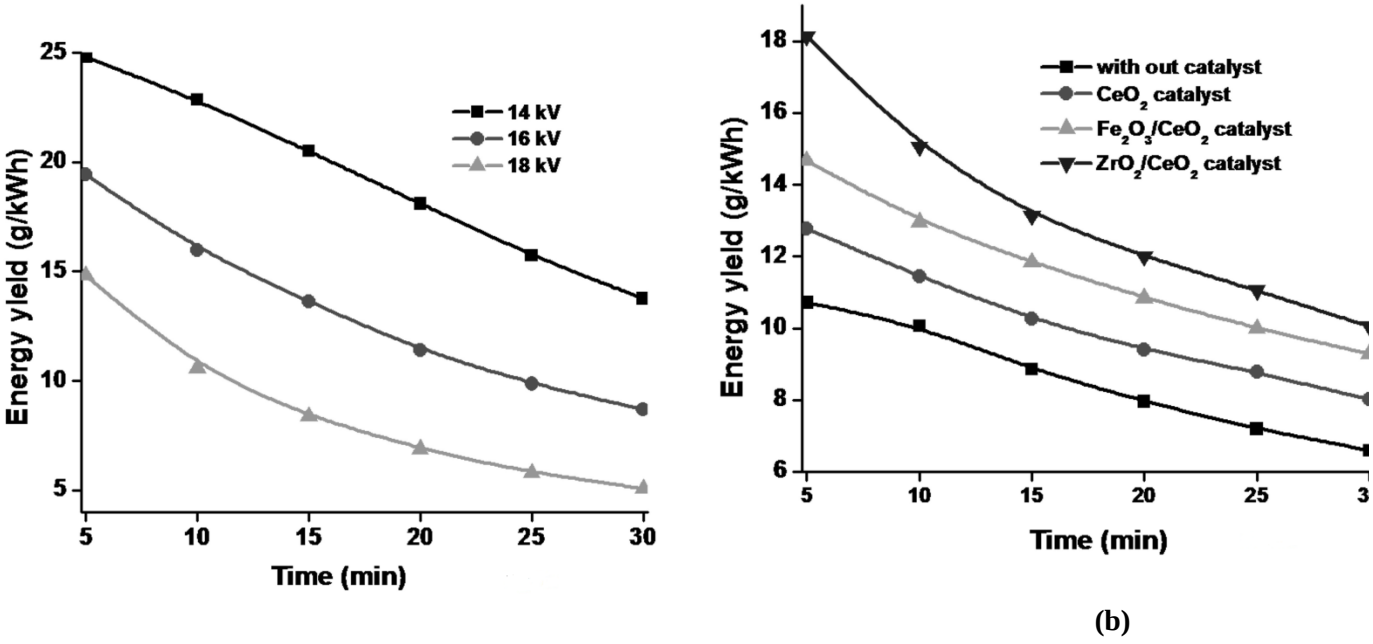

(a) **(b)**

Figure. 5.7: (a) Change in yield as a function of time for different applied voltages (b) Change in yield as a function of time for different catalyst addition.

5.3.6. Kinetics

In order to model the reaction and also for the purpose of up-scaling, understanding the reaction kinetics is important. During NTP plasma treatment, phenol degradation followed first-order kinetics as shown in Fig 5.8, where concentration of phenol decreases as a function of time and the rate constant was calculated from Eq-(5.9).

$$\ln(C/C_0) = -kt \qquad (5.9)$$

Where C_0, C and t denote the initial, final concentration and time, respectively. The values of the R^2 for different conditions are given in Table 5.1.

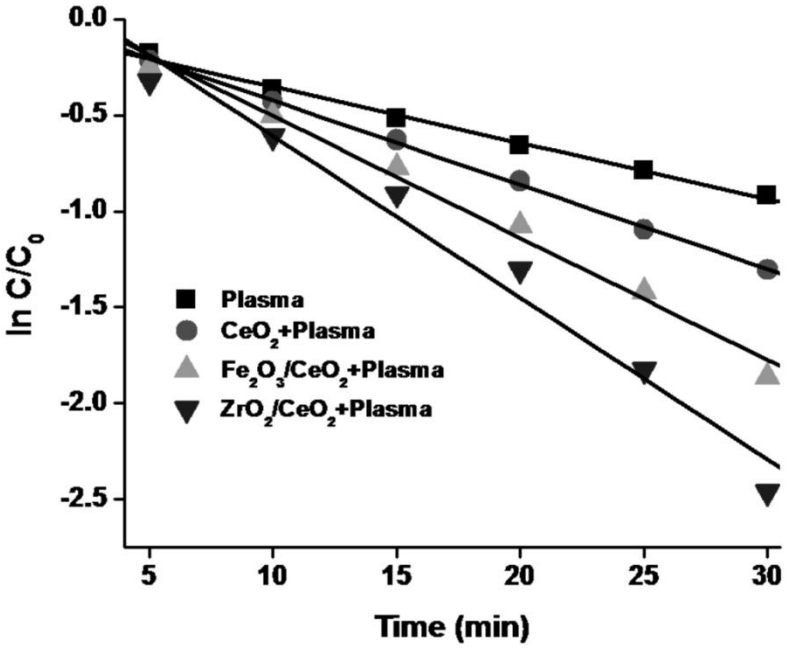

Figure. 5.8: First-order kinetics of phenol degradation at 18 kV and 100 ppm initial concentration.

5.3.7. Mineralization of phenol

Even though various techniques are reported for removal of pollutants in aqueous media, majority have reported the conversion of the pollutant. This may lead to secondary pollutants. Hence, mineralization is the preferred way of destroying the pollutant and promise of

any technique depends on degree of mineralization. In nonthermal plasma reactors, it is often believed that activated species drive the degradation and mineralization of pollutant to end products, such as CO, CO_2 and H_2O. Mineralization of phenol was determined by a total organic carbon content analyzer and the CO_2 formed was confirmed by a CO-CO_2 analyzer. Typical results presented in Table 5.1 and Fig 5.9 confirm that for 50 ppm phenol, 12.5, 18.5 and 24.5% mineralization was achieved at 14, 16 and 18 kV applied voltage, respectively. At 18 kV, for 50, 75 and 100 ppm phenol 24.5, 30.5 and 35.5% of the pollutant was mineralized. Interesting observation is that catalyst addition also improves mineralization. During removal of 100 ppm of phenol with plasma reactor at 18 kV, after 30 min mineralization was only 35.5% that increased to 47% on addition of catalyst.

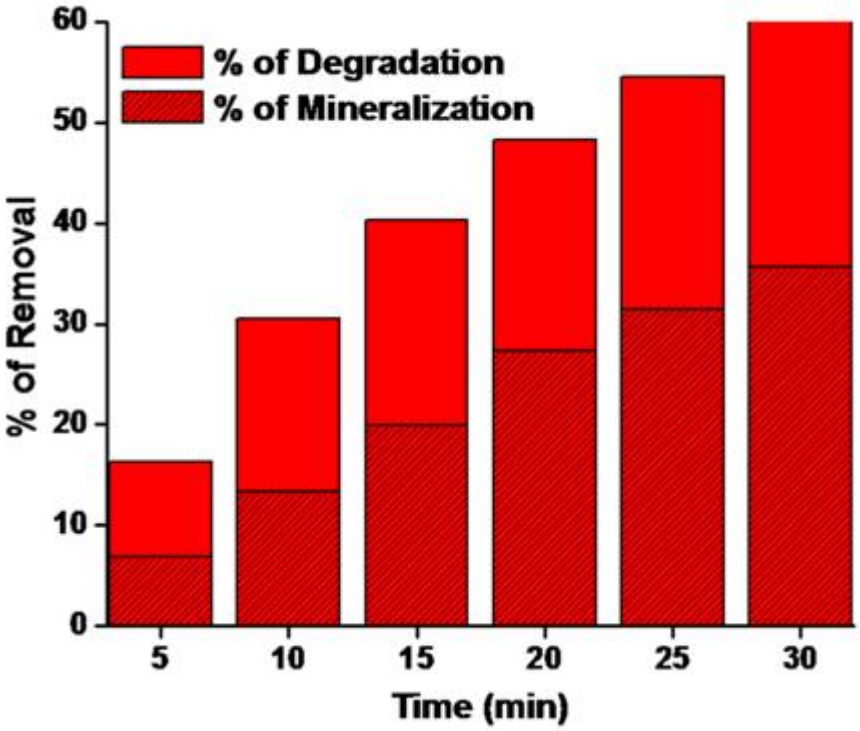

Figure. 5.9: % degradation and % mineralization as a function of time.

5.3.8 Plausible degradation mechanism

During the present study, discharge was created at gas-liquid interface that produces plasma containing various active species such as UV radiation, shock wave, ions (H^+, $H3O^+$, O^+,

H^-, O^-, OH^-, O_2^-), molecular species (H_2, O_3, H_2O_2) and most importantly reactive radicals (such as $O^\bullet$, $H^\bullet$, $OH^\bullet$), etc. Out of these reactive species, especially ozone and $^\bullet OH$ are the key oxidants. These active species may induce ultraviolet photolysis, electro hydraulic cavitations and supercritical water oxidation that may lead to mineralization [30, 150, 151]. As decreasing ozone concentration on addition of catalyst was established, it is logical to propose ozone induced radical reactions leading to the formation of OH radicals as shown in Eq-(5.10-5.15). Also, Dors et al., reported reactions between high energetic electrons present in the discharge streamer and the pollutant molecules in aqueous media that may produce •OH [151].

$$O + O_2 \rightarrow O_3 \quad (5.10)$$

$$O_3 + H_2O + hv \rightarrow 2\,{}^\bullet OH + O_2 \quad (5.11)$$

$$O_3 + H_2O \rightarrow H_2O_2 + O_2 \quad (5.12)$$

$$H_2O_2 + hv \rightarrow 2\,{}^\bullet OH \quad (5.13)$$

$${}^\bullet OH + H_2O_2 \rightarrow H_2O + {}^\bullet HO_2 \quad (5.14)$$

$$H_2O_2 + O_3 \rightarrow {}^\bullet OH + O_2 + {}^\bullet HO_2 \quad (5.15)$$

During the present study, GC-MS confirmed the formation of various intermediates like hydroquinone, pyrocatechol, p-benzoquinone and organic acids. From these results, a •OH initiated oxidation of phenol leading to the formation of Dihydroxycyclohexadienyl radical [$^\bullet C_6H_5(OH)_2$] (DHCHD) was proposed. Further reaction of DHCHD radicals with oxygen may produce dihydroxycyclohexadienylperoxyl (DHCHDP) radicals that decay in a first-order process to form pyrocatechol and hydroquinone. Hydroquinone further converts to 1,4-

benzoquinonethatmay have degraded into organic acids and finally to CO_2. A schematic representation of the phenol degradation in DBD plasma is shown in Fig 5.10.

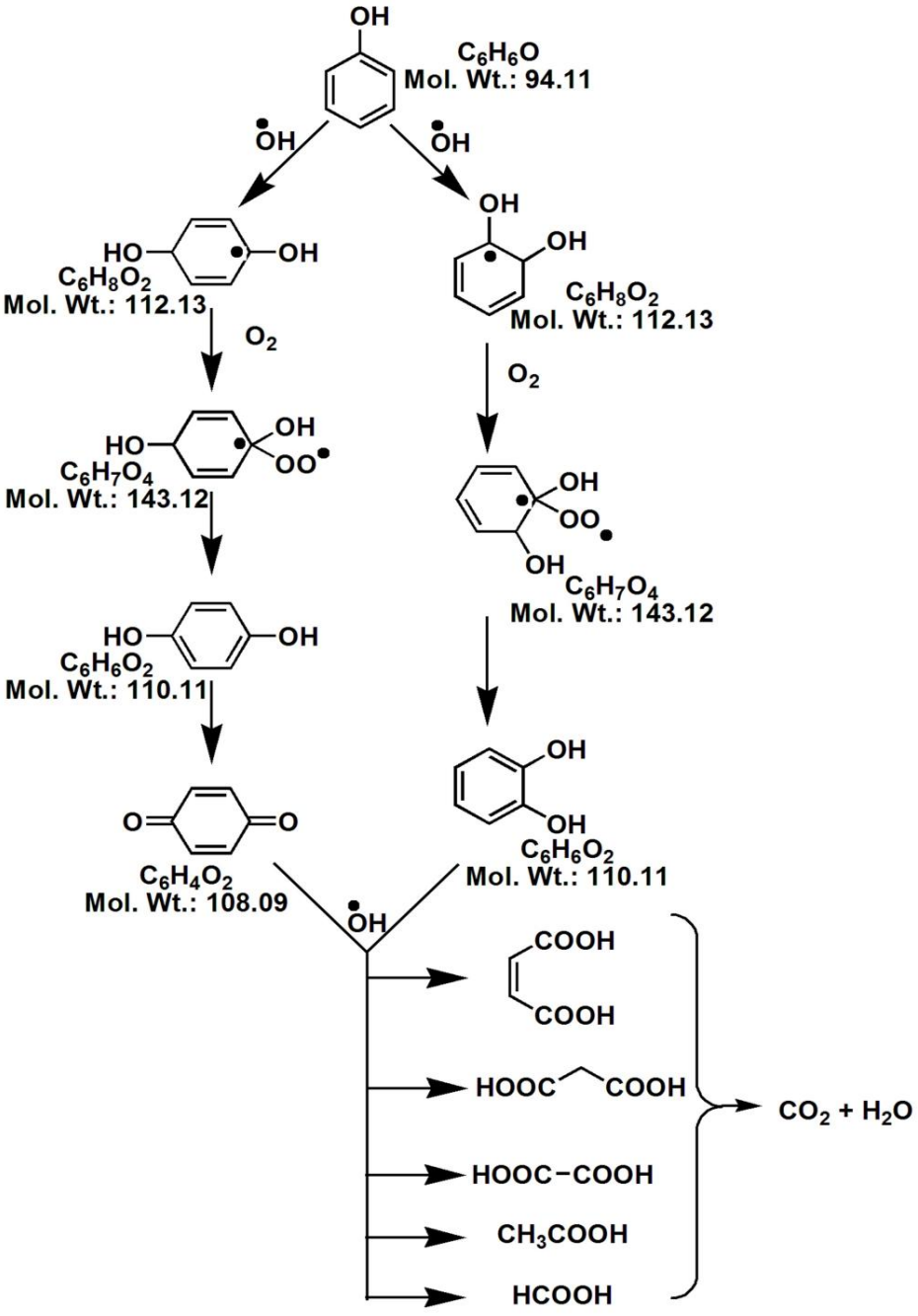

Figure. 5.10: Plausible Schematic representation of the phenol degradation mechanism.

5.4. Conclusions

Nonthermal plasma dielectric barrier discharge reactor was designed for the mineralization of aqueous phenol. Typical results indicated the improvement in the efficiency of the plasma reactor on addition of modified CeO_2 catalysts. Among the catalysts studied, 10 wt% ZrO_2/CeO_2 showed best activity due to oxygen vacancies, as confirmed by Raman spectra. Mineralization was confirmed by COx analyzer and quantified by total organic content analyzer. The best energy yield obtained was 20.5 g/kWh. A hydroxyl radical initiated reaction mechanism was proposed based on the intermediates observed by GC-MS.

Chapter 6

Catalytic Plasma Reactor for Mineralization of Sulfamethoxazole

6.1 Introduction

The presence of a large number of micro pollutants such as pesticides, pharmaceutical and personal care products (PPCPs) and dyes in surface waters have a negative impact on environment and ecology [152-154]. Even traces of PPCPs in water are of significant concern. PPCPs can enter the environment either in their original form or as metabolites or as degradation products. Conventional oxidative techniques are not effective for their mineralization. In this context advanced oxidation processes (AOPs) are highly promising for wastewater treatment without generating any sludge [35, 38]. In this direction, there is an increasing interest in an application of nonthermal plasma (NTP), as one of AOP for wastewater treatment [155-157]. Recent studies have demonstrated that electrical discharges in water can effectively treat/mineralize organic pollutants present in water [90, 94].

In general, application of AOPs proceeds via generation/utilization of several strong oxidants that are capable of maximizing efficiency of the treatment. In NTP-DBD ozone is one of important oxidant formed, whose *in-situ* decomposition may produce even more powerful oxidant atomic oxygen and hydroxyl radicals. As a result, several research groups have studied the application of NTP and solid catalysts for the removal of aqueous organic pollutants by *in-situ* decomposition of ozone [146, 158]. Of all the reactive species produced in the discharge in liquid phase, the hydroxyl radical is a very powerful and non-selective oxidant initiates the radical-involved reactions and transforms the target compounds into carbon dioxide and water if an adequate retention time is provided [159]. The mineralization of organic compounds by NTP-DBD processes is based on the oxidative degradation by active species, especially by the ozone and hydroxyl radicals. Sulfamethoxazole (SMX) represents an important class of sulfonamide antibiotics, which is widely used as one of human and veterinary pharmaceuticals. Objective of this research is to evaluate the effectiveness of NTP-DBD, catalytic NTP-DBD

reactor for the mineralization of SMX. The NTP-DBD processes may mineralize undesirable by products in water, hence the studies were conducted under various operational conditions in order to achieve the best degradation efficiency.

6.2. Experimental

6.2.1 Materials

The concentration of the SMX solution in all experiments was in the range 50 to 100 mg/L. It was prepared from a 1000 mg/L stock solution of SMX (Sigma Aldrich) prepared by 1000 mg of SMX in 1000 ml of Millipore water and filtered through a 0.45 μm filter.

6.2.2 Analysis

Aqueous samples were analyzed for SMX using high performance liquid chromatography (waters corp 515, HPLC) equipped with a C18 column (4.6mm×250mm) and PDI detector at a wavelength of 254 nm (mobile phase: acetonitrile /water = 70:30 (V/V), flow rate: 1 ml/min). Total organic carbon (TOC) was monitored as a function of time by a TOC-V_{CPH}, Shimadzu analyzer. The % degradation was calculated as follows

$$\text{Degradation percentage (\%)} = \frac{C_o - C_t}{C_o} \text{ x } 100 \qquad (6.1)$$

C_o is the initial and C_t is the concentrations at time t of SM, respectively.

The TOC removal was calculated from Eq-2

$$\%\text{TOC reduction} = [(TOC_i - TOC_t)/ TOC_i] \text{ x}100 \qquad (6.2)$$

Where, TOC_i= the initial total organic carbon of SMX and TOC_t= the total organic carbon at time t of treated SMX solution. H_2O_2 formation was confirmed by as reported previously.

6.2.3 Experimental setup

The experimental set-up was used nearly same as explained in previous sections.

6.3. Results and Discussion

6.3.1 Kinetics

The degradation of SMX was found to follow first order kinetics. From the curve fitting of the degradation profile for each variable, the apparent 1st order kinetic constants were calculated. Fig 6.1shows the first-order plots, for the removal of the SMX in the plasma reactor under catalytic conditions. The first-order kinetics equation is expressed as Eq-(6.3)

$$\ln(C_0/C) = kt \qquad (6.3)$$

where C_0, C, k, and t are the initial concentration of SMX, concentration at a given reaction time, the rate constant (min^{-1}), and reaction time (min), respectively. The rate constants of SMX under oxygen bubbling condition were higher than that of argon bubbling (Table 6.1).

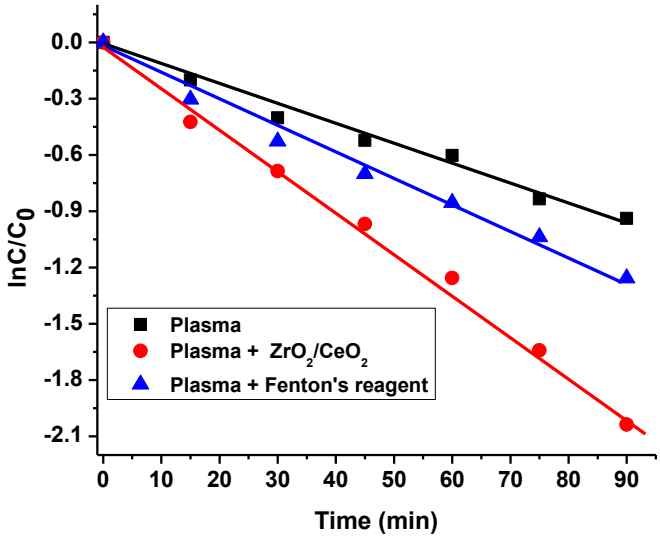

Figure. 6.1: First order kinetics of SMX degradation

6.3.2 Effect of Initial concentration

The initial concentration may have a significant influence on the rate of degradation. In order to understand the influence of the initial SMX concentration on the degradation, SMX concentration was varied from 50 to 100 ppm and results are shown in Fig 6.2. which confirms that the degradation efficiency of the reactor decreases with increasing concentration of SMX

(50-100ppm). The degradation of SMX was 94, 78, and 70 % respectively for 50, 75 and 100 ppm initial concentration at 18 kV applied voltage and the corresponding first-order rate constants were found to be 0.032, 0.021, and 0.017 min^{-1}. This may be due to the availability of a more number of active species at low concentrations.

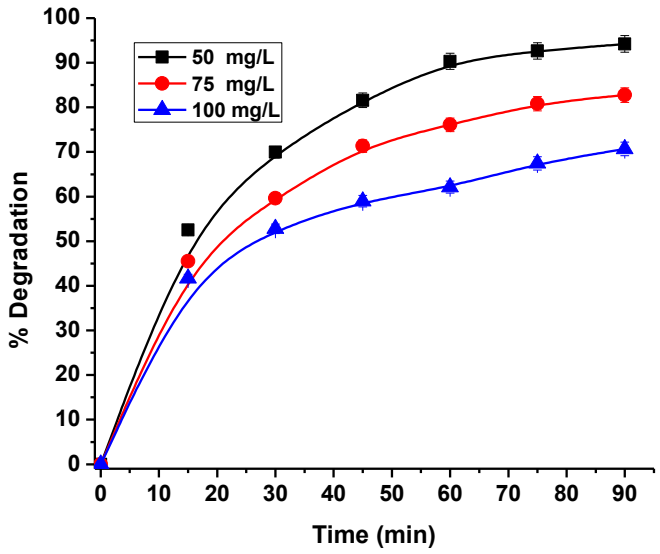

Figure. 6.2: Influence of initial concentration on degradation of SMX at 18 kV applied voltage.

6.3.3 Effect of feed gas

Feed gas may also influence the degradation of the pollutants in plasma reactors, as it may affect the formation of oxidants, positive and negative charged ions. On formation, these primary species react with each other or react with pollutant to produce secondary oxidant. During the present study oxygen, zero air and argon are bubbled through the SMX solution. As shown in Fig 6.3 oxygen bubbling is better than zero air and argon bubbling. The first-order rate constant SMX degradation also decreased in the order: oxygen> zero air > Argon > (0.017, 0.023, and 0.007 min^{-1} respectively). It is worth meaning that H_2O_2 formation is also effected by changing the gas. H_2O_2 during the present study was 68, 60 and 29 ppm respectively with oxygen, zero air and argon gases.

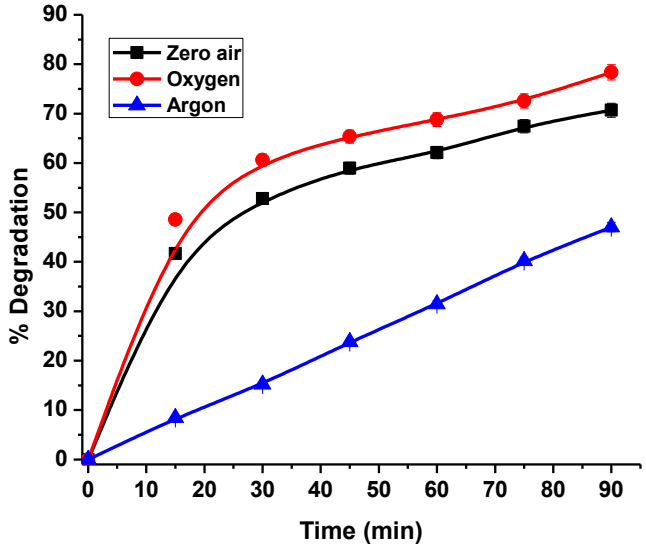

Figure.6.3. Effect of feeding gas on degradation of 100 ppm SMX at18 kV applied voltage.

C_0 (ppm)	Feeding gas	Catalyst	At 90 min of plasma treatment			Rate constant (min^{-1})	R^2
			% of degradation	% of TOC removal	Energy yield (g/kWh)		
50	Air	----	94.22	9.3	1.72	0.032	0.977
75	Air	----	75.68	14.6	2.07	0.021	0.969
100	Air	----	70.10	19.3	2.58	0.017	0.981
100	Oxygen	----	78.36	23.5	2.87	0.023	0.951
100	Argon	----	47.03	4.6	0.72	0.007	0.982
100	Air	Plasma/ Fentons	78.59	21.4	2.88	0.022	0.972
100	Air	ZrO_2/CeO_2	92.76	28.6	3.40	0.029	0.983

Table 6.1: % of degradation, decreasing in TOC%, energy yield values, and kinetic parameters during the SMX degradation at 18 kV applied voltage.

6.3.4 pH variation

Variation in the feed may alter the pH of the solution due to generation of various organic acids during the present study while using zero air, the pH of the solution dropped rapidly (Fig 6.4) when compared to other two feed gases. This decrease in pH may be due to the formation of strong nitrogen based acids like nitrous acid and nitric acid and some organic acids. Formation of nitric acid was ensured by acid-base titration.

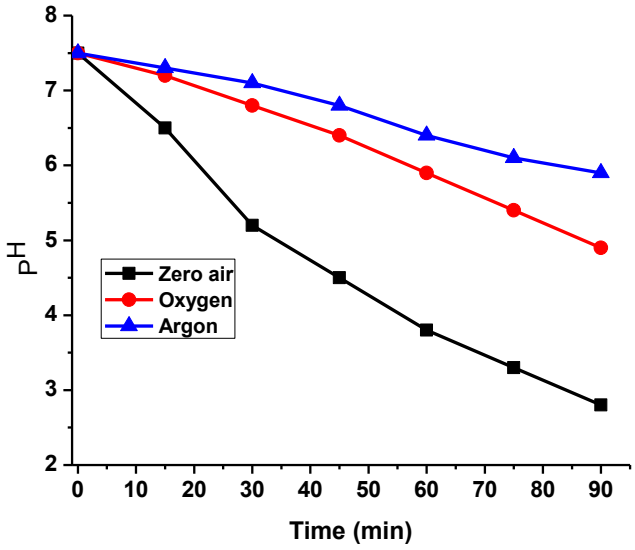

Figure. 6.4: Variations of pH during plasma treatment at 18 kV applied voltage, with different feeding gases.

6.3.5 Addition of catalyst

A combination of catalyst and NTP appears to be the best choice for the removal of SMX used in this study. Degradation and mineralization of the target compounds may be favored by the addition of suitable catalysts. During the present study at 18 kV, 60 ppm of H_2O_2 was confirmed. In order to facilitate Fenton type reactions 100 mg of Fe^{2+} was added. As seen from Figure 6.5, addition of Fe^{2+} improved the degradation. As seen from Fig 6.5 addition of Fe^{2+} improved the degradation to 78% against 70% with plasma alone. In a similar manner, formation of 330 ppm ozone at 18 kV was observed under air bubbling. In order to facilitate ozone decomposition, 10% ZrO_2/CeO_2 was added to SMX solution. The improved degradation for catalytic plasma reactor is shown in Figure 6.6, which confirms the degradation of 92%

against 70% for plasma alone. The better performance of the plasma catalytic technique may be due to *in-situ* decomposition of ozone to more active species in presence of catalyst. The better performance of 10% ZrO_2/CeO_2 may be due to its ozone decomposition ability that may lead to the formation of atomic oxygen, which is even a stronger oxidant than ozone. In order to ensure this observation, ozone concentration was measured during the reaction with ZrO_2/CeO_2,that conforms the decrease of ozone to 167 ppm.

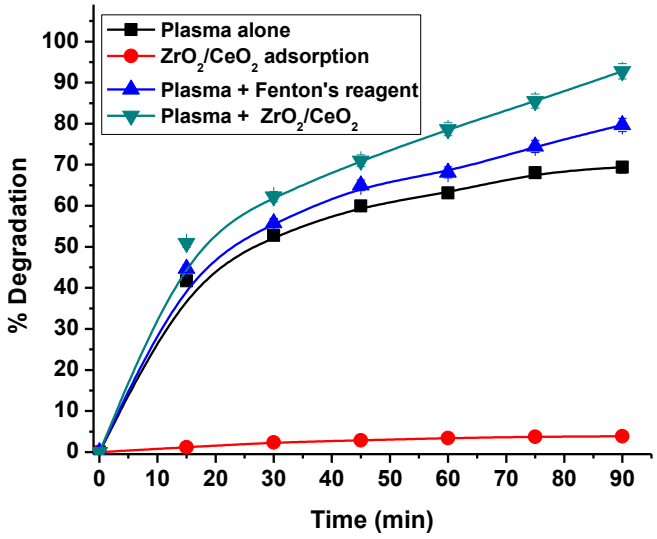

Figure 6.5: Effect of additives on enhancement of SMX degradation at 18 kV applied voltage,

6.3.6 Mineralization

Mineralization is the complete conversion of organic compound to CO_2 and H_2O. CO_2 formation was identified by COx analyzer, whereas TOC analyzer was used to estimate the mineralization. At 18 kV applied voltage for 100 ppm SMX initial concentration, plasma alone showed 19.3 % of mineralization while with the addition of Fentons and 10% ZrO_2/CeO_2 catalyst, it increased to 21.4 and 28.6% respectively (Table.6.1). These results show that the, addition of the catalyst improves the mineralization as well as the performance of the reactor towards the total oxidation.

6.3.7 Energy yield

The dye degradation efficiency may be better illustrated by widely accepted energy yield, which is a measure of the amount of pollutant decomposed per unit energy. Data on the energy yield under various operating conditions is given in Table 1. As a function of time, % degradation increases with decreasing energy yield; probably due to high energy consumption for longer durations. On increasing the concentration from 50 ppm to 100 ppm, the energy yield increases from 1.72 g/kWh to 2.58 g/kWh at 18 kV applied voltage. Interesting observation is that in presence of the catalyst energy yield increases to 2.88 and 3.40 g/kWh for plasma reactor combined with Fe^{2+} and 10% ZrO_2/CeO_2. This increase in the presence of Fe^{2+} may be due to the Fentons reaction leading to hydroxyl radical formation and whereas ZrO_2/CeO_2 may be due to the *in-situ* formation of oxidants like atomic oxygen by ozone decomposition.

Conclusion

As an alternative to the conventional techniques, the SMX degradation in aqueous medium was studied by NTP-DBD reactor. The advantage of NTP-DBD is the ease of operation, energy efficiency and improved mineralization on addition of the catalyst. The conversion efficiency decreased on increasing SMX concentration. Among the feed gases studied oxygen showed the best degradation, probably due to formation of more oxygen based active species. The degradation and mineralization efficiency of the reactor increased on addition of the Fe^{2+}, probably due to Fentons reactions. Whereas the best activity observed with ZrO_2/CeO_2 may be due to in situ decomposition of O_3, leading the formation of atomic oxygen.

Chapter 7-conclusions

Catalytic nonthermal plasma (NTP) dielectric barrier discharge (DBD) reactor was designed and tested for the degradation and mineralization of aqueous organic compounds. Model pollutants of different nature like dyes, pesticides and pharmaceutical compounds have been tested. The important findings may be summarized as follows:

NTP is an efficient approach for the degradation of aqueous organic compounds, whose efficiency mainly depends on the nature of the pollutant, input power and pollutant concentration. Electrical discharge in water have a great potential as a novel, chemical-free method of water treatment capable of mineralizing organic compounds.

It was observed that the principle reactive species involved in the degradation and mineralization process are hydroxyl radicals generated by the discharge. In addition, hydrogen peroxide, ozone, ultraviolet light and other active species produced by the discharge may play an important role in the oxidation processes. In situ generation of active species may facilitate the degradation and mineralization leading to the formation of CO_2 and H_2O.

During the present study, aqueous organic pollutants degradation followed first-order kinetics. In general, the efficiency of the process efficiency is limited by the primary oxidizing species, whereas in-situ decomposition of ozone on a suitable catalyst may increase the concentration of hydroxyl radicals.

It was identified that catalyst addition to NTP reactor improves the performance of the process. Hybrid gas-liquid DBD reactors were designed, characterized, optimization of various parameters like catalyst modification, concentration, gas flow rate, discharge gap, treatment time, applied voltage and chemical additives was done that highlighted the better performance of catalytic plasma approach.CO, CO_2 and NO_X analyzer was used for qualitative analysis of CO, CO_2 liberated conforming mineralization. Further mineralization was quantified by TOC analyzer.

The generation of hydrogen peroxide by the discharges in water has been investigated calorimetrically. The hydrogen peroxide formation increased with the increasing applied

voltage (power input), whereas Fe^{2+}addition increased the degree of mineralization, probably via Fenton reactions. During the degradation of methylene blue, addition of Fe^{2+} improved the degradation upto 97 %. Pseudo-first order kinetics were conformed and it was found that the rate constant depends on the initial pollutant concentration.

The performance of the plasma rector for endosulfan degradation was found to increase on addition of metal oxide catalyst and the same has been observed for the degradation of phenol and sulfamethoxazole. It was found that modified CeO_2 catalyst showed the best performance for in-situ decomposition of ozone in aqueous environment. Oxygen deficiency followed by its performance for ozone decomposition was improved on modification of CeO_2 with ZrO_2 and Fe_2O_3, due it increased oxygen vacancies, as evidenced by Raman spectroscopy. It was reasoned that the presence of oxygen vacancies on modified CeO_2 stabilizes the atomic oxygen formed by in-situ ozone decomposition, thereby improves the performance. Based on the intermediates identified by HR-MS, a hydroxyl radical initiated degradation mechanism was proposed.

The SMX degradation in aqueous medium was studied by NTP-DBD reactor. Energy efficiency was estimated and improved mineralization on addition of the catalyst was observed. Among the feed gases studied, oxygen showed the better degradation then nitrogen and air, due to formation of more oxygen based active species. The degradation and mineralization efficiency of the reactor increased on addition of the Fe^{2+}.

Finally to conclude, current advanced oxidation process based on electrical discharges in water is advantageous than conventional advanced oxidation process, whose efficiency can still be increased on utilizing combined catalytic plasma approach.

Much research has been done within the field of advanced oxidation processes and there is no doubt that this approach work efficiently for the oxidative degradation of small quantities of wastewater. This approach, in the present form, needs improvements for the real time application of large volumes of the waste water.

References

[1]. "Water Pollution." West's Encyclopedia of American Law. 2005. Retrieved July 07, 2014 from Encyclopedia.com: http://www.encyclopedia.com/doc/1G2-3437704663.html

[2]. R. O. Alves de Lima, A. P. Bazo, D. M. F. Salvadori, C. M. Rech, D. de Palma Oliveira and G. de Aragão Umbuzeiro Mutagenic And Carcinogenic Potential Of A Textile Azo Dye Processing Plant Effluent That Impacts A Drinking Water Source. Mutation Research/Genetic Toxicology and Environmental Mutagenesis 626, (2007) 53-60.

[3]. H. M. Pinheiro, E. Touraud and O. Thomas Aromatic Amines From Azo Dye Reduction: Status Review With Emphasis On Direct Uv Spectrophotometric Detection In Textile Industry Wastewaters. Dyes and Pigments 61, (2004) 121-139.

[4]. P. A. Carneiro, G. A. Umbuzeiro, D. P. Oliveira and M. V. B. Zanoni Assessment Of Water Contamination Caused By A Mutagenic Textile Effluent/Dyehouse Effluent Bearing Disperse Dyes. Journal of hazardous materials 174, (2010) 694-699.

[5]. C. N. Mulligan, R. N. Yong and B. F. Gibbs Remediation Technologies For Metal-Contaminated Soils And Groundwater: An Evaluation. Engineering Geology 60, (2001) 193-207.

[6]. V. Homem and L. Santos Degradation And Removal Methods Of Antibiotics From Aqueous Matrices – A review. Journal of Environmental Management 92, (2011) 2304-2347.

[7]. K. Dutta, S. Mukhopadhyay, S. Bhattacharjee and B. Chaudhuri Chemical Oxidation Of Methylene Blue Using A Fenton-Like Reaction. Journal of hazardous materials 84, (2001) 57-71.

[8]. N. Azbar, T. Yonar and K. Kestioglu Comparison Of Various Advanced Oxidation Processes And Chemical Treatment Methods For Cod And Color Removal From A Polyester And Acetate Fiber Dyeing Effluent. Chemosphere 55, (2004) 35-43.

[9]. I. Arslan, I. A. Balcioglu and T. Tuhkanen Advanced Oxidation of Synthetic Dyehouse Effluent by O_3, H_2O_2/O_3 and H_2O_2/UV Processes. Environmental Technology 20, (1999) 921-931.

[10]. W. H. Glaze, J.-W. Kang and D. H. Chapin The Chemistry of Water Treatment Processes Involving Ozone, Hydrogen Peroxide and Ultraviolet Radiation. Ozone: Science & Engineering 9, (1987) 335-352.

[11]. B. Sun, M. Sato and J. S. Clements Environmental Science Technology 34, (1999) 509.

[12]. E. Neyens and J. Baeyens A Review Of Classic Fenton's Peroxidation As An Advanced Oxidation Technique. Journal of hazardous materials 98, (2003) 33-50.

[13]. S. Chiron, A. Fernandez-Alba, A. Rodriguez and E. Garcia-Calvo Pesticide Chemical Oxidation: State-Of-The-Art. Water Research 34, (2000) 366-377.

[14]. G. Y. S. Chan and J. G. Wu, Efficacy of Ozone on Pesticide Residues. In *Ozone in Food Processing*, Wiley-Blackwell: 2012; pp 223-240.

[15]. T. Zhang, W. Li and J.-P. Croué A Non-Acid-Assisted And Non-Hydroxyl-Radical-Related Catalytic Ozonation With Ceria Supported Copper Oxide In Efficient Oxalate Degradation In Water. Applied Catalysis B: Environmental 121–122, (2012) 88-94.

[16]. B. Kasprzyk-Hordern, M. Ziółek and J. Nawrocki Catalytic Ozonation And Methods Of Enhancing Molecular Ozone Reactions In Water Treatment. Applied Catalysis B: Environmental 46, (2003) 639-669.

[17]. N. De la Cruz, L. Esquius, D. Grandjean, A. Magnet, A. Tungler, L. F. de Alencastro and C. Pulgarín Degradation Of Emergent Contaminants By Uv, Uv/H2o2 And Neutral Photo-Fenton At Pilot Scale In A Domestic Wastewater Treatment Plant. Water Research 47, (2013) 5836-5845.

[18]. A. Aleboyeh, M. E. Olya and H. Aleboyeh Electrical Energy Determination For An Azo Dye Decolorization And Mineralization By Uv/H2o2 Advanced Oxidation Process. Chemical Engineering Journal 137, (2008) 518-524.

[19]. M. Y. Ghaly, G. Härtel, R. Mayer and R. Haseneder Photochemical Oxidation Of P-Chlorophenol By Uv/H2o2 And Photo-Fenton Process. A comparative study. Waste Management 21, (2001) 41-47.

[20]. B. H. Hameed and T. W. Lee Degradation Of Malachite Green In Aqueous Solution By Fenton Process. Journal of hazardous materials 164, (2009) 468-472.

[21]. DR. Grymonpré, AK. Sharma, WC. Finney The Role Of Fenton's Reaction In Aqueous Phase Pulsed Streamer Corona Reactors. Chemical Engineering Journal 82, (2001) 189.

[22]. L. Núñez, J. A. García-Hortal and F. Torrades Study Of Kinetic Parameters Related To The Decolourization And Mineralization Of Reactive Dyes From Textile Dyeing Using Fenton And Photo-Fenton Processes. Dyes and Pigments 75, (2007) 647-652.

[23]. T. Aarthi and G. Madras Photocatalytic Degradation of Rhodamine Dyes with Nano-TiO2. Industrial & Engineering Chemistry Research 46, (2006) 7-14.

[24]. M. H. Priya and G. Madras Kinetics of TiO2-Catalyzed Ultrasonic Degradation of Rhodamine Dyes. Industrial & Engineering Chemistry Research 45, (2006) 913-921.

[25]. C. Pirola, C. L. Bianchi, S. Gatto, S. Ardizzone and G. Cappelletti Pressurized Photo-Reactor For The Degradation Of The Scarcely Biodegradable Dpc Cationic Surfactant In Water. Chemical Engineering Journal 225, (2013) 416-422.

[26]. N. Morales-Flores, U. Pal and M. E. Sanchez Photocatalytic Behavior Of Zno And Pt-Incorporated Zno Nanoparticles In Phenol Degradation. Applied Catalysis A 394, (2011) 269-275.

[27]. G. S. Son and J. W. Song Photodegradation of VOCs and Bad Smells in a TiO_2 Coated Honeycomb Monolith Reactor. Journal of Advanced Oxidation Technologies, 6 (2003) 80-92.

[28]. I. Kuehr and O. Núñez Titanium Dioxide Photoinduced Degradation Of Some Pesticide/Fungicide Precursors. Pest Management Science 63, (2007) 491-494.

[29]. P. Lukes, A. T. Appleton and B. R. Locke Hydrogen Peroxide And Ozone Formation In Hybrid Gas-Liquid Electrical Discharge Reactors. Industry Applications, IEEE Transactions on 40, (2004) 60-67.

[30]. L. Petr and R. L. Bruce Plasmachemical Oxidation Processes In A Hybrid Gas–Liquid Electrical Discharge Reactor. Journal of Physics D: Applied Physics 38, (2005) 4074.

[31]. L. Petr, C. Martin, B. Vaclav, J. Vaclav and S. Pavel Generation Of Ozone By Pulsed Corona Discharge Over Water Surface In Hybrid Gas–Liquid Electrical Discharge Reactor. Journal of Physics D: Applied Physics 38, (2005) 409.

[32]. D. R. Grymonpré, W. C. Finney, R. J. Clark and B. R. Locke Hybrid Gas−Liquid Electrical Discharge Reactors for Organic Compound Degradation. Industrial & Engineering Chemistry Research 43, (2004) 1975-1989.

[33]. R. L. Bruce and S. Kai-Yuan Review of the methods to form hydrogen peroxide in electrical discharge plasma with liquid water. Plasma Sources Science and Technology 20, (2011) 034006.

[34]. Ruma, P. Lukes, N. Aoki, E. Spetlikova, S. H. R. Hosseini, T. Sakugawa and H. Akiyama Effects Of Pulse Frequency Of Input Power On The Physical And Chemical Properties Of Pulsed Streamer Discharge Plasmas In Water. Journal of Physics D: Applied Physics 46, (2013) 125202.

[35]. W.-T. Shin, S. Yiacoumi, C. Tsouris and S. Dai A Pulseless Corona-Discharge Process For The Oxidation Of Organic Compounds In Water. Industrial & Engineering Chemistry Research 39, (2000) 4408-4414.

[36]. C. Subrahmanyam, A. Renken and L. Kiwi-Minsker Novel Catalytic Non-Thermal Plasma Reactor For The Abatement Of Vocs. Chemical Engineering Journal 134, (2007) 78-83.

[37]. A. A. Joshi, B. R. Locke, P. Arce and W. C. Finney Formation Of Hydroxyl Radicals, Hydrogen Peroxide And Aqueous Electrons By Pulsed Streamer Corona Discharge In Aqueous Solution. Journal of hazardous materials 41, (1995) 3-30.

[38]. E. Marotta, M. Schiorlin, X. Ren, M. Rea and C. Paradisi Advanced Oxidation Process For Degradation Of Aqueous Phenol In A Dielectric Barrier Discharge Reactor. Plasma Processes and Polymers 8, (2011) 867-875.

[39]. B. Peter and L. Christophe Non-Thermal Plasmas In And In Contact With Liquids. Journal of Physics D: Applied Physics 42, (2009) 053001.

[40]. P. Sunka, V. Babický, M. Clupek, P. Lukes, M. Simek, J. Schmidt and M. Cernák Generation Of Chemically Active Species By Electrical Discharges In Water. Plasma Sources Science and Technology 8, (1999) 258.

[41]. M. Zdenko, M. Marcela, M. Emmanuel and M. Imrich Removal Of Cyclohexanone In Transition Electric Discharges At Atmospheric Pressure. Journal of Physics D: Applied Physics 33, (2000) 3198.

[42]. C. Fitzsimmons, F. Ismail, J. C. Whitehead and J. J. Wilman The Chemistry of Dichloromethane Destruction in Atmospheric-Pressure Gas Streams by a Dielectric Packed-Bed Plasma Reactor. The Journal of Physical Chemistry A 104, (2000) 6032-6038.

[43]. K. J. Pringle, J. C. Whitehead, J. J. Wilman and J. Wu The Chemistry of Methane Remediation by a Non-thermal Atmospheric Pressure Plasma. Plasma Chemistry and Plasma Processing 24, (2004) 421-434.

[44]. G.-B. Zhao, S. John, J.-J. Zhang, J. C. Hamann, S. S. Muknahallipatna, S. Legowski, J. F. Ackerman and M. D. Argyle Production Of Hydrogen And Sulfur From Hydrogen Sulfide In A Nonthermal-Plasma Pulsed Corona Discharge Reactor. Chemical Engineering Science 62, (2007) 2216-2227.

[45]. L. Baars-Hibbe, P. Sichler, C. Schrader, C. Geßner, K. H. Gericke and S. Büttgenbach Micro-Structured Electrode Arrays: Atmospheric Pressure Plasma Processes And Applications. Surface and Coatings Technology 174–175, (2003) 519-523.

[46]. T. Hammer, T. Kappes and M. Baldauf Plasma Catalytic Hybrid Processes: Gas Discharge Initiation And Plasma Activation Of Catalytic Processes. Catalysis Today 89, (2004) 5-14.

[47]. HH Kim Nonthermal Plasma Processing For Air-Pollution Control: Current Issues, And Future Prospects, Plasma Processes and Polymers 1 (2004), 91-110.

[48]. R. Snoeckx, R. Aerts, X. Tu and A. Bogaerts Plasma-Based Dry Reforming: A Computational Study Ranging From The Nanoseconds To Seconds Time Scale. The Journal of Physical Chemistry C 117, (2013) 4957-4970.

[49]. F. Thevenet, L. Sivachandiran, O. Guaitella, C. Barakat and A. Rousseau Plasma–Catalyst Coupling For Volatile Organic Compound Removal And Indoor Air Treatment: A Review. Journal of Physics D: Applied Physics 47, (2014) 224011.

[50]. F. Thevenet, O. Guaitella, E. Puzenat, J. M. Herrmann, A. Rousseau and C. Guillard Oxidation Of Acetylene By Photocatalysis Coupled With Dielectric Barrier Discharge. Catalysis Today 122, (2007) 186-194.

[51]. S. Mahammadunnisa, P. Manoj Kumar Reddy, B. Ramaraju and C. Subrahmanyam Catalytic Nonthermal Plasma Reactor for Dry Reforming of Methane. Energy & Fuels 27, (2013) 4441-4447.

[52]. X. Zhang and M. S. Cha Partial Oxidation Of Methane In A Temperature-Controlled Dielectric Barrier Discharge Reactor. Proceedings of the Combustion Institute. (2014) doi:10.1016/j.proci.2014.05.089

[53]. H. Xiao, J. He, Y. Zhang, Y. Li, Y. Li, F. Shen, G. Yang, X. Yang, S. Deng, Y. Wang and L. Li Study Of A Novel High Voltage Pulsed Discharge Reactor With Porous Titanium Electrodes. Journal of the Taiwan Institute of Chemical Engineers 43, (2012) 597-603.

[54]. R. Aerts, X. Tu, W. Van Gaens, J. C. Whitehead and A. Bogaerts Gas Purification by Nonthermal Plasma: A Case Study of Ethylene. Environmental Science & Technology 47, (2013) 6478-6485.

[55]. J. Akhtar, N. S. Amin and A. Aris Combined Adsorption And Catalytic Ozonation For Removal Of Sulfamethoxazole Using Fe_2o_3/CeO_2 Loaded Activated Carbon. Chemical Engineering Journal 170, (2011) 136-144.

[56]. M. Magureanu, D. Piroi, N. B. Mandache, V. I. Pârvulescu, V. Pârvulescu, B. Cojocaru, C. Cadigan, R. Richards, H. Daly and C. Hardacre In Situ Study Of Ozone And Hybrid Plasma

Ag–Al Catalysts For The Oxidation Of Toluene: Evidence Of The Nature Of The Active Sites. Applied Catalysis B: Environmental 104, (2011) 84-90.

[57]. H. C. Wang, S. H. Chang, P. C. Hung, J. F. Hwang and M. B. Chang Synergistic Effect Of Transition Metal Oxides And Ozone On Pcdd/F Destruction. Journal of hazardous materials 164, (2009) 1452-1459.

[58]. L. Lei, X. Hao, X. Zhang and M. Zhou Wastewater Treatment Using A Heterogeneous Magnetite (Fe_3O_4) Non-Thermal Plasma Process. Plasma Processes Polymers. 4, (2007) 455-462.

[59]. M. Muhammad Arif Synergistic Effect Of Plasmacatalyst And Ozone In A Pulsed Corona Discharge Reactor On The Decomposition Of Organic Pollutants In Water. Plasma Sources Science and Technology 12, (2003) S26.

[60]. L. Sivachandiran, F. Thevenet and A. Rousseau Non-Thermal Plasma Assisted Regeneration of Acetone Adsorbed TiO_2 Surface. Plasma Chemistry and Plasma Processing 33, (2013) 855-871.

[61]. S.-p. Tong, W.-p. Liu, W.-h. Leng and Q.-q. Zhang Characteristics of MnO_2 Catalytic Ozonation Of Sulfosalicylic Acid And Propionic Acid In Water. Chemosphere 50, (2003) 1359-1364.

[62]. L. O. d. B. Benetoli, B. M. Cadorin, V. Z. Baldissarelli, R. Geremias, I. G. de Souza and N. A. Debacher Pyrite-Enhanced Methylene Blue Degradation In Non-Thermal Plasma Water Treatment Reactor. Journal of hazardous materials 237–238, (2012) 55-62.

[63]. B. R. Locke, M. Sato, P. Sunka, M. R. Hoffmann and J. S. Chang Electrohydraulic Discharge and Nonthermal Plasma for Water Treatment. Indistrial Engineering Chemistry Research 45, (2006) 882-905.

[64]. F. d. S. Gnokam, A. Doubla and J.-L. Brisset Temporal Post-Discharge Reactions In Plasma-Chemical Degradation Of Slaughterhouse Effluents. Chemical Engineering Communications 198, (2010) 483-493.

[65]. Q. Tang, W. Jiang, Y. Cheng, S. Lin, T. M. Lim and J. Xiong Generation of Reactive Species by Gas-Phase Dielectric Barrier Discharges. Industrial & Engineering Chemistry Research 50, (2011) 9839-9846.

[66]. J. Velikonja, M. A. Bergougnou, G. S. Peter Castle, W. L. Caims and I. I. Inculet Co-Generation of Ozone and Hydrogen Peroxide By Dielectric Barrier AC Discharge in Humid Oxygen. Ozone: Science & Engineering 23, (2001) 467-478.

[67]. F. Thevenet, J. Couble, M. Brandhorst, J. L. Dubois, E. Puzenat, C. Guillard and D. Bianchi Synthesis of Hydrogen Peroxide Using Dielectric Barrier Discharge Associated with Fibrous Materials. Plasma Chemistry and Plasma Processing 30, (2010) 489-502.

[68]. R. Burlica, K. Y. Shih and B. R. Locke Formation of H_2 and H_2O_2 in a Water-Spray Gliding Arc Nonthermal Plasma Reactor. Industrial & Engineering Chemistry Research 49, (2010) 6342-6349.

[69]. M. Magureanu, D. Piroi, F. Gherendi, N. Mandache and V. Parvulescu Decomposition of Methylene Blue in Water by Corona Discharges. Plasma Chemistry and Plasma Processing 28, (2008) 677-688.

[70]. F. Abdelmalek, R. A. Torres, E. Combet, C. Petrier, C. Pulgarin and A. Addou Gliding Arc Discharge (Gad) Assisted Catalytic Degradation Of Bisphenol A In Solution With Ferrous Ions. Separation and Purification Technology 63, (2008) 30-37.

[71]. C. Du, T. Shi, Y. Sun and X. Zhuang Decolorization Of Acid Orange 7 Solution By Gas-Liquid Gliding Arc Discharge Plasma. Journal of hazardous materials 154, (2008) 1192-1197.

[72]. R. Burlica and B. R. Locke Pulsed Plasma Gliding-Arc Discharges With Water Spray. Industry Applications, IEEE Transactions on 44, (2008) 482-489.

[73]. P. Westerhoff, G. Aiken, G. Amy and J. Debroux Relationships Between The Structure Of Natural Organic Matter And Its Reactivity Towards Molecular Ozone And Hydroxyl Radicals. Water Research 33, (1999) 2265-2276.

[74]. Y. S. Mok, J.-O. Jo and J. C. Whitehead Degradation Of An Azo Dye Orange Ii Using A Gas Phase Dielectric Barrier Discharge Reactor Submerged In Water. Chemical Engineering Journal 142, (2008) 56-64.

[75]. L. R. Grabowski, E. M. v. Veldhuizen, A. J. M. Pemen and W. R. Rutgers Breakdown Of Methylene Blue And Methyl Orange By Pulsed Corona Discharge. Plasma Sources Science and Technology 16, (2007) 226.

[76]. Y. Zhang, X. Xiong, Y. Han, H. Yuan, S. Deng, H. Xiao, F. Shen and X. Wu Application Of Titanium Dioxide-Loaded Activated Carbon Fiber In A Pulsed Discharge Reactor For Degradation Of Methyl Orange. Chemical Engineering Journal 162, (2010) 1045-1049.

[77]. M. Magureanu, D. Piroi, N. B. Mandache and V. Parvulescu Decomposition Of Methylene Blue In Water Using A Dielectric Barrier Discharge: Optimization Of The Operating Parameters. Journal of Applied Physics 104, (2008) -.

[78]. Q. Tang, W. Jiang, Y. Zhang, W. Wei and T. Lim Degradation of Azo Dye Acid Red 88 by Gas Phase Dielectric Barrier Discharges. Plasma Chemistry and Plasma Processing 29, (2009) 291-305.

[79]. H. Wang, J. Li, X. Quan and Y. Wu Enhanced Generation Of Oxidative Species And Phenol Degradation In A Discharge Plasma System Coupled With Tio2 Photocatalysis. Applied Catalysis B: Environmental 83, (2008) 72-77.

[80]. J. H. Yan, C. M. Du, X. D. Li, B. G. Cheron, M. J. Ni and K. F. Cen Degradation of Phenol in Aqueous Solutions by Gas–Liquid Gliding Arc Discharges. Plasma Chemistry and Plasma Processing 26, (2006) 31-41.

[81]. Y. J. Liu and X. Z. Jiang Phenol Degradation by a Nonpulsed Diaphragm Glow Discharge in an Aqueous Solution. Environmental Science & Technology 39, (2005) 8512-8517.

[82]. C. H. Wang, X. Zhang, T. C. Wang, N. Lu, J. Li and Y. Wu Role Of Energy Input Model On The Remediation Of The P-Nitrophenol Contaminated Over-Wet Soil By Pulsed Corona Discharge Plasma. Journal of Physics: Conference Series 418, (2013) 012135.

[83]. M. Sahni and B. R. Locke Degradation Of Chemical Warfare Agent Simulants Using Gas–Liquid Pulsed Streamer Discharges. Journal of hazardous materials 137, (2006) 1025-1034.

[84]. X. Jin, X. Wang, Y. Wang and H. Ren Oxidative Degradation of Amoxicillin in Aqueous Solution with Contact Glow Discharge Electrolysis. Industrial & Engineering Chemistry Research 52, (2013) 9726-9730.

[85]. D. Piroi, M. Magureanu, N. B. Mandache, V. David and V. Parvulescu In Pulsed Dielectric Barrier Discharge Generated At The Gas-Liquid Interface For The Degradation Of The Organic Dye Methyl Red In Aqueous Solution, Optimization Of Electrical And Electronic Equipment (Optim), 2010 12th International Conference on, 20-22 May 2010, 2010; 1323-1328.

[86]. L. R. Grabowski, E. M. Veldhuizen, A. J. M. Pemen and W. R. Rutgers Corona Above Water Reactor for Systematic Study of Aqueous Phenol Degradation. Plasma Chemistry and Plasma Processing 26, (2006) 3-17.

[87]. B. Jiang, J. Zheng, Q. Liu and M. Wu Degradation Of Azo Dye Using Non-Thermal Plasma Advanced Oxidation Process In A Circulatory Airtight Reactor System. Chemical Engineering Journal 204–206, (2012) 32-39.

[88]. X. Xu Dielectric Barrier Discharge — Properties And Applications. Thin Solid Films 390, (2001) 237-242.

[89]. U. Kogelschatz, B. Eliasson and W. Egli Delectric-barrier Dscharges. Principle and applications. Le Journal de Physique IV 07, (1997) 47-66.

[90]. H. Lee, S. Park, Y.-K. Park, B. Kim, S.-J. Kim and S.-C. Jung Rapid Destruction Of The Rhodamine B Using Tio2 Photocatalyst In The Liquid Phase Plasma. Chemistry Central Journal 7, (2013) 156.

[91]. R. Zhang, C. Zhang, X. Cheng, L. Wang, Y. Wu and Z. Guan Kinetics Of Decolorization Of Azo Dye By Bipolar Pulsed Barrier Discharge In A Three-Phase Discharge Plasma Reactor. Journal of hazardous materials 142, (2007) 105-110.

[92]. Y.-S. Chen, X.-S. Zhang, Y.-C. Dai and W.-K. Yuan Pulsed High-Voltage Discharge Plasma For Degradation Of Phenol In Aqueous Solution. Separation and Purification Technology 34, (2004) 5-12.

[93]. J.-j. Ruan, W. Li, Y. Shi, Y. Nie, X. Wang and T.-e. Tan Decomposition Of Simulated Odors In Municipal Wastewater Treatment Plants By A Wire-Plate Pulse Corona Reactor. Chemosphere 59, (2005) 327-333.

[94]. M. Young Sun and J. Jin-Oh Degradation of Organic Contaminant by Using Dielectric Barrier Discharge Reactor Immersed in Wastewater. Plasma Science, IEEE Transactions on 34, (2006) 2624-2629.

[95]. Z. Wang, D. Xu, Y. Chen, C. Hao and X. Zhang Plasma Decoloration Of Dye Using Dielectric Barrier Discharges With Earthed Spraying Water Electrodes. Journal of Electrostatics 66, (2008) 476-481.

[96]. H. Wang, J. Li and X. Quan Decoloration Of Azo Dye By A Multi-Needle-To-Plate High-Voltage Pulsed Corona Discharge System In Water. Journal of Electrostatics 64, (2006) 416-421.

[97]. V. I. Gibalov, J. Dřímal, M. Wronski and V. G. Samoilovich Barrier Discharge The Transferred Charge and Ozone Synthesis. Contributions to Plasma Physics 31, (1991) 89-99.

[98]. P. S. Lang, W. K. Ching, D. M. Willberg and M. R. Hoffmann Oxidative Degradation of 2,4,6-Trinitrotoluene by Ozone in an Electrohydraulic Discharge Reactor. Environmental Science & Technology 32, (1998) 3142-3148.

[99]. X. Tao, R. Lu and H. Li Electrical Characteristics of Dielectric-Barrier Discharges in Atmospheric Pressure Air Using a Power-Frequency Voltage Source. Plasma Science and Technology 14, (2012) 723.

[100]. G. Eisenberg Colorimetric Determination of Hydrogen Peroxide. Industrial & Engineering Chemistry Analytical Edition 15, (1943) 327-328.

[101]. I. D. Mall, V. C. Srivastava, N. K. Agarwal and I. M. Mishra Adsorptive Removal Of Malachite Green Dye From Aqueous Solution By Bagasse Fly Ash And Activated Carbon-Kinetic Study And Equilibrium Isotherm Analyses. Colloids and Surfaces A: Physicochemical and Engineering Aspects 264, (2005) 17-28.

[102]. Q. H. Hu, S. Z. Qiao, F. Haghseresht, M. A. Wilson and G. Q. Lu Adsorption Study for Removal of Basic Red Dye Using Bentonite. Industrial & Engineering Chemistry Research 45, (2005) 733-738.

[103]. Y. Badr, M. G. Abd El-Wahed and M. A. Mahmoud Photocatalytic Degradation Of Methyl Red Dye By Silica Nanoparticles. Journal of hazardous materials 154, (2008) 245-253.

[104]. M. A. Oturan An ecologically Effective Water Treatment Technique Using Electrochemically Generated Hydroxyl Radicals For In Situ Destruction Of Organic Pollutants: Application To Herbicide 2,4-D. Journal of Applied Electrochemistry 30, (2000) 475-482.

[105]. M. Magureanu, D. Piroi, N. B. Mandache, V. David, A. Medvedovici and V. I. Parvulescu Degradation Of Pharmaceutical Compound Pentoxifylline In Water By Non-Thermal Plasma Treatment. Water Research 44, (2010) 3445-3453.

[106]. P. Šunka Pulse Electrical Discharges In Water And Their Applications. Physics of Plasmas 8, (2001) 2587-2594.

[107]. C. Subrahmanyam, A. Renken and L. Kiwi-Minsker Ctalytic Aatement of Votile Oganic Cmpounds Asisted by Nn-thermal Pasma. Part ii. Optimized catalytic electrode and Orating Cnditions. Applied catalysis b: environmental 65, (2006) 157-162.

[108]. F. Huang, L. Chen, H. Wang and Z. Yan Analysis Of The Degradation Mechanism Of Methylene Blue By Atmospheric Pressure Dielectric Barrier Discharge Plasma. Chemical Engineering Journal 162, (2010) 250-256.

[109]. R. Burlica, M. J. Kirkpatrick and B. R. Locke Formation Of Reactive Species In Gliding Arc Discharges With Liquid Water. Journal of Electrostatics 64, (2006) 35-43.

[110]. F. Abdelmalek, M. R. Ghezzar, M. Belhadj, A. Addou and J.-L. Brisset Bleaching and Degradation of Textile Dyes by Nonthermal Plasma Process at Atmospheric Pressure. Industrial & Engineering Chemistry Research 45, (2005) 23-29.

[111]. P. Lukes and B. R. Locke Degradation of Substituted Phenols in a Hybrid Gas-Liquid Electrical Discharge Reactor. Industrial & Engineering Chemistry Research 44, (2005) 2921-2930.

[112]. M. Muruganandham and M. Swaminathan Photocatalytic Decolourisation And Degradation Of Reactive Orange 4 By Tio2-Uv Process. Dyes and Pigments 68, (2006) 133-142.

[113]. F. Minisci, A. Citterio and C. Giordano Electron-Transfer Processes: Peroxydisulfate, A Useful And Versatile Reagent In Organic Chemistry. Accounts of Chemical Research 16, (1983) 27-32.

[114]. X. Hao, X. Zhang and L. Lei The Catalytic Effect of Metal Ions on the Degradation of 4-Chlorophenol Induced by an Aqueous Pulsed Discharge Plasma. Plasma Science and Technology 15, (2013) 678.

[115]. F. Abdelmalek, S. Gharbi, B. Benstaali, A. Addou and J. L. Brisset Plasmachemical Degradation Of Azo Dyes By Humid Air Plasma: Yellow Supranol 4 Gl, Scarlet Red Nylosan F3 Gl And Industrial Waste. Water Research 38, (2004) 2339-2347.

[116]. I. Arslan and I. A. Balcioglu Effect Of Common Reactive Dye Auxiliaries On The Ozonation Of Dyehouse Effluents Containing Vinylsulphone And Aminochlorotriazine Dyes. Desalination 130, (2000) 61-71.

[117]. A. Mandal, K. Ojha, A. K. De and S. Bhattacharjee Removal Of Catechol From Aqueous Solution By Advanced Photo-Oxidation Process. Chemical Engineering Journal 102, (2004) 203-208.

[118]. C.-M. Ma, G.-B. Hong, H.-W. Chen, N.-T. Hang and Y.-S. Shen Photooxidation Contribution Study on the Decomposition of Azo Dyes in Aqueous Solutions by VUV-Based AOPs. International Journal of Photoenergy 2011, (2011) 8.

[119]. J. Pereira, S. Antunes, B. Castro, C. Marques, A. Gonçalves, F. Gonçalves and R. Pereira Toxicity Evaluation Of Three Pesticides On Non-Target Aquatic And Soil Organisms: Commercial Formulation Versus Active Ingredient. Ecotoxicology 18, (2009) 455-463.

[120]. K. Atreya, B. Sitaula, F. Johnsen and R. Bajracharya Continuing Issues In The Limitations Of Pesticide Use In Developing Countries. Journal of Agricultural and Environmental Ethics 24, (2011) 49-62.

[121]. C. A. Damalas and I. G. Eleftherohorinos Pesticide Exposure, Safety Issues, and Risk Assessment Indicators. International Journal of Environmental Research and Public Health 8, (2011) 1402-1419.

[122]. J. Weber, C. J. Halsall, D. Muir, C. Teixeira, J. Small, K. Solomon, M. Hermanson, H. Hung and T. Bidleman Endosulfan, A Global Pesticide: A Review Of Its Fate In The Environment And Occurrence In The Arctic. Science of The Total Environment 408, (2010) 2966-2984.

[123]. J. Varayoud, L. Monje, T. Bernhardt, M. Muñoz-de-Toro, E. H. Luque and J. G. Ramos Endosulfan Modulates Estrogen-Dependent Genes Like A Non-Uterotrophic Dose Of 17β-Estradiol. Reproductive Toxicology 26, (2008) 138-145.

[124]. M. H. Silva and D. Gammon an assessment of the developmental, reproductive, and neurotoxicity of endosulfan. Birth defects research part b: developmental and reproductive Toxicology 86, (2009) 1-28.

[125]. M. H. Silva and S. L. Beauvais Hman Halth Rsk Rsessment of Edosulfan. I: Txicology and Hzard Ientification. Regulatory Toxicology and Pharmacology 56, (2010) 4-17.

[126]. V. K. Gupta and I. Ali Removal of Endosulfan and Methoxychlor from Water on Carbon Slurry. Environmental Science & Technology 42, (2008) 766-770.

[127]. L. J. Banasiak, B. Van der Bruggen and A. I. Schäfer Sorption Of Pesticide Endosulfan By Electrodialysis Membranes. Chemical Engineering Journal 166, (2011) 233-239.

[128]. P. C. Mishra and R. K. Patel Removal Of Endosulfan By Sal Wood Charcoal. Journal of hazardous materials 152, (2008) 730-736.

[129]. K. Kravvariti, N. G. Tsiropoulos and D. G. Karpouzas Degradation And Adsorption Of Terbuthylazine And Chlorpyrifos In Biobed Biomixtures From Composted Cotton Crop Residues. Pest Management Science 66, (2010) 1122-1128.

[130]. A. Kar, Y. R. Smith and V. Subramanian Improved Photocatalytic Degradation Of Textile Dye Using Titanium Dioxide Nanotubes Formed Over Titanium Wires. Environmental Science & Technology 43, (2009) 3260-3265.

[131]. M. K. Dail and S. P. Mezyk Hydroxyl-Radical-Induced Degradative Oxidation of β-Lactam Antibiotics in Water: Absolute Rate Constant Measurements. The Journal of Physical Chemistry A 114, (2010) 8391-8395.

[132]. L. F. Gaunt, C. B. Beggs and G. E. Georghiou Bactericidal Action Of The Reactive Species Produced By Gas-Discharge Nonthermal Plasma At Atmospheric Pressure: A Review. IEEE Trans. Plasma Sci. 34, (2006) 1257-1269.

[133]. L. Jie, W. Tiecheng, L. Na, Z. Dandan, W. Yan, W. Tianwei and S. Masayuki Degradation Of Dyes By Active Species Injected From A Gas Phase Surface Discharge. Plasma Sources Science and Technology 20, (2011) 034019.

[134]. P. C. C. Faria, J. J. M. Órfão and M. F. R. Pereira Ozone Decomposition in Water Catalyzed by Activated Carbon: Influence of Chemical and Textural Properties. Industrial & Engineering Chemistry Research 45, (2006) 2715-2721.

[135]. T. Zhang, W. Li and J.-P. Croué Catalytic Ozonation of Oxalate with a Cerium Supported Palladium Oxide: An Efficient Degradation Not Relying on Hydroxyl Radical Oxidation. Environmental Science & Technology 45, (2011) 9339-9346.

[136]. X.-Y. Li, Y.-H. Cui, Y.-J. Feng, Z.-M. Xie and J.-D. Gu Reaction Pathways And Mechanisms Of The Electrochemical Degradation Of Phenol On Different Electrodes. Water Research 39, (2005) 1972-81.

[137]. V. Uberoi and S. K. Bhattacharya Toxicity And Degradability Of Nitrophenols In Anaerobic Systems. Water Environment Research 69, (1997) 146-156.

[138]. J. A. Zazo, J. A. Casas, A. F. Mohedano, M. A. Gilarranz and J. J. Rodríguez Chemical Pathway and Kinetics of Phenol Oxidation by Fenton's Reagent. Environmental Science & Technology 39, (2005) 9295-9302.

[139]. P. Ye and A. T. Lemley Adsorption Effect On The Degradation Of 4,6-O-Dinitrocresol And P-Nitrophenol In A Montmorillonite Clay Slurry By Aft. Water Research 43, (2009) 1303-1312.

[140]. R. Chandra, S. Yadav, R. N. Bharagava and V. Rai Phenol Degradation By Paenibacillus Thiaminolyticus And Bacillus Cereus In Axenic And Mixed Conditions. World Journal of Microbiology and Biotechnology 27, (2011) 2939-2947.

[141]. Y. Niu, M. Xing, J. Zhang and B. Tian Visible Light Activated Sulfur And Iron Co-Doped Tio2 Photocatalyst For The Photocatalytic Degradation Of Phenol. Catalysis Today. 201 (2013) 159-166.

[142]. Z. Guo, R. Ma and G. Li Degradation Of Phenol By Nanomaterial Tio2 In Wastewater. Chemical Engineering Journal (Amsterdam, Neth.) 119, (2006) 55-59.

[143]. D. H. Bremner, A. E. Burgess, D. Houllemare and K.-C. Namkung Phenol Degradation Using Hydroxyl Radicals Generated From Zero-Valent Iron And Hydrogen Peroxide. Applied catalysis b: environmental 63, (2006) 15-19.

[144]. S. Mahammadunnisa, P. M. K. Reddy, N. Lingaiah and C. Subrahmanyam Nio/Ce1− Xnixo2− Δ As An Alternative To Noble Metal Catalysts For Co Oxidation. Catalysis Science & Technology (2013).

[145]. A. Martínez-Arias, M. Fernández-García, L. N. Salamanca, R. X. Valenzuela, J. C. Conesa and J. Soria Structural And Redox Properties Of Ceria In Alumina-Supported Ceria Catalyst Supports. The Journal of Physical Chemistry B 104, (2000) 4038-4046.

[146]. F. J. Beltrán, F. J. Rivas and R. Montero-de-Espinosa Ozone-Enhanced Oxidation of Oxalic Acid in Water with Cobalt Catalysts. 2. Heterogeneous Catalytic Ozonation. Industrial & Engineering Chemistry Research 42, (2003) 3218-3224.

[147]. F. J. Beltrán, J. Rivas, P. Álvarez and R. Montero-de-Espinosa Kinetics of Heterogeneous Catalytic Ozone Decomposition in Water on an Activated Carbon. Ozone: Science & Engineering 24, (2002) 227-237.

[148]. J. Karuppiah, L. Sivachandiran, R. Karvembu and C. Subrahmanyam Catalytic Nonthermal Plasma Reactor For The Abatement Of Low Concentrations Of Isopropanol. Chemical Engineering Journal (Amsterdam, Neth.) 165, (2010) 194-199.

[149]. J. Villaseñor, P. Reyes and G. Pecchi Catalytic And Photocatalytic Ozonation Of Phenol On Mno2 Supported Catalysts. Catalysis Today 76, (2002) 121-131.

[150]. S. Kunitomo and S. Bing In Removal Of Phenol In Water By Pulsed High Voltage Discharge, Pulsed Power Plasma Science, 2001. PPPS-2001. Digest of Technical Papers, 2001, 2001; 1138-1141 vol.2.

[151]. M. Dors, G. V. Nichipor and J. Mizeraczyk In Modeling Of Phenol Decomposition Induced By Pulsed Corona Discharge In Water, Dielectric Liquids, 2005. ICDL 2005. 2005 IEEE International Conference on, 26 June-1 July 2005, 2005; 95-98.

[152]. L. Yang, C. Hu, Y. Nie and J. Qu Catalytic Ozonation of Selected Pharmaceuticals over Mesoporous Alumina-Supported Manganese Oxide. Environmental Science & Technology 43, (2009) 2525-2529.

[153]. D. Gerrity, B. D. Stanford, R. A. Trenholm and S. A. Snyder An Evaluation Of A Pilot-Scale Nonthermal Plasma Advanced Oxidation Process For Trace Organic Compound Degradation. Water Res 44, (2010) 493-504.

[154]. S. K. Khetan and T. J. Collins Human Pharmaceuticals in the Aquatic Environment: A Challenge to Green Chemistry. Chemical Reviews 107, (2007) 2319-2364.

[155]. A. T. Sugiarto, S. Ito, T. Ohshima, M. Sato and J. D. Skalny Oxidative Decoloration Of Dyes By Pulsed Discharge Plasma In Water. Journal of Electrostatics 58, (2003) 135-145.

[156]. Q. Tang, S. Lin, W. Jiang and T. M. Lim Gas Phase Dielectric Barrier Discharge Induced Reactive Species Degradation Of 2,4-Dinitrophenol. Chemical Engineering Journal 153, (2009) 94-100.

[157]. J. L. Wang and L. J. Xu Advanced Oxidation Processes for Wastewater Treatment: Formation of Hydroxyl Radical and Application. Critical Reviews in Environmental Science and Technology 42, (2011) 251-325.

Research Publications:

1. **P. Manoj Kumar Reddy** and Ch. Subrahmanyam., Green Approach for Wastewater Treatment-Degradation and Mineralization of Aqueous Organic Pollutants by Discharge Plasma, ACS **Industrial & Engineering Chemistry Research,** 51, (2012) 11097-11103.

2. **P. Manoj Kumar Reddy**, B. Ramaraju, J. Karuppiah, E.L. Reddy and Ch. Subrahmanyam., Degradation and Mineralization of methylene blue by dielectric barrier discharge non-thermal plasma reactor, **Chemical Engineering Journal**, 217, (2013) 41-47.

3. **P. Manoj Kumar Reddy,** B. Ramaraju and Ch. Subrahmanyam., Degradation of Malachite Green by Dielectric Barrier Discharge Plasma, **Water Science and Technology,** 67.5, (2013) 1097-1104.

4. **P. Manoj Kumar Reddy,** Sk. Mahammadunnisa, B. Raju, B. Sreedhar and Ch. Subrahmanyam, Low cost adsorbents from bio-waste for the removal of dyes from aqueous solution, **Environmental Science and Pollution Research**, 20, (2013) 4111-4124.

5. **P. Manoj Kumar Reddy,** A. Dayamani, Sk. Mahammadunnisa and Ch. Subrahmanyam., Mineralization of Phenol in water by Catalytic Non-Thermal Plasma Reactor – An Eco-Friendly Approach for Wastewater, **Plasma Processes and Polymers** 10(11), (2013) 1010-1017.

6. **P. Manoj Kumar Reddy,** Sk. Mahammadunnisa and Ch. Subrahmanyam., Mineralization of Endosulfan from Water by Nonthermal Plasma: A Green Approach for Treatment of Pesticide Contaminated Water, **Chemical Engineering Journal**, 238, (2014) 157-163.

7. **P. Manoj Kumar Reddy,** K. Krushnamurty, Sk. Mahammadunnisa and Ch. Subrahmanyam., Preparation of activated carbons from bio-waste – Effect of surface

functional groups on methylene blue adsorption, **International journal of Environmental Science and Technology**, (10.1007/s13762-014-0506-2).

8. **P. Manoj Kumar Reddy,** Sk. Mahammadunnisa and Ch. Subrahmanyam., Catalytic plasma reactor for pollutants mineralization, **Indian Journal of Chemistry A,** 53, (2014) 499-503.

9. **P. Manoj Kumar Reddy** and Ch. Subrahmanyam., Surface modification of carbon fabric for isopropanol removal from gas stream, **Microelectronic Engineering**, (In press).

10. **P. Manoj Kumar Reddy** and Ch. Subrahmanyam., Non-Thermal Plasma: Aqueous Organic Pollutant Degradation, **Taylor & Francis LLC Encyclopedia**, (Revision submitted).

11. B. Ramaraju, **P. Manoj Kumar Reddy** and Ch. Subrahmanyam., Low cost adsorbents from agricultural waste for removal of dyes, **Environmental Progress & Sustainable Energy 33(1), (2014) 38-46.**

12. **P. Manoj Kumar Reddy and** Ch. Subrahmanyam., Surface modification of carbon fabric for isopropanol removal from gas stream, **Microelectronic Engineering, (In press).**

Oral presentations:

1. **P. Manoj Kumar Reddy,** Sk. Mahammadunnisa and Ch. Subrahmanyam*., Catalytic NTP-DBD reactor for mineralization of aqueous organic pollutants. 2012 International Symposium on Plasmas for Catalyses and Energy Materials (ISPCEM-2012) September 21-24, 2012; Tianjin, China.

2. **P. Manoj Kumar Reddy*** and Ch. Subrahmanyam., Degradation of textile dye methylene blue using non-thermal plasma, First International Conference on Plasma

Processing of Organic Materials and Polymers (PPOMP 2011), November 25-27, 2011; Kottayam, Kerala. **(Invited talk)**

3. **P. Manoj Kumar Reddy** and Ch. Subrahmanyam*., Nonthermal plasma reactor for wastewater treatment. XX International conference on Chemical Reactors (CHEMREACTOR-20) December 3-7, 2012; Luxemburg, United Kingdom.

4. **P. Manoj Kumar Reddy***, Sk. Mahammadunnisa and Ch. Subrahmanyam., Catalytic plasma reactor for pollutants mineralization-a new ecofriendly process for wastewater treatment., 21st National Symposium on Catalysis (CATSYMP-21) 10-13 February, 2013; IICT Hyderabad, India. **(Best Orel presentation award)**

5. **P. Manoj Kumar Reddy*** and Ch. Subrahmanyam., Surface Modification of Carbon Nanofibres by dielectric barrier discharge., 8th International Conference on Surfaces, Coatings and Nanostructured Materials (NANOSMAT) 22-25 September 2013;

Awards and Recognitions:

- **Research excellence award from IIT-Hyderabad for the year of 2013.**
- **Hindustan Platinum Best Oral presentation award for presentation at CATSYMP-21, IICT Hyderabad, India.**